## Title

Electrochemically Enhanced Amine Regeneration Process for Next Generation Carbon Dioxide Capture



## Author

Tseng, Yen-Wen

## Publication Date

2022

Peer reviewed|Thesis/dissertation

UNIVERSITY OF CALIFORNIA

Los Angeles

# Electrochemically Enhanced Amine Regeneration Process for Next Generation Carbon Dioxide Capture

A dissertation submitted in partial satisfaction of the requirements for the degree

Doctor of Philosophy in Chemical Engineering

by

Yen-Wen Tseng

2022

ABSTRACT OF THE DISSERTATION

Electrochemically Enhanced Amine Regeneration Process for Next Generation Carbon Dioxide Capture

by

Yen-Wen Tseng
Doctor of Philosophy in Chemical Engineering
University of California, Los Angeles, 2022
Professor Dante Simonetti, Chair

Resulting of fossil fuel usage, $CO_2$ concentration in the atmosphere has increased drastically throughout the past century. This increase in $CO_2$ concentration has led to global warming and more frequent extreme weather events that threaten the habitability of the planet. Therefore, it is essential to decrease the $CO_2$ concentration in the atmosphere to mitigate global warming. Post-combustion capture using amine absorbent is one of the most widely used methods, given its feasibility in retrofitting existing fossil fuel-consuming facilities. However, several challenges, including high energy requirements and low cyclic capacity, limit the commercialization of the post-combustion capture technology. In this work, an electrochemically enhanced amine regeneration process is developed to tackle these challenges.

The electrochemically enhanced amine regeneration system utilizes the hydrolysis reaction, generating proton and hydroxide to complete an acid- and base-swing regeneration cycle. The electrochemical amine regeneration cell was constructed by stacking multiple ion exchange membranes, acrylic spacers, and rubber gaskets. Several studies were conducted to test, build and optimize the electrochemical amine regeneration system.

Amine absorption and desorption baseline were established in different amine-based absorbents to understand the $CO_2$ absorption and desorption profile. Proton-induced $CO_2$ desorption from the absorbent was studied by HCl addition to the $CO_2$-loaded amines. This study validated that complete $CO_2$ desorption can be achieved under ambient temperature. The regeneration of amine by the combination of acid-swing and base-swing was validated by HCl and NaOH addition. The electrochemical cell was then used to perform the acid swing. Different cell structures, exchange membranes, and ionic solutions usage were tested. The acid swing of amine and complete $CO_2$ desorption can be achieved using a four-compartment cell. The base swing of acidified amine was performed by anion exchange. It is validated that electrochemical acid-swing and anion exchange base-swing can successfully regenerate amine. The reabsorption capacity of regenerated amine is the same regardless of the regeneration method used.

The optimization study of the electrochemical amine regeneration system focuses on improving energy efficiency and reducing process complexity. Proton requirements for complete $CO_2$ desorption and $CO_2$ loading capacity of various amine absorbents were characterized. It is found that Piperazine has the lowest proton to $CO_2$ ratio, which will result in less energy requirement for electrochemical amine regeneration. A five-compartment electrochemical cell is designed to replace the need for anion exchange resin for base swing. It is validated that the five-compartment cell can complete acid-swing and base-swing to achieve amine regeneration in a continuous operation mode. This cell design reduces the complexity of the process, increases energy efficiency, and facilitates the system's scale-up.

In conclusion, an electrochemical amine regeneration system has been developed. Compared to the state-of-art method, it can achieve >80% cyclic capacity with low energy

consumption. With further optimization studies, the energy consumption can be further reduced, and this system can potentially serve as the method for the next generation of $CO_2$ capture.

This dissertation of Yen-wen Tseng is approved.

Carlos Morales-Guio

David Jassby

Philippe Sautet

Dante Simonetti, Committee Chair

University of California, Los Angeles

2022

TABLE OF CONTENT

LIST OF FIGURES

LIST OF TABLES

ACKNOWLEDGMENTS

This work would not have been done without the help, guidance, and support from my family, advisor, committee members, colleagues, and friends. I would like to express my appreciation for all I have received from everyone. However, given my limited time ane memory, I unfortunately may have missed some names in this section. For those who are not named, you have my thanks and apology.

First of all, Mom and Dad, I would like to thank you for all they have done for me throughout my whole life. You provided me with an excellent environment and domestic education when I grew up and raised me into a cultivated person. I would not have been who I am now without you. In addition, I would like to also thank you for your continual love and support. Your love and support accompany me through all my ups and downs, and it is essential for my Ph.D. study. I want to thank you, too, my dear wife, Molly, for your love, help, and support. You have done so much, caring for, accompanying, and supporting me unconditionally. My Ph.D. journey would have been much more challenging without you in my life. It is truly my blessing to marry you and have you for the rest of my life. Kevin, thanks for your encouragement and belief in me. Your pep talk works out great every time, and I am grateful to have such a good brother like you.

To my advisors, professor Simonetti and professor Jassby, thank you for your valuable advice on the project and your time shaping me into a logical thinker and qualified Ph.D. In addition, your patience and tolerance in guiding me through my errors made have helped me grow into a better researcher. I would also like to thank my committee members, professor Sautet and professor Morales-Guio. Your constructive questions and suggestions have helped this work and me improve.

For the Simonetti group members, I would like to thank you all for all the great times we had in our office and lab, and for the sparks we generated through our intellectual collisions. Dr.

Luke Minardi, you helped me the most with almost everything when I just joined the group. So, thank you for that, and thank you for the great time we had at the softball and basketball game we had together. Eric, Anas, Steven, and Dr. Xin Chen, thanks for all the help you have provided me, both intellectually and practically. Despite that we did not work directly in the lab, I would like to thank Dr. Aziz Alturki, Dr. Juan Carlos Vega, Jenny and Mario for making my lab life much more fun and for always being there for help. Finally, for my undergrad, whom I have worked with, Jovy, thank you for all the great help on the experiments and python scripts.

I would also like to thank my former advisor, professor Liao. Thank you for admitting me into the Ph.D. program at UCLA. None of this work would happen without you recognizing me as a qualified student. I would also like to thank my other former advisor, professor Sun. The virology knowledge I acquired in your group has helped me stay calm during a hard time of the COVID pandemic. Finally, I want to thank the members of my former Liao and Sun lab members- Dr. Tony Wu, Dr. Paul Lin, Dr. Charlie Chen, Dr. Freddy Chen, Dr. Yushen Du, Dr.Yuan Shi, Dr. Dangyan Gong, and Tianhao Zhang. Your help in and outside the lab is deeply appreciated.

I would also like to thank professor Yu-chen Hu and Dr. Chiu-ling Chen, whom I met at National Tsing Hua University during my undergraduate time. Thank you for providing me with the necessary training and guiding me into scientific research. Those training and guidance are valuable experiences that help me foster and grow.

Finally, I would like to thank all my friends for being my friend and supporting me during my Ph.D. journey. To Dr. Rick Tsai, Dr. Kylie Chung, Dr. Mike Lo, Dr. Steve Lu, Dr. Wayne Horng, Dr. Chris Wu, Dr. Sheng-Feng Hsieh, Andy Huang, Huiling Chung, Jasper Zhao, Lisa Chen, Max Chang, Jaxon Tsai, Yawen Yu, Gena Yu, Jill Tsai, and Hanshen Huang, thank you all for the support and great time we had together.

# VITA

| | |
|---|---|
| 2010-2014 | B.S. Chemical Engineering<br>National Tsing Hua University<br>Hsinchu, Taiwan |
| 2016-2022 | Graduate Student Researcher<br>Department of Chemical Engineering<br>University of California, Los Angeles |
| 2017-2022 | Teaching Assistant<br>Department of Chemical Engineering<br>University of California, Los Angeles |
| 2019-2021 | Teaching Assistant<br>Department of Civil Engineering<br>University of California, Los Angles |

# PUBLICATIONS


1. Du Y, Hultquist JF, Zhou Q, et al. mRNA display with library of even-distribution reveals cellular interactors of influenza virus NS1. *Nat Commun*. 2020;11(1):1-13.
2. Du Y, Xin L, Shi Y, et al. Genome-wide identification of interferon-sensitive mutations enables influenza vaccine design. 2018;296(January):290-296.
3. Lin M, Tseng Y, Shen C, et al. Synthetic switch-based baculovirus for transgene expression control and selective killing of hepatocellular carcinoma cells. 2018;46(15). doi:10.1093/nar/gky447
4. Chen C-L, Tseng Y-W, Wu J-C, et al. Suppression of hepatocellular carcinoma by baculovirus-mediated expression of long non-coding RNA PTENP1 and MicroRNA regulation. *Biomaterials*. 2015;44:71-81.
5. Chen C-L, Wu J-C, Chen G-Y, et al. Baculovirus-mediated miRNA regulation to suppress hepatocellular carcinoma tumorigenicity and metastasis. *Mol Ther*. 2015;23(1):79-88.

# Chapter 1 Introduction and background

## 1.1 Motivation

$CO_2$ emission from fossil fuels is a significant contributor to the accumulation of $CO_2$ in the atmosphere. With the increasing demand for fossil fuels, annual $CO_2$ emissions increase from 17.05 to 34.81 billion metric tons per year from 1975 to 2020[1,2]. Consequently, atmospheric $CO_2$ levels increased drastically from 331 ppm to 414 ppm during this period of time[3]. The 2011-2020 decade became the warmest decade on record, with the surface average temperature being +0.82 ℃ above the 20$^{th}$ century average[4]. This global warming leads to climate change contributing to detrimental consequences and economic loss. The rise of sea level threats the long-term habitability of the pacific island countries like the Republic of Tuvalu[5]. Extreme weather events have led to massive losses in agricultural industries[6]. These consequences show the urgency to stop global warming.

To limit the temperature increase to below 2 °C compared to the pre-industrial level, International Energy Agency (IEA) proposes the removal of 10-20 Gt $CO_2$ per year[7]. In addition to switching from fossil-based energy sources to $CO_2$-neutral renewable energy sources, IEA urges carbon capture and storage (CCS) to reduce anthropogenic $CO_2$ during the transition to a low-carbon energy system[8,9]. With the soaring demands on CCS technologies, studies on novel methods, sorbents, thermodynamics, and kinetics have been carried out[10–14].

## 1.2 Introduction to $CO_2$ Capture Technologies

Conventional Carbon capture and storage technology can be categorized into pre-combustion, post-combustion, and oxyfuel combustion[15]. In pre-combustion capture, fossil fuels (coal or hydrocarbon) undergo partial oxidation or steam reforming reaction to generate syngas. Syngas then undergoes the water-gas shift reaction, turning themselves into a mixture of $CO_2$ and $H_2$ before combustion[14,16]. In oxyfuel

combustion capture, pure oxygen rather than air is used to provide oxidant for fossil fuel combustion. As a result, $CO_2$ in the flue gas is ready to be sequestrated without further absorption, as $CO_2$ and $H_2O$ are the only species present in the flue gas. In post-combustion capture, fossil fuel is combusted in air, creating flue gas consisting of $N_2$, $CO_2$, $H_2O$, $NO_x$, and $SO_x$. $CO_2$ is captured by absorption, adsorption, or membrane separation[13]. Among these $CO_2$ capture technologies, post-combustion capture is the most popular with its potential to capture $CO_2$ from the air and its ability to retrofit current fossil fuel-consuming facilities. This capability of "direct air capture" (DAC) allows for negative emission of $CO_2$, making the post-combustion capture method a potential solution to reduce the $CO_2$ concentration in the atmosphere.

### 1.2.1 Pre-Combustion Capture Technology

#### 1.2.1.1 Process description

The schematic of pre-combustion capture is shown in **Figure *1***. Pre-combustion capture is a method that removes the carbon before the hydrocarbon fuel is combusted. As shown in **Figure *1***, two reactors are required for syngas generation and water-gas shift. Hydrocarbon fuel is converted into hydrogen and carbon dioxide with these two reactions. The carbon dioxide and hydrogen are separated at the separation unit, and hydrogen is used as fuel for combustion. $H_2O$ will be the only product after combustion.

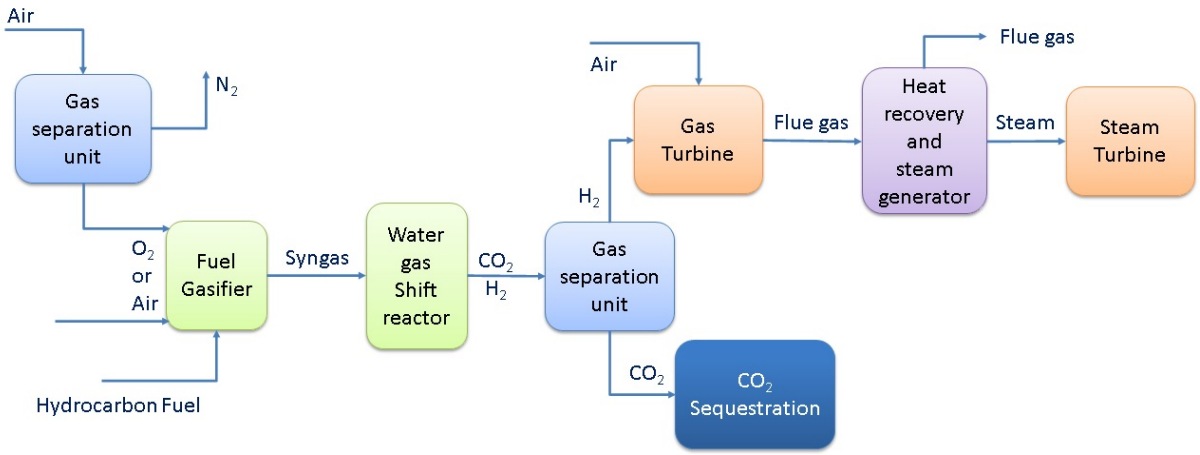


**Figure 1.** Process diagram of Pre-combustion capture method.

1.2.1.2 Mechanism

Pre-combustion capture technology utilizes syngas production and water-gas shift reaction to convert hydrocarbon into hydrogen fuel and carbon dioxide[16]. Syngas production from hydrocarbon fuel can be done via the following two reaction paths: steam-reforming and partial oxidation.

$$C_xH_y + xH_2O \leftrightarrow xCO + \left(x + \frac{y}{2}\right) H_2 \; \Delta H_{CH_4} = 206kJ\; mol^{-1} \qquad (1)$$

$$C_xH_y + \frac{1}{2}O_2 \leftrightarrow xCO + \frac{y}{2}H_2 \; \Delta H_{CH_4} = -36kJ\; mol^{-1} \qquad (2)$$

In a steam-reforming reaction, steam is reacted with hydrocarbon fuel to form carbon monoxide and hydrogen at 750-900 °C and 20-30 bar. On the other hand, partial oxidation of $CH_4$ occurs at 700°C-900°C with oxygen as reactant[17]. Oxygen required for partial oxidation is typically purified from the air[16]. Water gas shift reaction follows the syngas generation and converts CO into $CO_2$ by adding steam.

$$CO + H_2O \leftrightarrow CO_2 + H_2 \; \Delta H = -41kJ\ mol^{-1} \quad (3)$$

$CO_2$ is then isolated from the product stream, and hydrogen can be used as a carbon-neutral fuel.

1.2.1.3 Advantages and disadvantages

There are several advantages of using the pre-combustion capture method over other capture methods. The relatively higher $CO_2$ concentration at the point of capture makes the capture less energy intensive compared to post-combustion capture[18,19]. The concentration and pressure of $CO_2$ at the inlet stream of the capture unit can be up to 60% and 7MPa[16]. The relatively high concentration and pressure significantly reduce the energy penalty required to separate and compress $CO_2$. However, some disadvantages prevent its board application for $CO_2$ capture. It is challenging to fit this capture method to existing hydrocarbon-consuming facilities, like the power plant, as it requires a significant investment in modifying existing infrastructure. Reactors are needed for syngas generation and water gas shift reaction. A unique hydrogen-fueled turbine would need to be used. In addition, the pre-combustion method can only reduce the amount of $CO_2$ emission as it cannot remove CO2 from the atmosphere directly.

1.2.2 Oxyfuel Combustion

1.2.2.1 Process Description

The schematic of the oxyfuel combustion process is shown in ***Figure 2***. First, a gas separation unit is required to purify $O_2$ from the air. Next, purified Oxygen is used for hydrocarbon fuel combustion. Then, another gas separation unit separates $H_2O$ and $CO_2$ after combustion. Typically, a condenser would be used to separate the $CO_2$ and $H_2O$, given the simplicity of the condensing process compared to other separation methods.

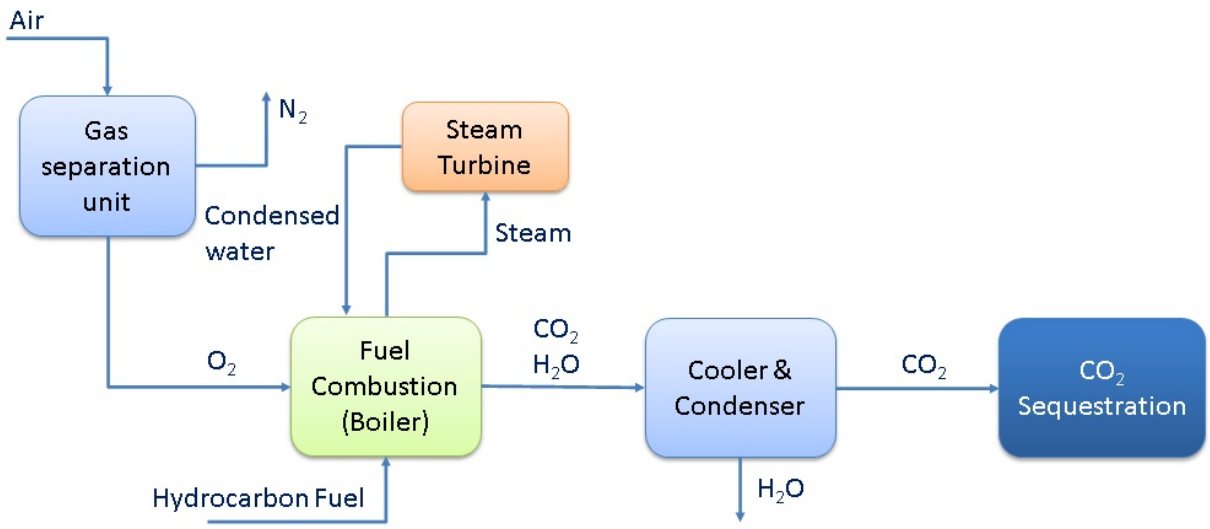


**Figure 2.** Process diagram of oxyfuel combustion

1.2.2.2 Mechanism

Pure oxygen rather than air is used to combust hydrocarbon fuels in the oxyfuel combustion capture method[13,20]. Hydrocarbon combustion with pure $O_2$ generates a $CO_2$ and $H_2O$ mixture in the flue gas. $CO_2$ can be separated simply by cooling the combustion exhaust to condense $H_2O$. Equation ( 4 ) shows the reaction of oxyfuel combustion. No other reaction is required to capture $CO_2$.

$$C_xH_y + \left(x + \frac{y}{2}\right) O_2 \leftrightarrow xCO_2 + \frac{y}{2} H_2O \qquad (4)$$

1.2.2.3 Advantages and disadvantages

Process simplicity and feasibility of easy $CO_2$ isolation are the main advantages of oxyfuel combustion[21]. Unlike the pre-combustion capture method, oxyfuel combustion does not require significant infrastructure modifications. Also, the isolation of $CO_2$ requires no additional material or solvent, making it easier and cheaper[22]. Some studies also showed that less $NO_x$ and $SO_x$ are generated than in the post-combustion capture method[23]. Despite these advantages, oxyfuel

combustion is not economically feasible. The high cost of pure oxygen generation is the main factor limiting its application[13]. In addition, oxyfuel combustion cannot be used for carbon dioxide removal from the atmosphere.

### 1.2.3 Post-combustion capture

#### 1.2.3.1 Process Description

A schematic of post-combustion capture is provided in **Figure 3.** Hydrocarbon fuel is combusted without any pretreatment. Flue gas produced by this combustion mainly contains $N_2$, $CO_2$, $H_2O$, and a trace amount of $NO_x$ and $SO_x$. Flue gas is purged into the absorption column, where amine-based absorbent is in contact with the flue gas. The $CO_2$-loaded absorbent is transported to a stripping unit where the amine solution is heated to over 120 °C, and $CO_2$ is desorbed. Regenerated amine is then circulated back to the absorption unit for $CO_2$ re-absorption.

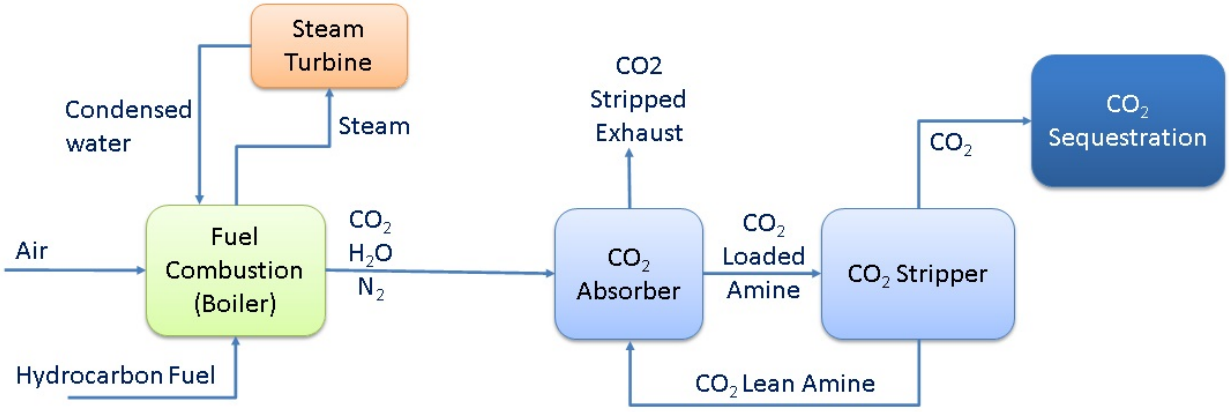


**Figure 3.** Process diagram of post-combustion capture

#### 1.2.3.2 Mechanism

Post-combustion capture method captures $CO_2$ using amine absorbent after the hydrocarbon fuel combustion. $CO_2$ containing flue gas is purged through an absorption column in a conventional amine scrubbing process. Aqueous amine solution (20-50% v/v) is in contact with flue gas in the absorption column to absorb $CO_2$. Absorption occurs via an exothermic reaction of

$CO_2$ and amine. The zwitterion mechanism is the most commonly accepted mechanism proposed for $CO_2$ absorption in amine. In the following equations, monoethanolamine (MEA) is used as an example (R= $CH_2CH_3OH$ )[24].

$$CO_2 + RNH_2 = RNH_2^+COO^- \quad (5)$$

$$RNH_2^+COO^- + RNH_2 = RNHCOO^- + RNH_3^+ \quad (6)$$

$CO_2$ is reacted with monoethanolamine to form a zwitterion as an intermediate. This intermediate zwitterion then instantly reacts with another monoethanolamine to form a carbamate and protonated amine[25]. Some recent studies suggest that the absorption of $CO_2$ in MEA may involve several molecules, including carbonate and bicarbonate, at higher $CO_2$ loading[26,27]. Lv. et al. show that carbonate and bicarbonate formation is the dominant $CO_2$ absorption mechanism at higher $CO_2$ loading (>0.4mol$CO_2$ mol$MEA^{-1}$)[26]. In addition, $CO_2$ can be hydrolyzed into carbonate or bicarbonate and reacted with MEA to form carbamate. The proposed mechanism is shown in **Figure *4***.

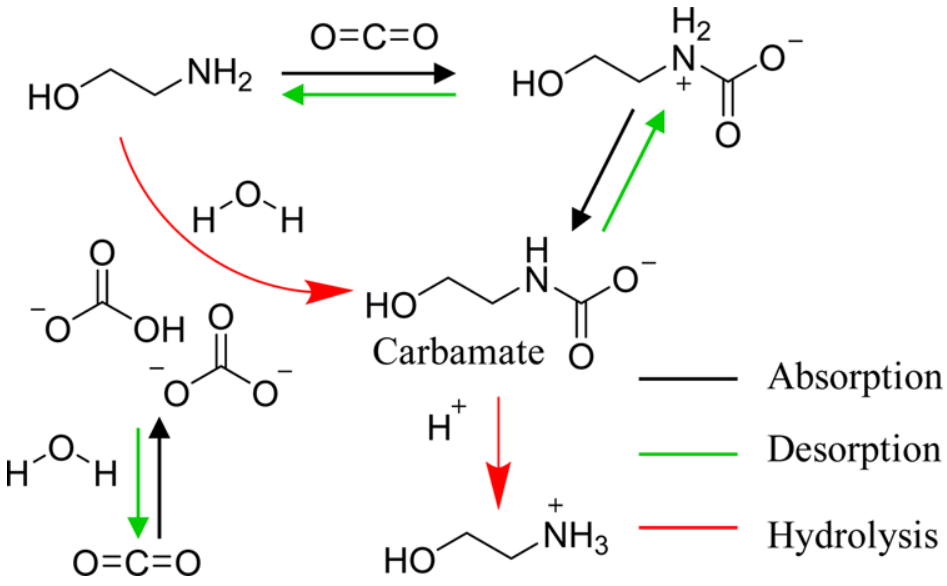


**Figure 4.** Mechanism of CO2 absorption in MEA.[26]

The desorption of CO2 from the amine solution is simply the reverse reaction of the absorption. As the absorption of $CO_2$ in amine is exothermic, CO2 desorption is expected to be endothermic, and heat input into $CO_2$ loaded amine solution is required. MEA solution needs to be heated to over 120℃ for $CO_2$ desorption[28–30]. As a result, a significant amount of heat duty is required for $CO_2$ desorption and amine regeneration.

#### 1.2.3.3 Maximum $CO_2$ loading in different amines

Maximum $CO_2$ loading in amines is affected by various factors, including amine types, $CO_2$ concentration, and solution temperature[25,31]. For example, tertiary amines typically have higher loading than primary and secondary amines; however, at a lower reaction rate, due to different reaction mechanism[32,33]. In addition, Higher $CO_2$ concentration used for absorption can also increase the $CO_2$ loading in various amine[34–36]. For example, with 30% $CO_2$ concentration, $CO_2$ loading of MEA solution at 40℃ can be around 0.45-0.5 mol $CO_2$ molMEA$^{-1}$. On the other hand, if using air (400 ppm $CO_2$) as a $CO_2$ source for absorption, the maximum $CO_2$ loading of MEA can reach around 0.25-0.3 mol $CO_2$ molMEA$^{-1}$. On the other hand, high solution temperature can decrease the maximum (equilibrium) loading of $CO_2$ in amine solutions[35–37]. For example, at a $CO_2$ partial pressure of 300 pa, the maximum $CO_2$ loading capacity of 40℃ MEA is about 0.5 molCO2 molMEA$^{-1,}$ while maximum loading can only reach 0.35 mol$CO_2$ mol MEA$^{-1}$ at a solution temperature of 80℃[35].

#### 1.2.3.4 Cyclic capacity and heat duty requirements for amine regeneration

The cyclic capacity of the amine is defined to be the difference in $CO_2$ loading between absorption and regeneration in a $CO_2$ capture cycle[38]. The cyclic capacity of amine absorbent is affected by multiple factors, including amine types, regeneration temperatures, and rich loading of

the amine absorbent. It is reported that higher cyclic capacity can be achieved with higher regeneration temperature and heat duty[30]. With a rich loading of 0.5mol$CO_2$ mol$MEA^{-1}$ and reboiler duty of 2000kJ $kgCO_2^{-1}$, cyclic capacity is ~0.15 mol$CO_2$ mol$MEA^{-1}$. At the same rich loading, cyclic capacity can reach 0.28 mol$CO_2$ mol$MEA^{-1}$ at a reboiler duty of 10000kJ $kgCO_2^{-1}$. At a rich loading of 0.3 mol$CO_2$ mol$MEA^{-1}$, cyclic capacity is less than 0.1 mol$CO_2$ mol$MEA^{-1}$ even at a reboiler duty of > 18000kJ $kgCO_2^{-1}$. This result shows that rich loading can significantly affect the cyclic capacity and reboiler duty required.

#### 1.2.3.5 Advantages and disadvantages

Post-combustion capture can retrofit old hydrocarbon-fueled power plants without changing existing infrastructure significantly, making post-combustion capture more favorable than other capture methods. Also, post-combustion capture can apply to direct air capture and capture $CO_2$ from the atmosphere. However, post-combustion capture is not yet a market-driven technology, and capture cost needs to be reduced to facilitate this technology. In addition, several challenges limit the application of post-combustion capture. First, the $CO_2$ desorption and amine regeneration process is highly energy intensive because of the massive heat requirement to regenerate the amine[30,31,39]. Additionally, the cyclic capacity of MEA is smaller than 50% of its maximum capacity even when operating at optimized condition[40].

## 1.3 Introduction to water electrolysis

Water electrolysis is first demonstrated experimentally by Adriaan Paets van Troostwijk and Jan Rudolph Deiman more than two hundred years ago[41]. A powerful friction-based electrostatic generator powered the experiment with two gold electrodes immersed in water[41]. With material science, electrochemistry, and membrane technology advancements, water electrolysis has been applied to different fields, including hydrogen production and acid & base production.

### 1.3.1 Hydrolysis using ion-exchange membrane

#### 1.3.1.1 Alkaline electrolysis

Alkaline electrolysis is an electrochemical process where hydrolysis occurs in an alkaline solution (NaOH/KOH) with a diaphragm separating anode and cathode. The schematics and the reaction on the anode and cathode are provided in ***Figure 5***. Hydroxide ions and hydrogen are generated at the anode by oxidation of water. Hydrogen is released in the gas phase, and hydroxide is transported through the porous diaphragm to the cathode. Hydroxide ion is reduced at the cathode, generating hydrogen. In summary, hydroxide is transported between the cathode anode to complete the hydrolysis reaction. Material of electrode, electrocatalyst, and separator material are highlighted research focus to improve the cell efficiency and reduce the cost of alkaline electrolyzer[42].

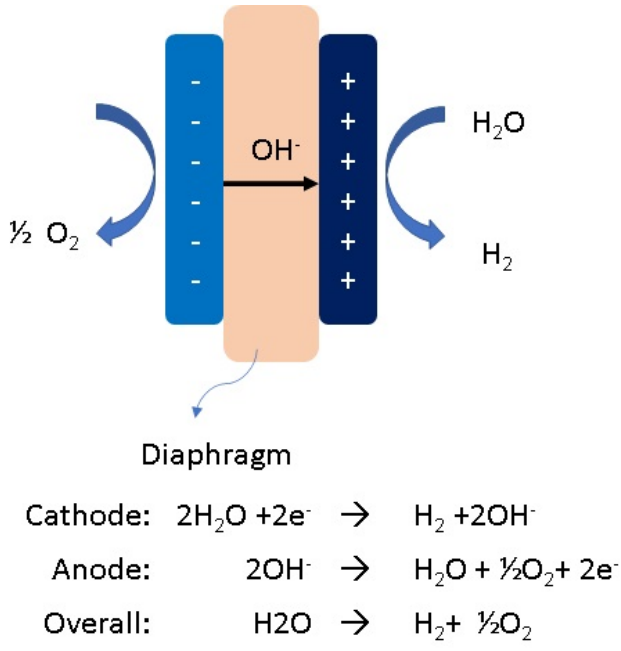


**Figure 5.** Schematics of Alkaline electrolysis cell

### 1.3.1.2 PEM electrolysis

Proton exchange membrane (PEM) electrolysis is another water electrolysis method; however, using proton as an ion transporter. A schematic of cell structure and reaction on electrodes is shown in **Figure *6.*** Water is oxidized at the anode, creating oxygen and proton. Proton is then transported through PEM and is reduced at the cathode to create hydrogen. PEM water electrolysis has several advantages over alkaline electrolysis[43]. It has a higher current density, a more compact system design, and a quick response to allow more flexibility[43]. Also, it produces ultrapure hydrogen without the need for further purification[44,45]. However, the requirement of noble metal for the electrode (Pt/Pd cathode, $IrO_2$/$RuO_2$ anode) increases the overall price for PEM water electrolysis[46–48]. Therefore, a significant amount of research is done on electrode materials and membrane electrode assembly to reduce the overall cost of PEM water electrolysis[49–53].

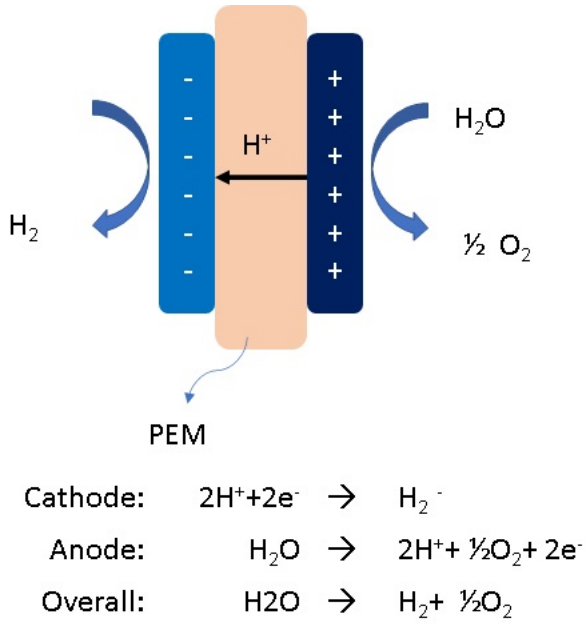


**Figure 6.** Schematics of proton exchange membrane water electrolyzer

#### 1.3.1.3 Bipolar membrane water dissociation

A bipolar membrane is a membrane that consists of an anion-exchange layer (AEL) and a cation-exchange layer (CEL) on two sides of the membrane. Bipolar junction is used to term the interface between AEL and CEL. Unlike monopolar membranes, the bipolar membrane does not allow cation or anion to transport. It dissociates water into proton and hydroxide at the bipolar junction, without the oxygen and hydrogen evolution[54]. Water dissociation occurs at the bipolar junction when the membrane is under reverse bias. Schematics of the bipolar membrane under forward bias and reverse bias are shown in **Figure 7**. The Second Wien effect describes the phenomenon that weak electrolyte's ion mobility and dissociation constant increase under a high electric field. It was used to describe the water dissociation in bipolar membrane[55–58]. It is assumed that AEL and CEL are sharply bound to create a sharp bipolar junction with a thin charge region where water is dissociated like a weak electrolyte. Another mechanism suggests a protonation-deprotonation mechanism where $H^+$ and $OH^-$ are generated by the proton-transfer reaction between water and ionic group on the membrane[59]. In the case of the weak base, the reaction mechanism is shown in equation ( 7 ) & ( 8 ). In the case of the weak acid, the reaction is shown in equation ( 9 ) & ( 10 ). The overall reaction equation is shown in equation ( 11 ), where MX is the electrolyte used, MOH is the base, and HX is the acid generated. Strathmann et al.[60] develop a model to explain water dissociation in bipolar membrane combining the second Wien effect and protonation-deprotonation mechanism. Water dissociation and proton and hydroxide formation are proposed to compensate for the ion transport into the bipolar junction when the limiting current is exceeded. Water dissociation provides a new way to generate proton and hydroxide electrochemically without oxygen and hydrogen evolution.

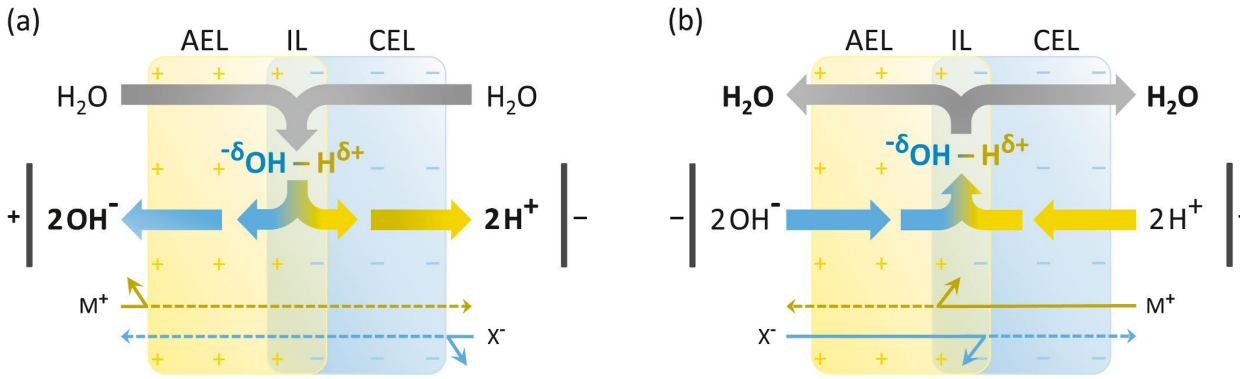


**Figure 7. (a)** Bipolar membrane under reverse bias. **(b)** Bipolar membrane under forward bias.[54]

$$B + H_2O \leftrightarrow BH^+ + OH^- \quad (7)$$

$$BH^+ + H_2O \leftrightarrow B + H_3O^+ \quad (8)$$

$$AH + H_2O \leftrightarrow A^- + H_3O^+ \quad (9)$$

$$A^- + H_2O \leftrightarrow AH + OH^- \quad (10)$$

$$MX + H_2O \leftrightarrow MOH + HX \quad (11)$$

## 1.4 Scope and Organization

This thesis focuses on developing a next-generation electrochemical amine regeneration system for carbon dioxide capture with the following studies: (i) understanding the absorption and desorption kinetics, capacity, and thermodynamics by breakthrough experiment, discussed in Chapter 3, (ii) effect of acid- and base- swing on $CO_2$ absorption capacity and kinetics of amine, discussed in Chapter 3, (iii) develop electrochemical acid-swing cell and anion exchange base-swing for amine regeneration, discussed in Chapter 4, and (iv) optimizing operating parameters to improve the amine regeneration kinetics, energy efficiency, process simplicity and $CO_2$ absorption capacity, discussed in Chapter 5.

# Chapter 2 Experimental Material and Methods

## 2.1 Amine Absorbent Characterization

### 2.1.1 Experiment Apparatus for $CO_2$ Absorption and Desorption Characterization

A home-built reactor is constructed to characterize amine absorbent's $CO_2$ absorption and desorption behavior. The schematic of the reactor is shown in **Figure 8**. Two Mass flow controllers (MFC, Model number: GE50A013502RMV020) are used to control carbon dioxide ($CO_2$) and nitrogen ($N_2$) flow rate from a gas cylinder flowing into a boiling bottle. $CO_2$ and $N_2$ are mixed before entering the boiling bottle, and the $CO_2$ and $N_2$ flow rate ratio can control the $CO_2$ concentration of the mixed gas. $N_2$ and $CO_2$ mixed gas are introduced into the boiling bottle with a gas sparger to provide better gas dispersion. A rubber stopper is used to seal one opening of the boiling bottle and hold the sparger at a certain height so that it does not interfere with the spinning of the stir bar. A pH probe is held by another rubber stopper that seals the second outlet of the boiling bottle. This pH probe can provide us with a pH reading of amine during $CO_2$ absorption and desorption. The third outlet of the boiling bottle is connected with a glass condenser to trap $H_2O$ and amine from evaporating. This glass condenser can minimize $H_2O$ and amine evaporation during $CO_2$ desorption by temperature swing. The gas coming from the condenser is mixed with extra nitrogen diluent before entering the $CO_2$ sensor ($CO_2$meter.com, Model: CM-0122). The flow rate of all gas streams can be measured and validated by a soap film flowmeter that is mounted at the outlet of the $CO_2$ sensor.

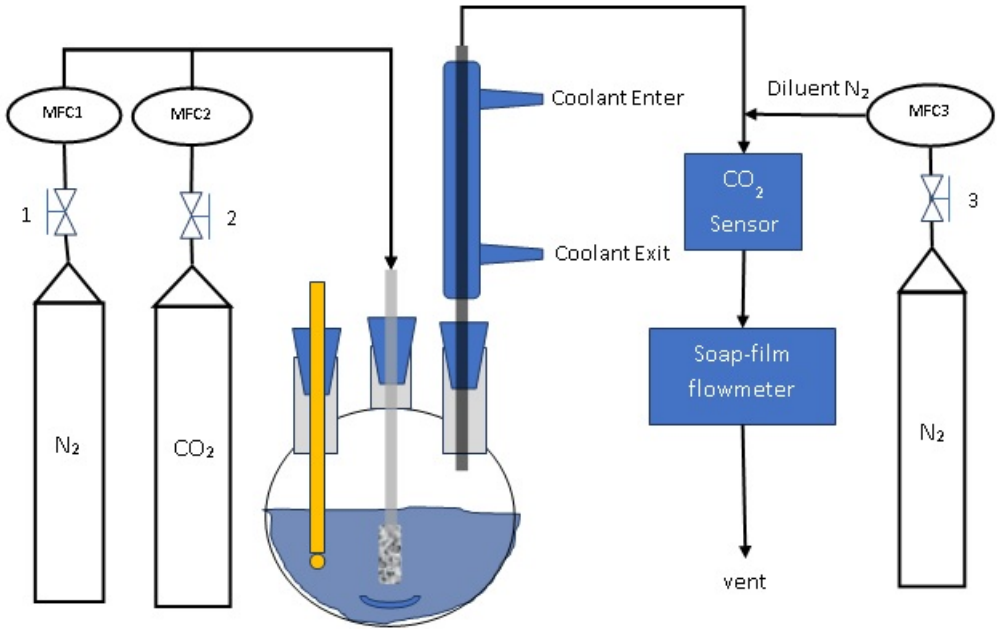


**Figure 8.** Experiment apparatus for characterization of $CO_2$ absorption and desorption of amine absorbents.

### 2.1.2 $CO_2$ absorption and CO2 breakthrough experiment

$CO_2$ breakthrough experiments were conducted in the reactor described in the previous paragraph to test the $CO_2$ absorption capacity of different amines. First, MFC1 and MFC2 are set to a constant value to acquire a $CO_2$ stream used for absorption. **Table 1** shows the flow rate setting of MFCs for different $CO_2$ concentrations used for absorption. $N_2$ diluent (flow rate set by MFC3) is supplied to the system if 100% $CO_2$ is used for the absorption experiment. After the MFCs setting is configured, the system is purged with that MFC configuration until saturated. The saturation can be verified by saturation $CO_2$ reading ($x_{sat}$) on the $CO_2$ sensor. The value of $x_{sat}$ is determined by the flow rate ratio of $N_2$ and $CO_2$ supplied to the system. Saturation $CO_2$ reading ($x_{eq}$) is maintained for 5 minutes before the start of the absorption experiment. When starting the experiment, the rubber stopper holding the pH probe is removed from the boiling bottle, and an amine absorbent to be tested is added. The rubber stopper is placed back on the boiling bottle after

amine addition. Amine absorbent is purged with $CO_2$ until it is fully saturated. $N_2$ diluent and $CO_2$ supply flow rate were measured by a soap film flowmeter before and after the breakthrough experiment to verify that the flow rates were kept constant during the whole breakthrough experiment.

**Table 1.** MFC Flowrate setting at different $CO_2$ concentrations used for absorption

| $CO_2$ concentration used for Absorption (%) | MFC 1 (ml $min^{-1}$) | MFC 2 (ml $min^{-1}$) | MFC 3 (ml $min^{-1}$) | Equilibrium $CO_2$ Reading $x_{sat}$ (%) |
|---|---|---|---|---|
| 100 | 0 | 100 | 400 | 20 |
| 20 | 400 | 100 | 0 | 20 |
| 5 | 475 | 25 | 0 | 5 |
| 1 | 495 | 5 | 0 | 1 |

### 2.1.3 $CO_2$ Desorption from $CO_2$-loaded amine absorbents

$CO_2$ desorption experiments are also conducted in the same home-built reactor described before. MFC 2 and MFC 3 are set to 0 ml $min^{-1}$, and MFC 1 is set to 350 ml $min^{-1}$ to purge the boiling bottle with $N_2$ at room temperature until the bottle is saturated with $N_2$. $N_2$ flow rate can be validated by a soap-film flowmeter. Purging the boiling bottle with $N_2$ can ensure that all $CO_2$ is depleted before starting the $CO_2$ desorption experiment. $N_2$ saturation can be verified by a zero $CO_2$ concentration reading on the $CO_2$ sensor. $CO_2$-loaded amine is then placed into the boiling flask to start the $CO_2$ desorption experiment. $CO_2$ desorption can be driven by heating, acid addition, or both. When inducing $CO_2$ desorption by acid addition, HCl is added to the boiling bottle by a syringe and needle that pokes through the rubber stopper. Adding HCl with a syringe and needle makes sure the whole experiment apparatus is perfectly sealed during HCl addition. Using a syringe and needle for HCl addition can ensure all desorbed $CO_2$ will enter the $CO_2$ sensor for accurate quantification. 25mmol (5M 5ml) HCl is added to the boiling bottle every 15 minutes

until all $CO_2$ is desorbed. When performing $CO_2$ desorption by elevating the temperature, the boiling bottle is soaked in a heat bath at the target temperature (40, 60, or 80 ℃) for at least an hour. A $CO_2$ sensor measures desorbed CO2 throughout the desorption process. The total $N_2$ flow rate was measured again at the end of the experiment to validate the constant $N_2$ supply during the desorption process.

### 2.1.4 Infrared Spectroscopy

Infrared Spectroscopy (PerkinElmer, Spectrum Two FT-IR Spectrometer) was used to characterize amine absorbent reactions ($CO_2$ loading, $CO_2$ desorption, and amine regeneration). 0.1 ml of amine samples were placed on the diamond crystal. Samples were pressurized by the pressure arm during the measurement. Samples that were highly acidic or basic (pH<1 or pH>13) were neutralized by HCl or NaOH before putting on the diamond crystal. The highly caustic or acidic sample may damage the diamond crystal and interfere with the reading of the spectrum. Background spectrum is taken before sample measurement using deionized water with the same pressurization.

### 2.1.5 Gas Chromatography-Mass Spectroscopy

Gas Chromatography-Mass Spectroscopy (Agilent Technology, 7890a) is used to quantify amines and characterize any by-product that may have formed during the electrochemical process. Amine samples sample is collected during the electrochemical process, and 0.5 micro liters of samples are injected into the front inlet port of GC. GC operation parameter is shown in **Table 2**.

**Table 2.** GC-MS operation parameter

| | Parameter | Set-Value |
|---|---|---|
| **Inlet Ports** | Temperature | 250 ℃ |
| | Pressure | 19.438 psi |
| | Total flow | 64.2 ml/min |
| | Septum purge flow | 3 ml/ min |
| | Split ratio | 50: 1 |
| **Columns** | Column type | HP-5, Agilent Technology |
| | He flowrate | 5 ml/ min |
| | Pressure | 0.2171 psi |
| **Oven** | Start temperature | 150 ℃ |
| | Ramp rate | 10 ℃ /min |
| | Ramp target temperature | 200 ℃ |
| | Hold at the target temperature | 8 min |
| **Detector** | Detector type | FID |
| | Temperature | 300 ℃ |
| | Air flow | 400 ml/min |
| | H2 flow | 30 ml/min |
| | N2 makeup flow | 5 ml/min |

## 2.2 Electrochemical Cell Design and Fabrication

A schematic of a home-built 4-compartment electrochemical cell stack is shown in **Figure 9**. A cell stack consists of side caps, rubber gaskets, plastic spacers, and membranes. The following rules are followed during the electrochemical stacking. First, silicone rubber gaskets (McMaster-Carr, 1460N22) are used to sandwich and secure membranes in the cell stack. Second, at least one layer of gasket must be present between plastic parts, including the spacer or side cap. Spacers, gaskets, and membranes can be added or taken away from the electrochemical cell stack depending on the number of compartments needed for different experiments.

The side cap and plastic spacer are acrylic (McMaster-Carr, 4615T133) or PTFE sheets (McMaster-Carr, 8545K35). Acrylic and PTFE are stable when in contact with sulfuric acid, sodium hydroxide, and amines. Therefore, they are suitable materials for fabricating parts used for an electrochemical cell. Plastic sheets with various thicknesses are constructed into the spacer to

provide flexibility in changing the volume of each compartment. A laser cutter is used to cut the acrylic spacer and silicone rubber gasket into the configuration shown in **Figure *10***. Next, membranes are cut with scissors into a shape that fits the gasket and spacer configuration. Platinum or platinum-coated titanium is used as the electrode material to prevent anode degradation during electrochemical cell operation. Super corrosion-resistant screws (McMaster-Carr, 92186A554) and nuts (McMaster-Carr, 94804A029) are used, and a wrench tightens nuts to secure the cell stack.

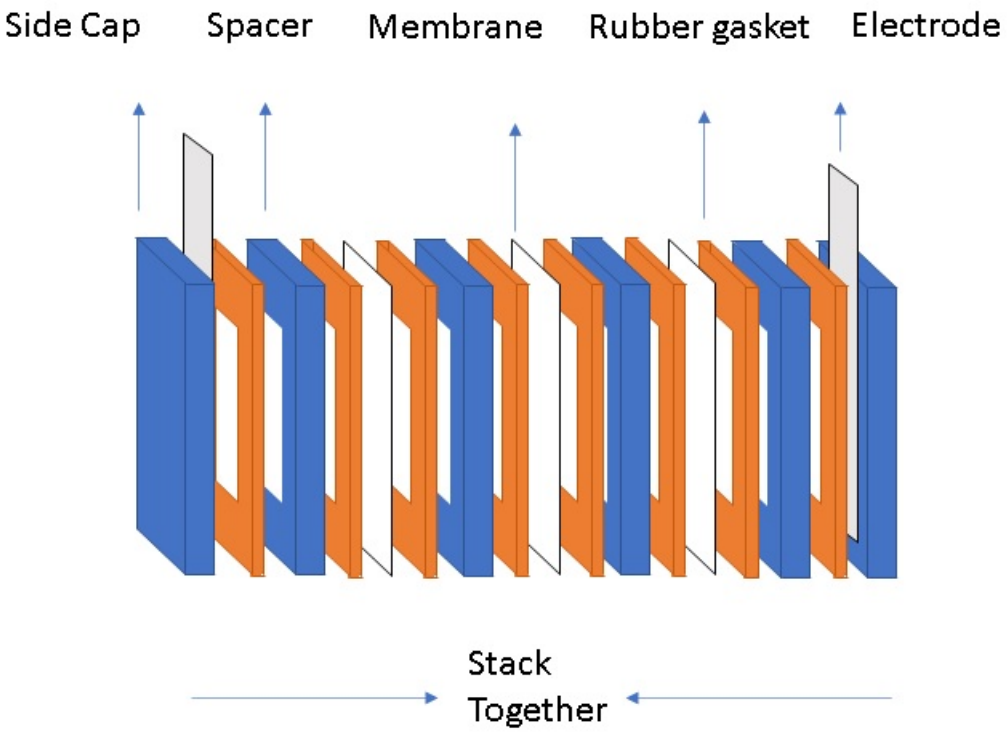


**Figure 9.** Schematics of the electrochemical cell stack structure

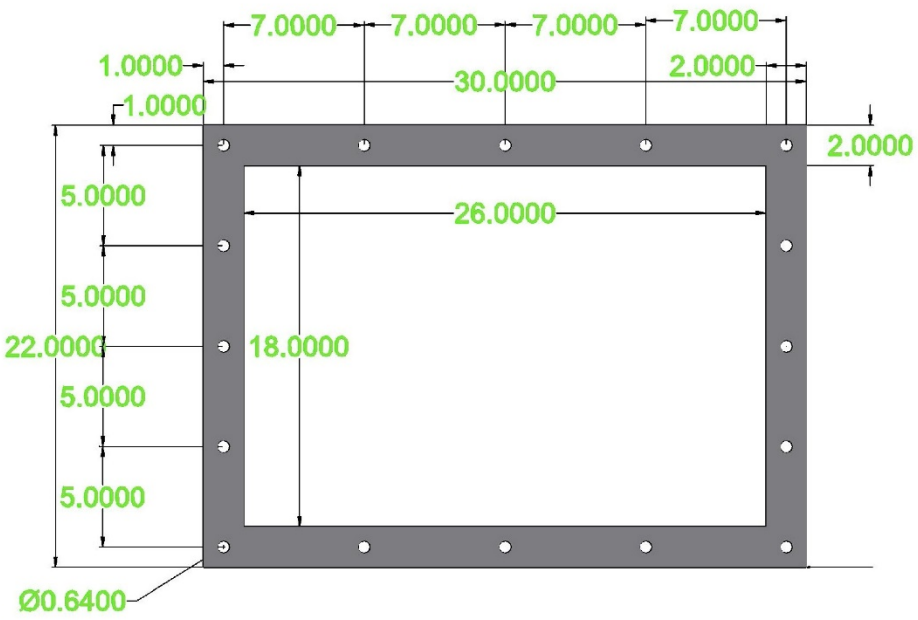


**Figure 10.** Design of Spacer and Rubber Gasket of Electrochemical cell. Unit: cm

## 2.3 Quantification of $CO_2$ Absorption and Desorption Capacity of Different Amines

Simplified schematics of the experimental apparatus are provided in **Figure *11*** with notations of molar flowrate (***J***, *mol* $sec^{-1}$) and $CO_2$ molar fraction (***X***, *dimensionless*) labeled on each stream. Representation of each notation and its properties can be found in **Table 3**.

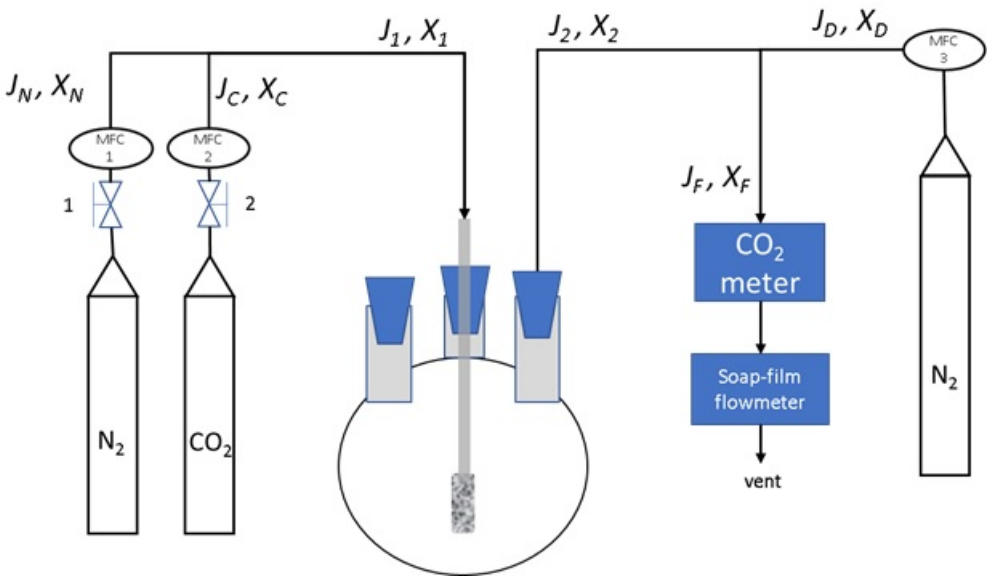


**Figure 11.** Simplified schematics of experiment apparatus with notations on molar flowrate and CO2 fraction

**Table 3.** Notations used in CO2 absorption capacity calculation

| Notation | Representation | Property |
|---|---|---|
| $J_N$ | Molar flowrate of $N_2$ source | Constant, Set by MFC 1 |
| $J_C$ | Molar flowrate of $CO_2$ source | Constant, Set by MFC 2 |
| $J_1$ | Molar flowrate of mixed gases entering boiling bottle | Constant, Sum of $J_N$ and $J_C$ |
| $J_2$ | Molar flowrate of gases exiting boiling bottle | Variable, Function of time |
| $J_D$ | Molar flowrate of Diluent $N_2$ | Constant, Set by MFC 3 |
| $J_F$ | Molar flowrate of gases entering $CO_2$ sensor | Variable, Function of time |
| $X_N$ | Molar fraction of $CO_2$ in $N_2$ source | Constant, Equal to 0 |
| $X_C$ | Molar fraction of $CO_2$ in $CO_2$ source | Constant, Equal to 1 |
| $X_1$ | Molar fraction of $CO_2$ in mixed gases entering boiling bottle | Constant, Determine by ratio of $J_N$ and $J_C$ |
| $X_2$ | Molar fraction of $CO_2$ in gases exiting boiling bottle | Variable, Determine by |
| $X_D$ | Molar fraction of $CO_2$ in Diluent $N_2$ | Constant, Equal to 0 |
| $X_F$ | Molar fraction of $CO_2$ in gases entering $CO_2$ sensor | Variable, Function of time, Measured by a $CO_2$ sensor |

The following equation can describe the amount of $CO_2$ absorbed or desorbed in a specific time *t*.

$$n_{CO_2-Absorbed} = n_{CO_2-in} - n_{CO_2-out} = \int_0^t J_1 X_1 \, dt - \int_0^t J_2 X_2 dt \qquad (12)$$

$n_{CO_2-in}$ and $n_{CO_2-out}$ is the mole of $CO_2$ going in and out of the boiling bottle. Therefore, the subtraction of these two numbers will give us the amount of $CO_2$ absorbed in time *t*. $CO_2$ desorption from the boiling bottle will result in a negative value in equation ( *12* ) $J_1, X_1, J_2$ and $X_2$ cannot be directly measured by $CO_2$ sensor or soap-film flowmeter. Therefore, they need to be substituted with other measurable variables.

To relate $J_2$ and $X_2$ with measurable variables, the following equations are needed.

$$J_2 X_2 = J_F X_F + J_D X_D = J_F X_F \quad (13)$$

Equation ( 13 ) shows the $CO_2$ mole balance in the outlet streams. The $CO_2$ flow rate from the boiling bottle equals the $CO_2$ flow rate that flows into the $CO_2$ sensor. However, $J_F$ cannot be measured in a real time manner, the substitution of $J_F$ with other measurable variables is needed in equation ( 14 ).

$$J_F (1 - X_F) = J_D + J_N \quad (14)$$

Equation ( 14 ) depicts the $N_2$ mole balance of the whole system. Assuming that $N_2$ and $CO_2$ are the only two types of molecules in the systems, the molar fraction of $N_2$ in any stream can be expressed by $(1 - X)$ . With this assumption, $J_F (1 - X_F)$ would be the molar flowrate of $N_2$ flowing into the $CO_2$ sensor. This value is equal to the total supply rate of $N_2$ into the system, $J_D + J_N$, and it is a constant as $N_2$ would not be involved in $CO_2$ absorption or desorption reaction. When we apply equation ( 14 ) to equation ( 13 ) and substitute $J_F$, we get the following equation

$$J_2 X_2 = J_F X_F = (J_D + J_N) \frac{X_F}{1 - X_F} \quad (15)$$

In this equation, $J_D$ and $J_N$ are set by MFC and can be measured in a real-time manner. This equation perfectly relates $J_2 X_2$ with measurable variables. With equation ( 15 ) applied to $n_{CO_2-out} = \int_0^t J_2 X_2 \, dt$, we can acquire the following equation.

$$n_{CO_2-out} = \int_0^t (J_D + J_N) \frac{X_F}{1 - X_F} dt \quad (16)$$

This equation allows us to quantify the amount of $CO_2$ coming out of the boiling bottle by recording $CO_2$ readings on the $CO_2$ sensor in a real-time manner.

On the other hand, $n_{CO_2-in}$ need to be calculated to determine the amount of $CO_2$ supplied. To relate $J_1$ and $X_1$ with measurable variables, the following equations are used.

$$J_1 = J_C + J_N \quad (17)$$

$$J_1 X_1 = J_C X_C + J_N X_N = J_C X_C = J_C \quad (18)$$

Equation ( *17* ) shows the mole balance of gases in all the inlet streams, and it is used to relate $J_1$ with other measurable variables. $J_C$ and $J_N$ and are molar flowrate of the $CO_2$ and $N_2$ from a gas cylinder, and its flow rate can be set by MFC and validated by a soap film flowmeter. Equation ( 18 ) shows the mole balance of $CO_2$ molecules in the same inlet streams. It can be further simplified given that $X_N$ is equal to 0 and $X_C$ is equal to 1. With these two equations applied to $n_{CO_2-in} = \int_0^t J_1 X_1 \, dt$, we can acquire the following equation.

$$n_{CO_2-in} = \int_0^t J_C \, dt \quad (19)$$

We can also acquire $n_{CO_2-in}$ by concentration reading of $CO_2$ sensor before start of absorption experiment. As described in Chapter 2, we need to purge $N_2$ and $CO_2$ mix gas before the start of the absorption experiment, with no amine added to the boiling bottle at that point. Therefore, $n_{CO_2-in}$would equals to $n_{CO_2-out}$ during the purging stage. The following equation can describe the amount of CO2 supplied to the system.

$$n_{CO_2-in} = \int_0^t (J_D + J_N) \frac{X_{Sat}}{1 - X_{Sat}} dt \quad (20)$$

$X_{Sat}$ is the saturation $CO_2$ sensor reading. If we substitute equation ( 12 ) with equation ( 20 ) and ( 16 ), we get the following equation.

$$n_{CO_2-in} - n_{CO_2-out} = (J_D + J_N)\left(\int_0^t \frac{X_{Sat}}{1 - X_{Sat}} dt - \int_0^t \frac{X_F}{1 - X_F} dt\right) \quad (21)$$

This equation quantifies the amount of $CO_2$ absorption and desorption and is derived with several assumptions. First, the nitrogen supply in the system is constant. Second, $CO_2$ and $N_2$ are dominant

species in the gas phase of the system. Therefore, extra care must be taken during the experiments to ensure these two assumptions hold. A Python script based on equation ( *21* ) used for the $CO_2$ quantification is provided in **Appendix *A***.

# Chapter 3 Amine-based Absorbent $CO_2$ Capture Studies

This chapter mainly focuses on understanding the absorption and desorption profile of various amine absorbents. The reaction kinetics and capacity of absorption and desorption are measured. $CO_2$ absorption capacity is measured on different types of amines and $CO_2$ concentration. 3.6M MEA, 0.9M MEA, and 0.9M piperazine are tested for their $CO_2$ loading under various $CO_2$ concentrations. The type of amine and $CO_2$ concentration used can significantly impact the loading capacity of the $CO_2$. For example, the maximum loading of 0.9M piperazine with 5% CO2 is 1.01 mol$CO_2$ molPiperazine$^{-1}$. $CO_2$-loading of 0.9M MEA with the same $CO_2$ concentration is 0.55 mol$CO_2$ mol$MEA^{-1}$. The maximum loading of 3.6M MEA is 0.66 mol$CO_2$ mol$MEA^{-1}$ with 100% $CO_2$. Desorption methods, including temperature swing, acid swing, and a combination of both swings, are tested. $CO_2$ is desorbed from 3.6M MEA by increasing the solution temperature to 80℃ or by hydrochloric acid addition. $CO_2$ can be desorbed with hydrochloric acid addition. The amount of $CO_2$ desorbed is positively correlated to the amount of added acid. ASPEN is used to simulate the absorption and desorption process using an equilibrium-based model. The simulation result is consistent with the experiment data. The study in this chapter is used to establish a baseline of absorption and desorption. We can use the baseline as a reference for comparison with future experiments. The design of the electrochemical amine regeneration system and its operation parameter would be based on the understanding of amine absorption capacity and the proton-driven $CO_2$ desorption.

## 3.1 $CO_2$ Absorption studies in amine absorbents

The absorption capacity of amine solution of different concentrations was tested under different $CO_2$ concentrations using the method described in Chapter 2. 50ml of 0.9M MEA or 0.9M piperazine was placed in the boiling bottle and purged with 5% $CO_2$ with a flowrate of 421

ml/min until amine is fully loaded with $CO_2$. **Figure 12** (a) shows the breakthrough curve of both amines. The absorption capacity of MEA and piperazine are 0.55 mol$CO_2$ mol$MEA^{-1}$ and 1 mol$CO_2$ mol$Piperazine^{-1}$. The breakthrough time for piperazine is significantly higher than MEA. This result is consistent with the fact that piperazine exhibit higher $CO_2$ loading capacity. The rate of $CO_2$ absorption was also quantified during the breakthrough experiment. A similar rate of reaction is found at the start of the absorption. The rate of $CO_2$ determines the initial $CO_2$ absorption rate supplied as the rate of $CO_2$ transport between the gas-liquid interface and amine-$CO_2$ reaction rate is not yet a limiting factor. The rate of $CO_2$ absorption decreases significantly when the $CO_2$ loading of MEA reaches ~0.4mol$CO_2$ mol$MEA^{-1}$. This rate decrease results from the change of the primary absorption mechanism from carbamate formation to carbonate/bicarbonate formation[26]. The $CO_2$ absorption rate of piperazine exhibits a similar trend. The absorption rate starts to decrease when $CO_2$ loading reaches 0.85 mol$CO_2$ mol$Piperazine^{-1}$.

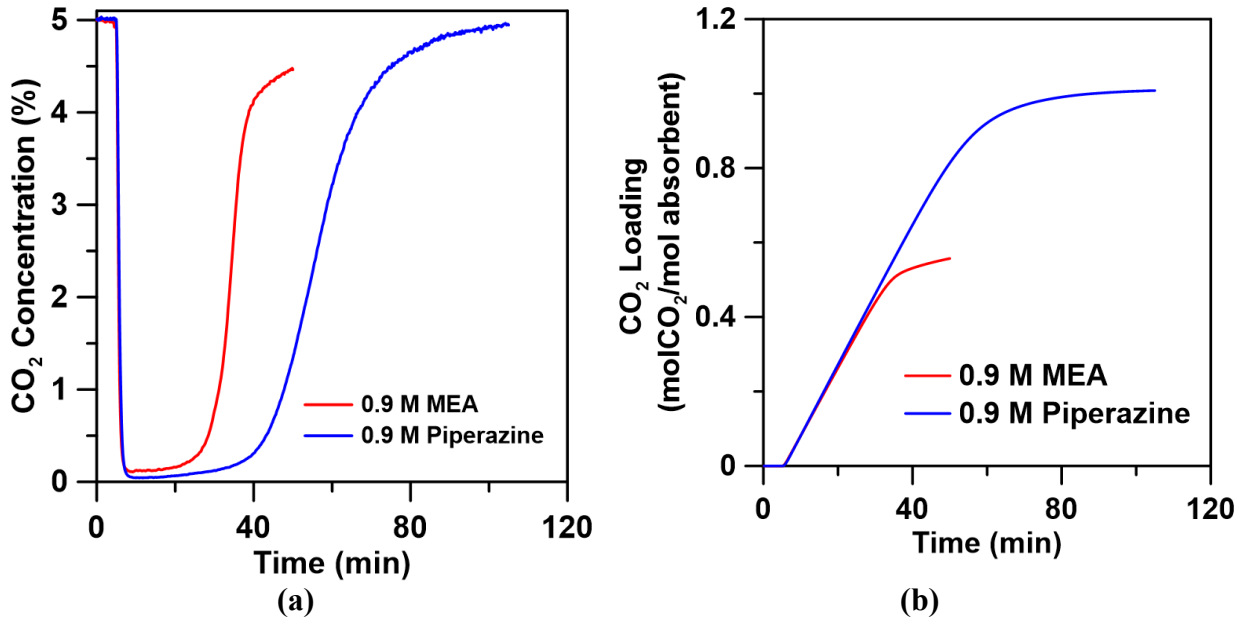


**Figure 12. (a)** The breakthrough curve of 50ml of 0.9M MEA and 0.9M Piperazine with 5% $CO_2$ (flow rate: 421ml/min). **(b)** Cumulative $CO_2$ loading in 0.9M MEA and Piperazine.

3.6M Diethanolamine (DEA), triethanolamine (TEA), monoethanolamine (MEA), 2-ethylaminoethanol, 2-dimethylaminoethanol (2-DMAE) were purged with 5% $CO_2$ at a flow rate of 360 ml/min. Their loading capacity and absorption rate were measured and quantified as described in Chapter 2. 2-Ethylaminoethanol has the highest absorption capacity among the amine tested. The loading capacity of each amine tested is shown in **Table 4**.

**Table 4.** $CO_2$ loading of amines (3.6M, load with 5% $CO_2$)

| Amine | $CO_2$ Loading (mol $CO_2$ mol Absorbent $^{-1}$) |
|---|---|
| Monoethanolamine | 0.51 |
| Diethanolamine | 0.48 |
| Triethanolamine | 0.098 |
| 2-ethylaminoethanol | 0.61 |
| 2-dimethylaminoethanol | 0.45 |

MEA, DEA, and 2-ehylaminoethanol have similar initial $CO_2$ absorption rates; however, they decrease at different rates as the loading of $CO_2$ goes higher. 2-DMAE and TEA have significantly lower absorption rates compared to other amine tested. This result is consistent with the literature that tertiary amine and sterically hindered amines have a slower absorption rate than primary or secondary amines[12,32].

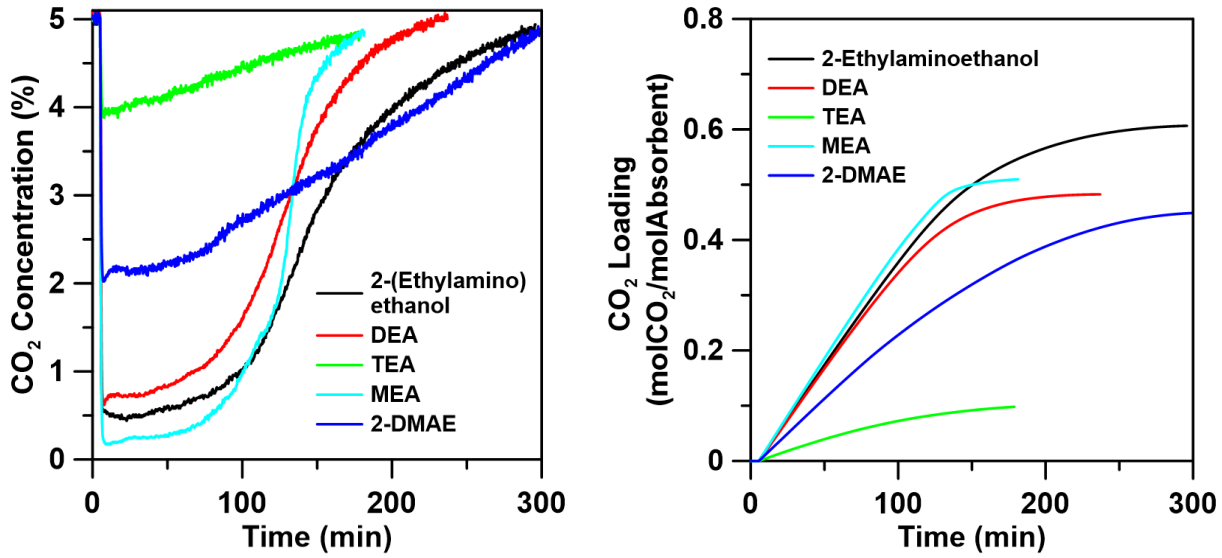


(a) (b)

**Figure 13. (a)** The breakthrough curve of various amines (50ml 3.6M) with 5% $CO_2$ flowrate of 360ml/min. **(b)** Cumulative $CO_2$ loading in various amines (50 ml 3.6M)

Breakthrough experiments were performed on diamines and triamines, including diethylenetriamine (DETA), ethylenediamine (EDA), and piperazine (Pz) (50ml 1.8M), to quantify absorption capacity and absorption rate using 5% $CO_2$ with a flowrate of 366 ml/min. These amines have more than one nitrogen nucleophile in a molecule and exhibit higher loading capacity. For example, the loading capacity of DETA, EDA, and Pz is 1.3 mol $CO_2$ molDETA$^{-1}$, 0.93 mol $CO_2$ molEDA$^{-1}$ and 0.85 mol $CO_2$ molPz$^{-1}$ respectively.

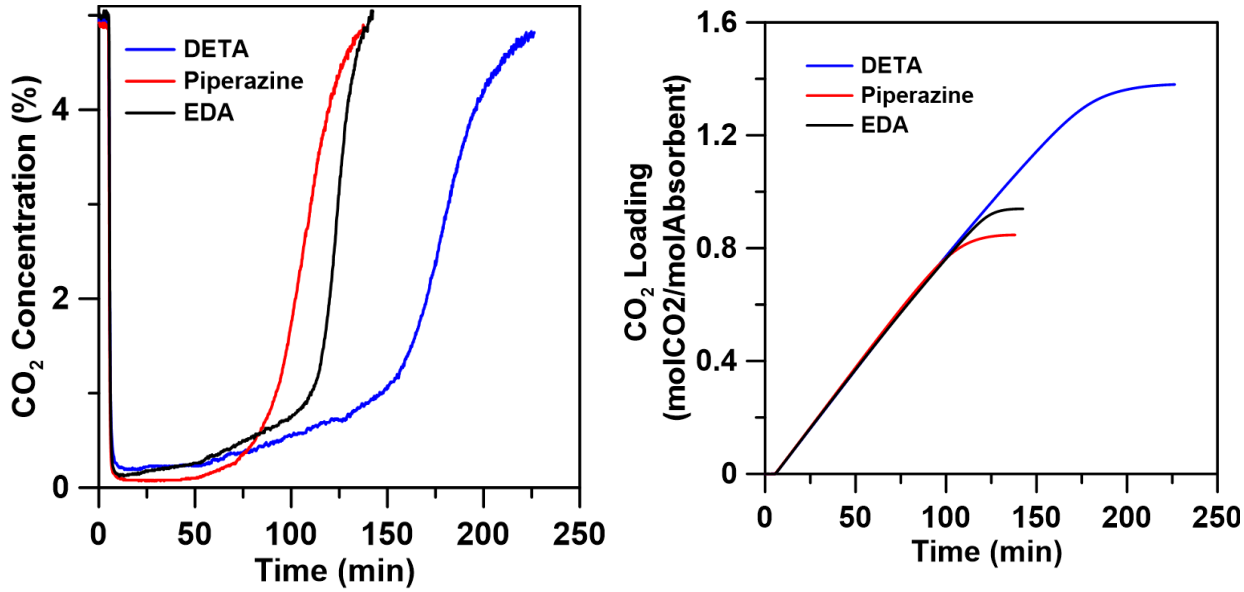


(a) (b)

**Figure 14. (a)** The breakthrough curve of EDA, DETA, and Pz (1.8M) with 5% $CO_2$ of 360ml **(b)** Cumulative $CO_2$ loading of EDA, DETA, and Pz.

## 3.2 $CO_2$ desorption studies by temperature and acid swing

$CO_2$ desorption from amine absorbent can be induced by temperature swing or acid swing of the solution. The following studies were performed to understand the desorption profile and set up a desorption baseline to be the reference for future experiments. First, a 100ml 3.6M MEA solution was loaded with $CO_2$ until the $CO_2$ loading reached 0.485mol$CO_2$ mol$MEA^{-1}$. Next, the $CO_2$-loaded MEA solution was split into two 50 ml aliquots. One aliquot was immersed in a water bath of 40, 60, and 80 ℃ for 1 hour. The other aliquot of loaded MEA was mixed with 50mmol HCl and then immersed in a water bath in the same manner. The amount of $CO_2$ desorption was quantified using the method described in **Chapter 2**. **Figure 15** shows the $CO_2$ desorption profile of $CO_2$ under the acid swing and temperature swing ($N_2$ flow rate: 444ml/min). **Figure 16** shows the cumulative extent of desorption of the desorption process. Cumulative $CO_2$ desorption (%) is calculated by the ratio of the amount of $CO_2$ desorbed and $CO_2$ loading of loaded amine.

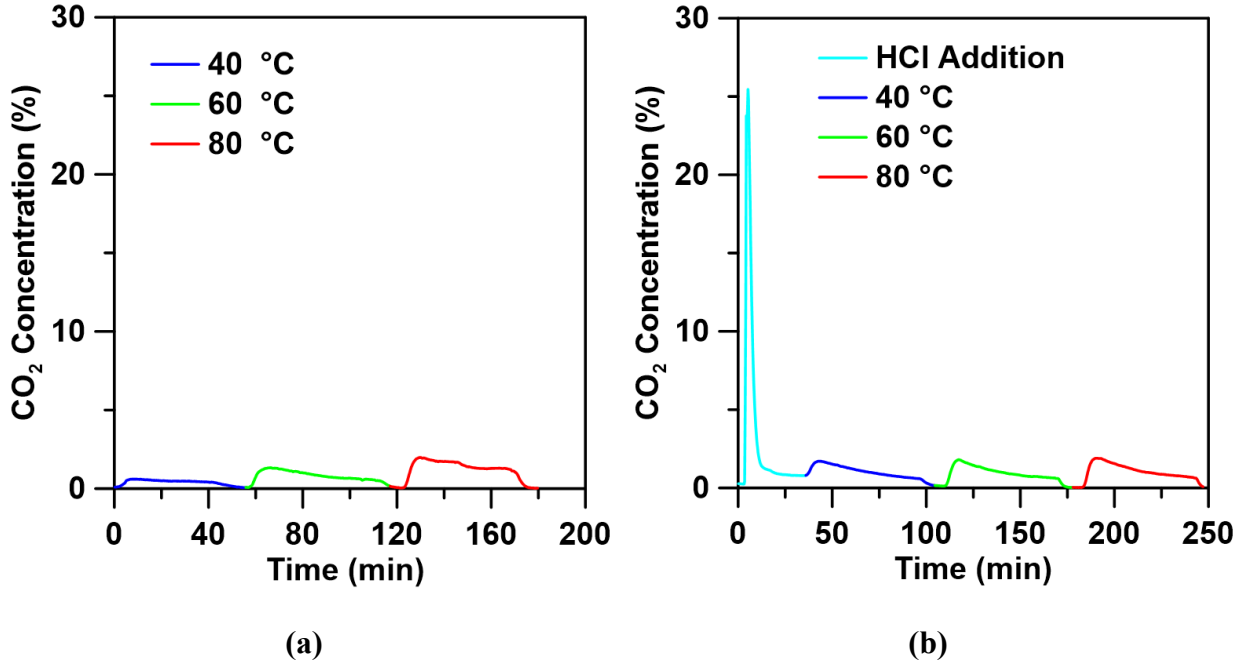


**Figure 15. (a)** Desorption profile of 50ml 3.6M MEA (50ml, 3.6M, loading: 0.485 mol$CO_2$ mol$MEA^{-1}$) under temperature swing (40, 60 and 80 ℃) **(b)** Desorption profile of MEA (50ml, 3.6M, loading: 485 mol$CO_2$ mol$MEA^{-1}$) under acid swing (50 mmol HCl) and subsequent temperature swing (40, 60 and 80 ℃).

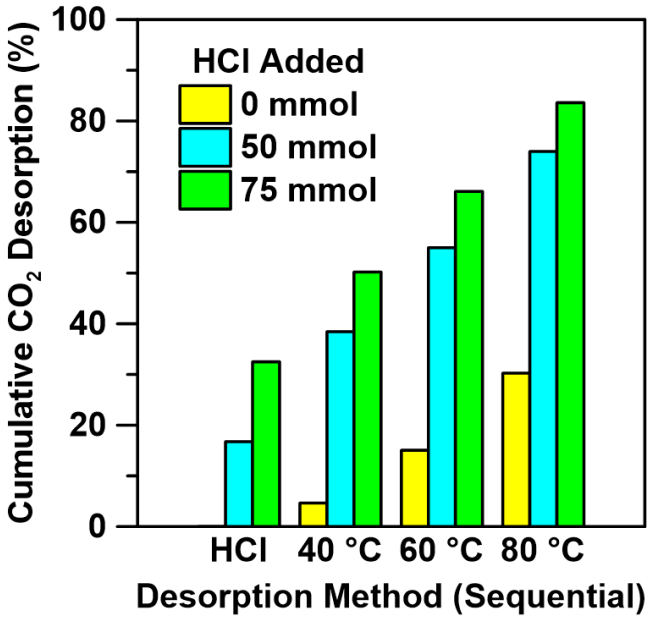


**Figure 16.** Cumulative $CO_2$ desorption from loaded MEA solution. (Loading: 0.485mol $CO_2$ mol$MEA^{-1}$)

**Figure 15** (a) shows a higher peak $CO_2$ concentration when the loaded amine solution is immersed in a water bath of higher temperature. The peak concentration is ~ 2% when the amine is immersed in 80 ℃, while the peak $CO_2$ concentration is 0.6% when immersed in a 40 ℃ water bath. This result validates that the rate of $CO_2$ desorption induced by temperature swings increases with the increase of water bath temperature. On the other hand, the rate of $CO_2$ desorption induced by acid addition is significantly higher than that of $CO_2$ desorption induced by temperature swing. Instant $CO_2$ desorption can be observed after adding 50mmol HCl into the loaded amine, as shown in **Figure 15** (b). The peak $CO_2$ concentration is ~25% with acid addition, while less than ~2% when desorption is induced by a temperature swing at 80℃. The desorption rate is more than ten times higher when induced by acid than that induced by temperature swing. In addition, HCl addition can induce $CO_2$ desorption from MEA. It can also facilitate $CO_2$ desorption for subsequent temperature swings, especially at low temperatures.

**Table 5** shows the $CO_2$ desorption % of each desorption step. Without acid swing, only 4.65% of loaded $CO_2$ can be desorbed from MEA solution at 40 ℃. However, 21.69% of loaded $CO_2$ can be desorbed from MEA solution at 40 ℃ if 50 mmol HCl is added before the temperature swing. A similar desorption profile is observed when more HCl is used for desorption (75 mmol). These results show that acid addition to the loaded MEA solution can induce not only $CO_2$ desorption but also catalyze temperature-induced $CO_2$ desorption. Therefore, the heat requirement for $CO_2$ desorption can be reduced with acid addition into amine absorbent. This result is consistent with recent studies where organic acids are used[61–63].

**Table 5.** Percentage of $CO_2$ desorption from loaded MEA solution

| Desorption Method | 0 mol HCl | 50 mmol HCl | 75 mmol HCl |
|---|---|---|---|
| HCl Addition @ 20 ℃ | 0 % | 16.75 % | 32.5 % |
| 40 °C / 1hr | 4.65 % | 21.69 % | 17.7 % |
| 60 °C / 1hr | 10.4 % | 16.57 % | 15.9 % |
| 80 °C / 1hr | 15.2 % | 18.97 % | 17.5 % |

To understand if 100% of $CO_2$ desorption can be achievable without temperature swing, excessive HCl was added to the loaded MEA solution. 5ml of 5M HCl was added to 50ml 3.6M MEA (Loading: (1) 0.25 mol$CO_2$ mol$MEA^{-1}$ (2) 0.5 mol$CO_2$ mol$MEA^{-1}$) solution every 10-15 min in the boiling bottle and $CO_2$ desorption is measured as described in Chapter 2. Cumulative $CO_2$ desorption amounts from 3.6M MEA solution at various loading are shown in **Figure 17 (a)**. This data proves that 100% of $CO_2$ desorption can be achieved with acid addition only under ambient temperature. Proton to MEA ratio of 1: 1 is required for complete $CO_2$ desorption regardless of the initial loading of MEA solution. Although the proton requirement for complete $CO_2$ desorption is similar among amines with different loading, the $CO_2$ desorption profiles differ. $CO_2$ does not desorb at a low loading at a low proton to MEA ratio. Only 0.43 % of $CO_2$ was desorbed from MEA (loading: 0.25 mol$CO_2$ mol$MEA^{-1}$) at a proton to MEA ratio of 0.14. Similarly, 8.78 % of $CO_2$ is desorbed from MEA (loading: 0.5 mol$CO_2$ mol$MEA^{-1}$) at the same proton to MEA ratio. If the $CO_2$ desorbed is compared on a mol$CO_2$ mol$MEA^{-1}$ basis, the difference between the amount of $CO_2$ desorbed is even more apparent. 0.9M piperazine solution is tested similarly, and similar results are acquired (**Appendix *B***).

$CO_2$ desorption was verified by IR spectrum of the amine solutions at various pH, and the IR spectrum of loaded-MEA and acidified MEA is shown in **Figure *17* (b)**. The carbamate peaks (1486 $cm^{-1}$, 1568 $cm^{-1}$, and 1320 $cm^{-1}$ [64]) gradually disappear with decreasing pH. Furthermore, at low pH (pH = 1.86), a peak at 1517 $cm^{-1}$ indicates the presence of protonated amine molecules.

The IR spectrum remains unchanged as pH decreases further (i.e., from 6.0 to 1.8), indicating near complete carbamate decomposition/$CO_2$ desorption. This observation is consistent with the data shown in **Figure 17 (a),** where>80% desorption is achieved at pH = 6 for a $CO_2$-rich amine solution with initial 0.5 mol $CO_2$ per mol MEA loadings.

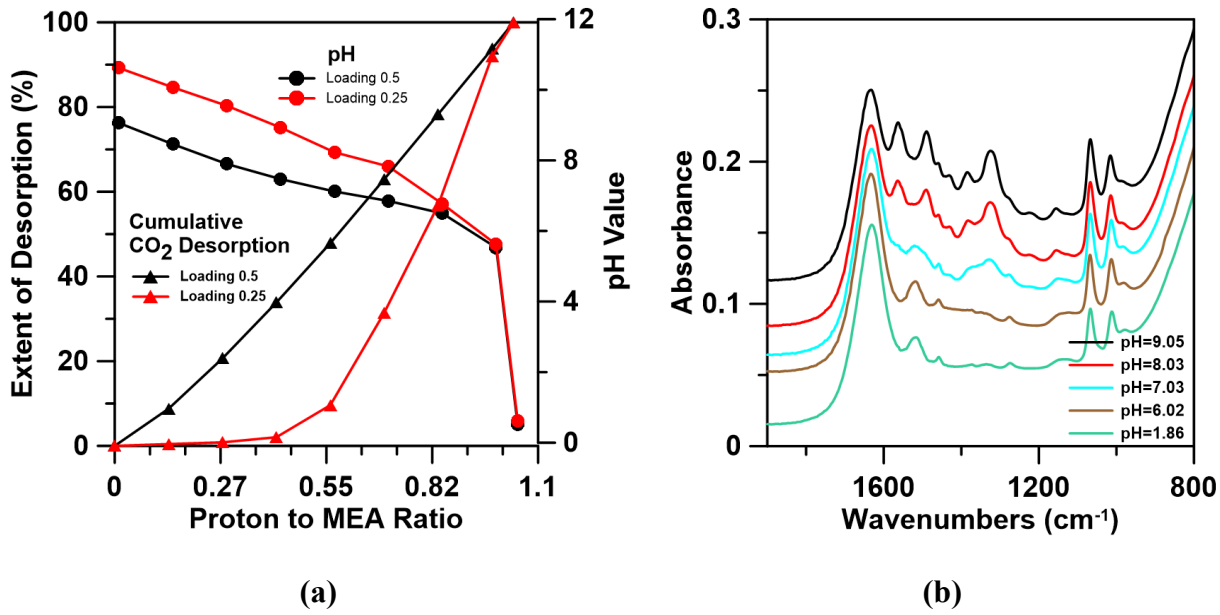


**Figure 17. (a)** Desorption profile of proton-induced $CO_2$ desorption from loaded MEA of various $CO_2$ loading (unit: mol $CO_2$ mol$MEA^{-1}$). **(b)** IR-spectrum of loaded MEA and acidified MEA.

## 3.3 ASPEN Simulation on $CO_2$ absorption and desorption

A simple ASPEN model simulates absorption and desorption by temperature and acid swing. The schematics of the simulation module used are shown in **Figure 18**. The simulation was performed using two adiabatic flash tanks under a vapor-liquid equilibrium-based model. In this simulation, the flow rate of $CO_2$ is set to be 1kmol $CO_2$/hour in FLUGAS stream, and the flow rate of the MEA stream is set to 3kmol MEA/hour. Under this setup, 90% of $CO_2$ is stripped from FLUGAS, and the $CO_2$ flow rate in STRIPFLU is 0.1kmol$CO_2$/hour. Absorbed $CO_2$ is in

carbamate from in LOADMEA stream with a flow rate of 0.9kmol$MEACOO^-$/hour. $CO_2$ desorption using a temperature and acid swing combination is simulated by the parameter set described in **Table 6**.

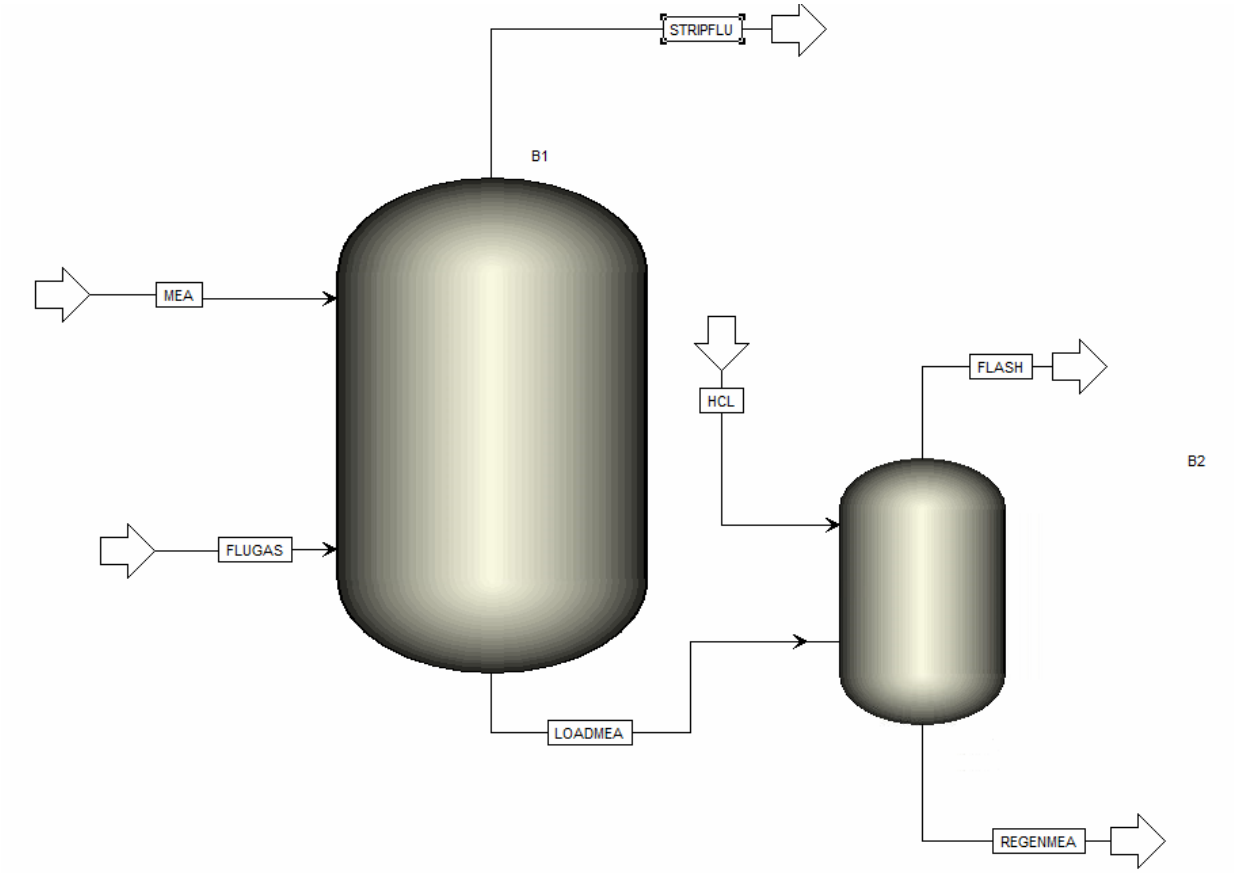


**Figure 18.** Schematics of ASPEN simulation modules.

**Table 6.** Parameter of ASPEN simulation on $CO_2$ with temperature swing

| **Unit** | Equilibrium Parameter | Setting |
|---|---|---|
| Flash tank 1 | Temperature | 20 ℃ |
| | Pressure | 1 atm |
| | Duty | 0 kJ/hour |
| Flash tank 2 | Temperature | 40-140 ℃ |
| | Pressure | 1atm |
| | Duty | 0 kJ/hour |
| **Stream** | **Composition** | **Flowrate** |
| MEA | 30 % MEA | 3kmol MEA /hour |
| FLUGAS | 15 % $CO_2$ | 1kmol $CO_2$/hour |
| HCL | 5% HCl | 0-3kmolHCl/hour |

**Figure 19** shows the simulation result of the flow rate and the composition of REGENMEA and FLASH stream at the outlet of flash tank 2. **Figure 19 (a)** shows the composition and flow rate change in REGENMEA stream at an HCl to MEA ratio of 0 to 1 (without HCl addition). At a temperature below 100 ℃, no $CO_2$ can be found in FLASH stream. $CO_2$ start to desorb when the temperature reaches 110 ℃, as shown by the increase of $CO_2$ flow rate in FLASH stream and decrease of $MEACOO^-$ flow rate in REGENMEA stream. The amount of MEA increase indicates the amine is regenerated when temperature increases. A minimal amount of bicarbonate and protonated MEA are found. However, when the temperature is higher than 120 ℃, loss of MEA occurs. MEA started to evaporate and leave the tank as a gas phase component (FLASH stream). At 140 ℃, 1.32 kmol/hour of MEA is lost from FLASH stream. This solvent loss is not desired as it would increase the operation cost for the $CO_2$ capture process. In addition, only 0.69 kmol/hour of $CO_2$ exits Flash tank 2 from FLASH stream at 140 ℃, while the amount of carbamate input from LOADMEA stream is 0.9 kmol/hour. This result indicates that $CO_2$ is not fully desorbed even when loss of absorbent occurs.

**Figure *19*** (b) shows the composition and flow rate of REGENMEA stream with an HCl to MEA ratio of 0.33 to 1. With HCl addition, the molar flow rate of protonated MEA increases to 1.9kmol/hour at 40 ℃. Carbamate flow rate does not change as no $CO_2$ is desorbed at 40 ℃ under this HCl to MEA ratio. With the temperature increase, $CO_2$ starts to desorb when the temperature reaches 90 ℃, which is 20 ℃ lower than the amine without acid addition. This result indicates that HCl addition facilitates $CO_2$ desorption at a lower temperature. At an even higher HCl to MEA ratio, $CO_2$ can desorb without heating, as shown in Figures (c) and (d).

Furthermore, it is shown in **Figure *19*** (d) that all loaded $CO_2$ is desorbed at 40 ℃ with HCl to MEA ratio of 1: 1. Temperature swing is not needed for $CO_2$ desorption at this HCl to MEA ratio. Although HCl addition can facilitate CO2 desorption or allow for complete CO2 desorption without any heating, it has a drawback concerning MEA regeneration. HCl addition to the $CO_2$ absorbent, facilitates the formation of protonated amine, which cannot absorb the $CO_2$. Therefore, bases need to be added to protonated amine to neutralize the proton added and convert protonated amine into a non-protonated form.

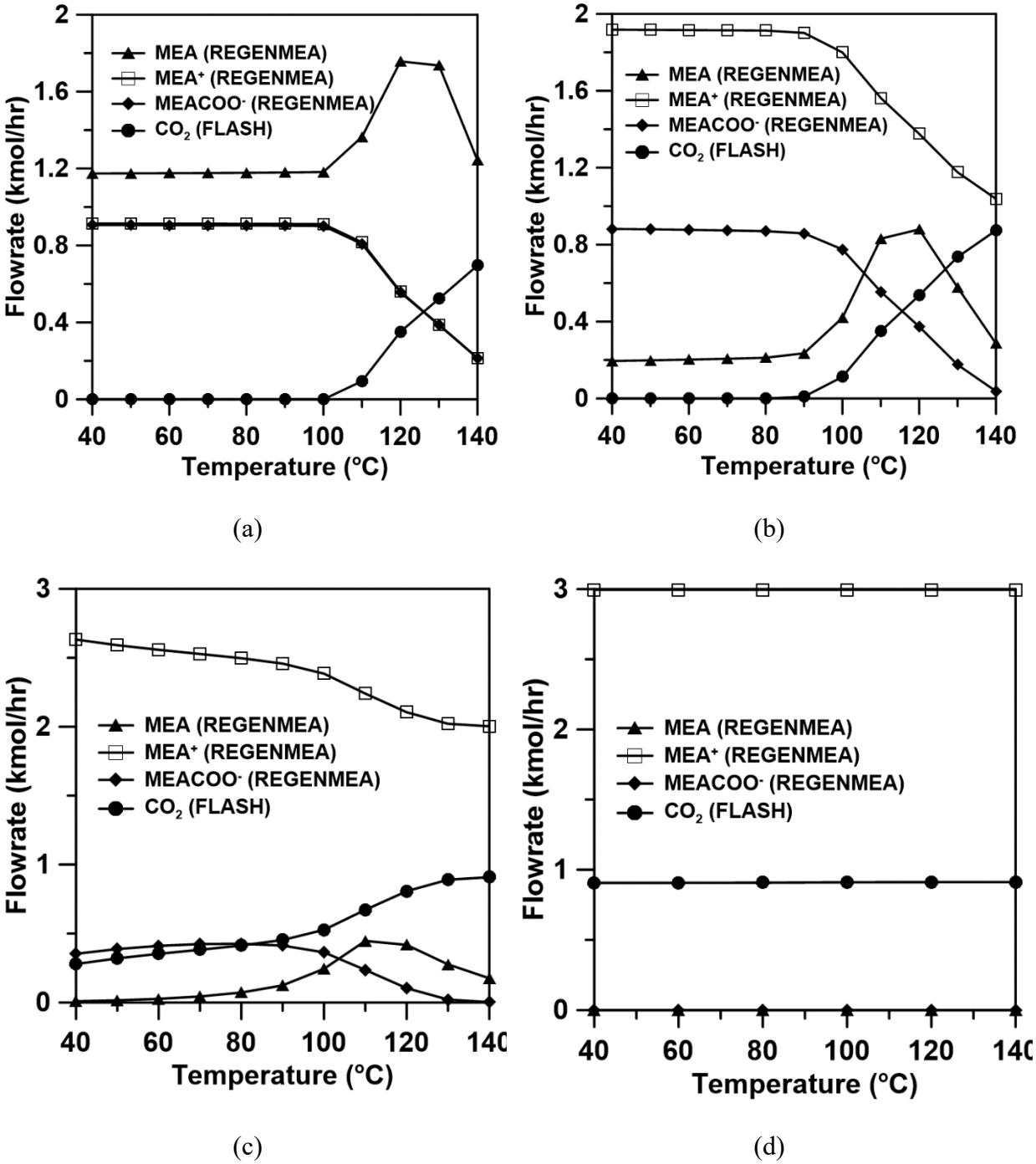


**Figure 19.** Composition and flow rate of REGENMEA and FLASH stream at different HCl to MEA ratio. **(a)** 0:1 **(b)** 0.33: 1 **(c)** 0.66: 1 **(d)** 1:1

# Chapter 4 Development of Electrochemical Amine Regeneration System

## 4.1 Studies on the feasibility of acid-base swing amine regeneration

To understand the feasibility of acid- and base-swing as an amine regeneration method, several experiments need to be done to understand the amine property after acid-base swing regeneration. First, absorption capacity and rate were measured to validate that no decrease in these two parameters occurred after the acid-base swing. Then, fresh MEA, acid-added MEA, and acid and base-added MEA were purged with 5% $CO_2$ until saturation. The acid-added MEA is prepared by adding 15mmol HCl (5M 3ml) to 50 ml 0.9M MEA solution. Subsequently, 15 mmol of NaOH is added to the acid-added MEA to prepare acid-base-added MEA. The loading capacity and rate of absorption of these amine samples are shown in **Figure 20.** It is shown that HCl addition to MEA can reduce the loading capacity to 0.375 mol$CO_2$ mol$MEA^{-1}$. This result from HCl converting MEA into protonated form, and protonated MEA cannot absorb $CO_2$. However, this loss of capacity is not permanent, and the capacity can be restored by NaOH addition. The acid-base-added MEA solution has a similar capacity to that of fresh MEA (~0.54mol$CO_2$ mol$MEA^{-1}$). In addition, the rate of $CO_2$ absorption is not changed after acid and base addition. In summary, the absorption capacity and absorption rate are not changed after acid and base addition. This result shows that acid-base swing can serve as an amine regeneration method without the concern of loss of capacity and rate of absorption.

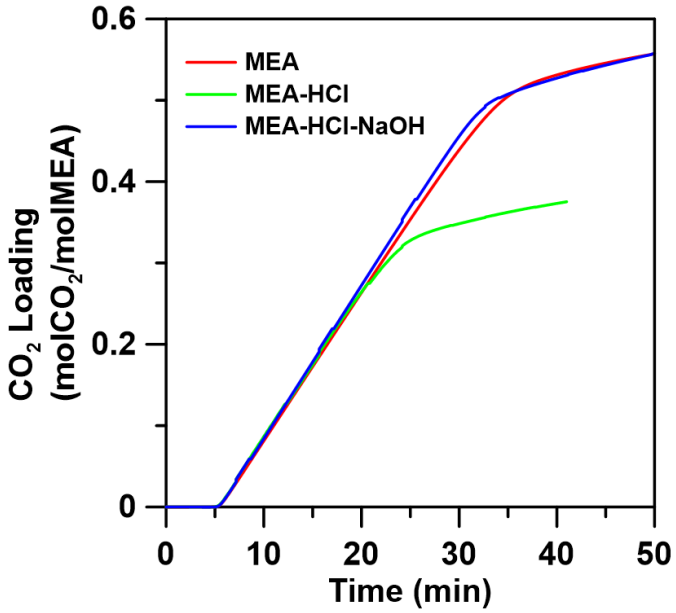


**Figure 20.** $CO_2$ absorption of 50ml 0.9M MEA solution with different acid-base treatment under 5% $CO_2$ (384 ml $min^{-1}$).

A similar validation process was also performed on $CO_2$-loaded MEA. $CO_2$-rich MEA solutions (0.5 mol $CO_2$ per mol MEA) were acidified with 5 M HCl to different pH values (pH = 6, 7, and 8) to achieve different extents of desorption. Subsequently, stoichiometric amounts of NaOH (to neutralize the added protons) were added to the acidified MEA, and the capacity of these solutions was quantified via the method described in Chapter 2. **Figure 21 (a)** shows that the extent of $CO_2$ reabsorption (compared to the maximum $CO_2$ loading) increases as the extent of the pH swing increases, indicating that NaOH addition can facilitate the conversion of protonated MEA to non-protonated MEA, thereby restoring absorption capacity. The absorption of $CO_2$ by hydroxides at corresponding pH is negligible as quantified by $CO_2$ absorption experiments in aqueous solutions of NaOH (See **Appendix B Figure 49**). This data validates that the reabsorption capacity results from mainly regenerated MEA, not from the alkalinity of the hydroxides. IR analysis of the solutions is shown in **Figure 21 (b).** It shows that the intensity of the peak at 1517 $cm^{-1}$ decreased while the peak at 955 $cm^{-1}$ increased, indicating the disappearance of protonated

MEA and the formation of MEA. These results demonstrate the required pH swing necessary to desorb >80% of $CO_2$ from a rich amine solution for subsequent absorption cycles.

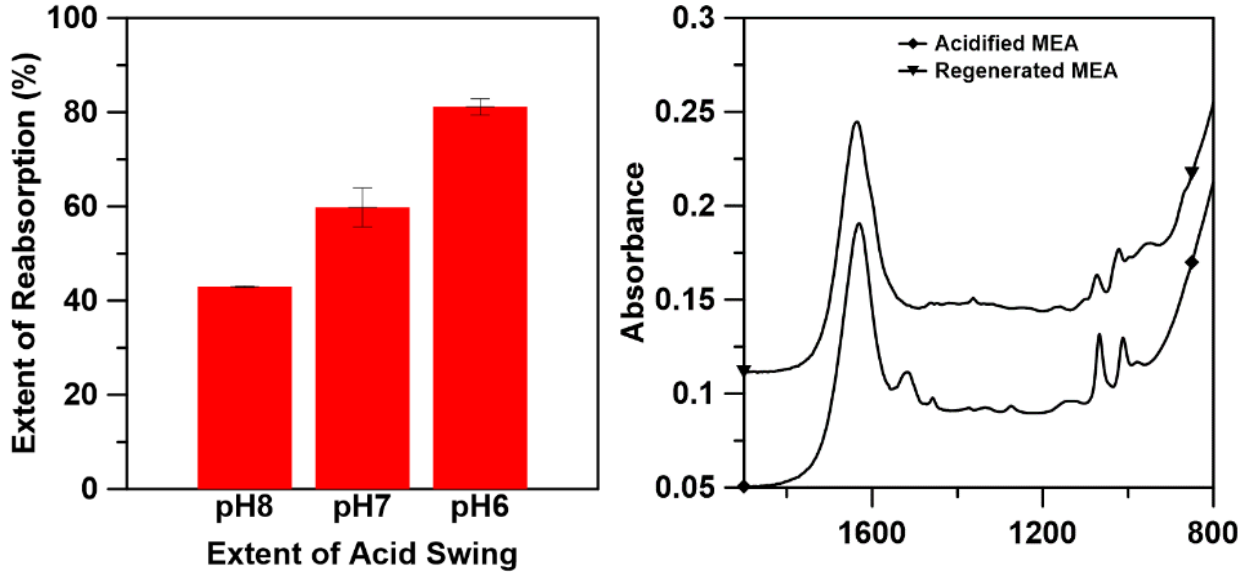


(a) (b)

**Figure 21. (a)** Reabsorption extents of MEA solutions for various pH swing cycles (b) IR spectrum of Acidified MEA and regenerated MEA.

## 4.2 Development of electrochemical acid swing cell

### 4.2.1 Two-compartment acid swing cells

Water electrolysis reaction is used to generate proton used for amine acid swing. Two-compartment-based cell design is shown in **Figure 22 (a).** One cation exchange membrane separates the cell into two compartments in this design. Pt is used as the cathode, and 316 stainless steel is used as the cathode. The proton will be generated at the anode and decrease the pH of the solution at the anodic compartment. Therefore, the MEA solution must be placed in the anodic compartment to perform an electrochemical acid swing. However, this design is not optimal for several reasons.

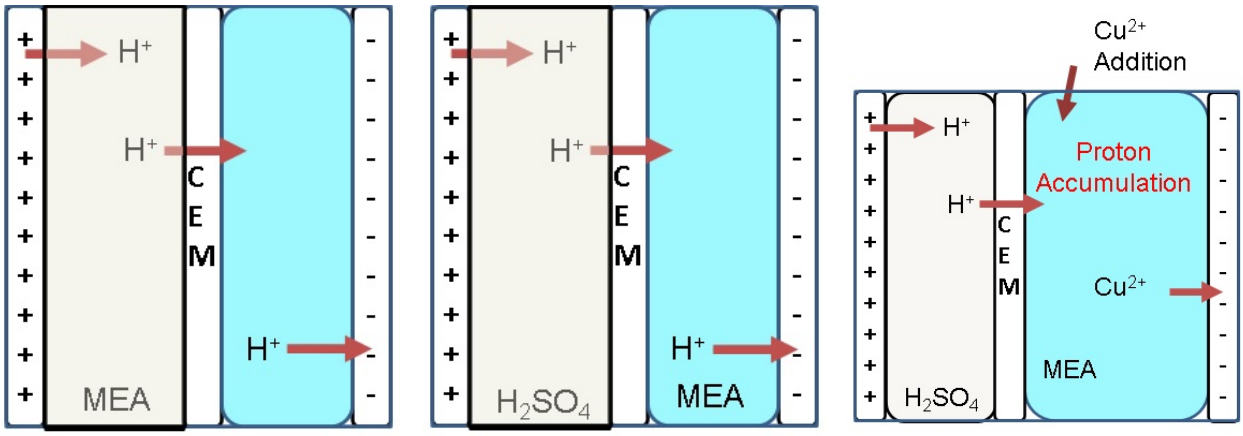


**(a)** **(b)** **(c)**

**Figure 22.** Schematics of a two-compartment electrochemical cell for the acid swing of MEA solution **(a)** MEA placed in the anodic compartment. **(b)** MEA was placed in the cathodic compartment. **(b)** MEA placed in the cathodic compartment with copper (II) ion added

First, MEA can be oxidized at the anode[65]. In **Figure 23**, it is shown that an oxidative wave appears at -0.3 to 0.1 V during the positive scan, resulting from the formation of polyalcohols and ketoses[66]. Water oxidation occurs at V > 0.6 and is associated with a peak around 0.6V. This result demonstrates that MEA oxidation can occur at a voltage lower than that required for oxygen evolution. As a result, MEA oxidation reaction would be prioritized over oxygen evolution reaction if MEA solution is placed in an anodic compartment. Therefore, the electrochemical cell design in **Figure 22 (a)** is not optimal as it leads to severe MEA degradation. The cell configuration needs to be modified to prevent MEA oxidation.

**Figure 22 (b)** shows the modified cell configuration that segregates MEA from the anode to prevent oxidation of MEA. In this configuration, 1M $H_2SO_4$ is placed in the anodic compartment, and MEA solution is placed in the cathodic compartment. The dominant reaction at the anode would be water oxidation without the presence of MEA. This design ensures the generation of protons and prevents MEA oxidation. Proton generated at the anode can migrate through the cation exchange membrane and reaches the cathodic compartment to acidify the MEA solution. However,

the reaction that occurred at the cathode limits the acid swing of the MEA solution. The dominant reaction at the cathode is either proton consumption or water reduction, depending on the pH of the cathodic solution. Protons that migrate through the cathode compartment can be consumed or neutralized by the hydroxide generated at the cathode. Therefore, the modified configuration cannot be used for MEA acid swing.

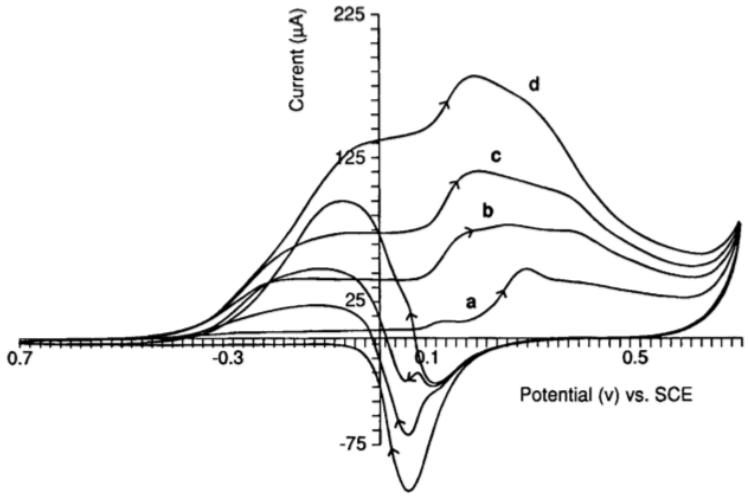


**Figure 23.** Voltametric response of monoethanolamine as a function of concentration at the Au RDE in $O_2$-free 0.1 M NaOH. Rotation speed: 500 rev $min^{-1}$. Scan rate: 5.0 V min-'. Conc. (mM): (a) 0.00, (b) 0.10, (c) 0.20, (d) 0.40. [65]

The two-compartment cell is modified to tackle the undesired proton consuming and hydroxide generating reactions. First, copper nitrate is added to the cathodic compartment's MEA solution, as shown in **Figure *22*** (c). The presence of copper (II) ions in the cathodic compartment change the dominant cathode reaction. **Table 7** lists the potential reactions that can occur at the cathode after adding copper ion to the cathode compartment.

**Table 7.** Cathodic Reactions

| | | | |
|---|---|---|---|
| $Cu^{2+} + 2e^-$ | → | $Cu$ | V= + 0.337 |
| $2H^+ + 2e^-$ | → | $H_2$ | V = 0.00 |
| $2H_2O + 2e^-$ | → | $H_2 + 2OH^-$ | V = -0.8277 |

It is shown that copper reduction exhibits higher reduction potential, indicating that copper plating on the cathode would be the preferred reaction in a solution containing copper ion, water, and proton. Therefore, adding copper ions to the MEA solution at the cathode compartment could reduce proton consumption or hydroxide generation, as shown in Figure 22 (c). This fact allows for the accumulation of proton at the cathode compartment, and acid swing of MEA solution can potentially be done. An electrochemical amine regeneration system for $CO_2$ capture is designed based on this cell configuration, and the system is shown in **Figure *24***.

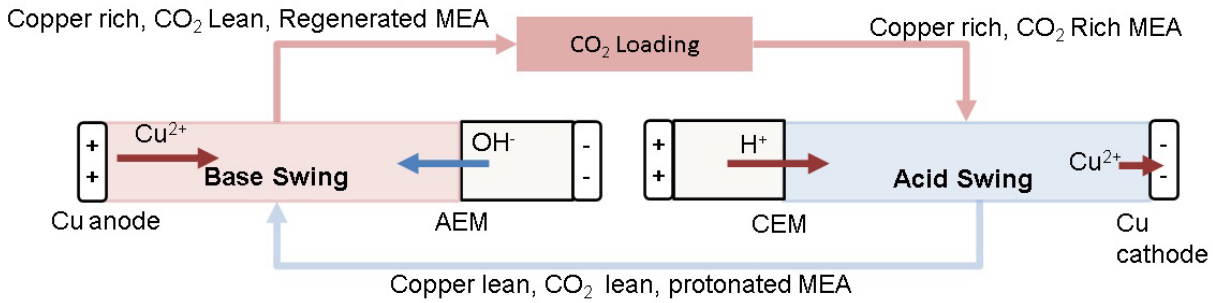


**Figure 24.** Electrochemical amine regeneration system for $CO_2$ capture with two-compartment electrochemical cell

$CO_2$ is loaded to MEA at a $CO_2$ loading unit, and $CO_2$-rich MEA is transported to an acid swing cell for $CO_2$ desorption. In the acid swing cell, proton generated by anode migrates through CEM, and copper ion is reduced and plate on the cathode of the acid swing cell. Protonated MEA is formed in the acid swing cell, along with the desorption of $CO_2$ and reduction of copper ions. The copper lean, $CO_2$ lean protonated MEA solution is transported into the base swing cell for amine regeneration. In the base swing cell, hydroxide is generated from cathode transport through

the AEM while the copper anode is oxidized, releasing copper (II) ion into the base swing cell. The protonated amine will be regenerated into a non-protonated form by the hydroxide generated. The copper (II) ion rich, $CO_2$ lean regenerated MEA is then transported into the $CO_2$ absorption unit for $CO_2$ capture and starts the following $CO_2$ capture & amine regeneration cycle. This design expected that a non-negligible amount of copper ion would be present in regenerated amine. Therefore, we must examine whether copper ions do not change the $CO_2$ absorption properties of MEA.

To measure the $CO_2$ absorption characteristic of MEA in the presence of copper (II) ion, 5 mmol or 25 mmol of copper nitrate was added to MEA (50ml, 3.6M), and 40ml of 100% $CO_2$ was used to purge the MEA for absorption. $CO_2$ absorption capacity and rate of absorption were measured. **Figure 25** shows that the $CO_2$ absorption capacity drops significantly with copper addition. This capacity loss is a result of the fact that MEA and cupper can form a complex and decrease the absorption capacity of MEA and facilitate $CO_2$ desorption from MEA[67]. This result indicates that the proton and copper ion exhibit the same functions as they can decrease absorption capacity and facilitate $CO_2$ desorption. This property is not desired for the amine regeneration system as copper presented in regenerated amine decreases the absorption capacity. In addition, the $CO_2$ desorption triggered by the acid swing cell will not be effective as the acid swing cell exchange the copper in MEA solution with the proton. Therefore, there would be no change in the amount of $CO_2$ desorption stimulant ($H^+$ and $Cu^{2+}$), and acid swing cells will not effectively desorb $CO_2$.

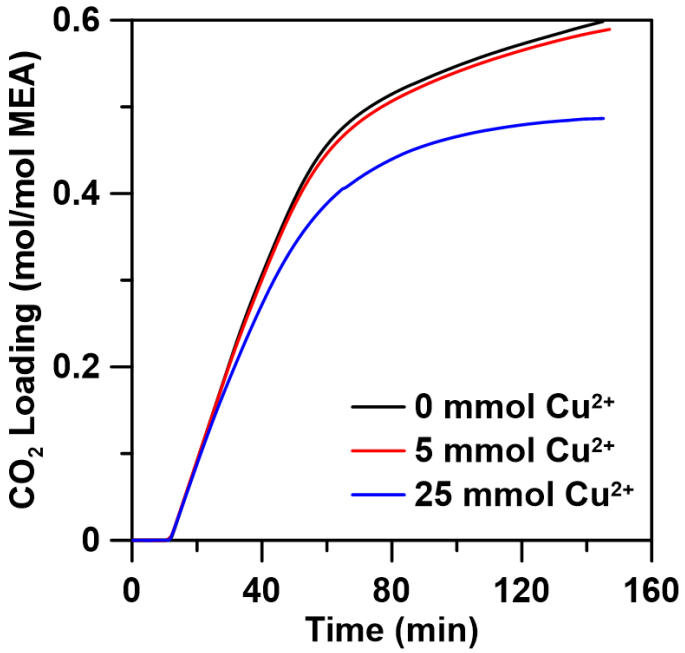


**Figure 25.** Cumulative $CO_2$ absorption in MEA solution (3.6M 50mol) with copper nitrate addition (100% $CO_2$, 40ml/min)

There are several pathways to tackle this issue. First, substitute copper (II) ion with other metal ions that do not complex with MEA to avoid capacity loss of MEA. Alternatively, an amine absorbent that does not complex with copper (II) ion can be used. Third, simply segregate MEA from copper ion using another ion exchange membrane. One of these three methods can tackle the MEA capacity loss resulting from copper (II) ion addition.

However, the first two methods are not realistic solutions. First, almost all metal ions can be complex with amine species[68]. These metal ions will include but are not limited to cobalt (III)[69], Nickel (II)[70], and silver(I)[71]. Therefore, it is nearly impossible to have a metal ion that meets the requirement described in the first solution. The second solution is also a challenging method to go for, as most amines can coordinate with copper and form a complex. Studies have shown that various amines commonly used for $CO_2$ capture can coordinate with copper (II) ions. These amines will include but are not limited to MEA[67], DEA[72], TEA[72], piperazine[73], and ethylenediamine

(EDA)[74]. Adding an extra ion exchange membrane to segregate copper ions and MEA would be the most feasible solution. Therefore, a three-compartment electrochemical cell is designed and built.

### 4.2.2 Three-compartment acid swing cell

The three-compartment cell is made by adding one more cation exchange membrane to the two-compartment cell shown in **Figure 22 (c)**, separating the cathodic compartment into a bridge and cathodic compartment. The schematic of the three-compartment cell is shown in **Figure 26**. The three compartments are the anode compartment, bridge compartment, and cathode compartment. In this design, the MEA solution is placed in the bridge compartment. A cation exchange membrane separates MEA from the anode to prevent anodic oxidation. Acid swing is expected to be done in the bridge compartment with this three-compartment cell design. The acid swing capability of this three-compartment cell design (**Figure 26**) is tested with the following experiments.

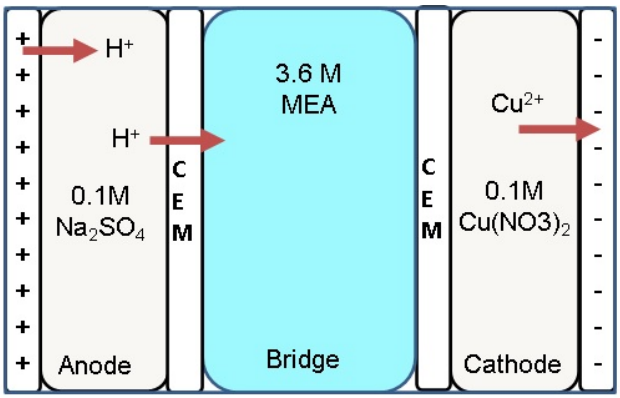


**Figure 26.** Schematic of a three-compartment electrochemical cell with two CEMs. Buffers in each compartment can be changed as required for different experiments.

First, the hypothesis was tested that copper ions in the cathode compartment can decrease proton consumption and hydroxide generation. 0.1M $Na_2SO_4$ solution was placed in the anode

compartment, and 0.1M NaCl was placed in the bridge compartment. Next, two different cathodic solutions were tested in the cathodic compartment. 0.1M NaCl and 0.1M $Cu(NO_3)_2$ solutions were placed in the cathode compartment in two trials. A platinum wire was used as the anode, and a 316 stainless steel mesh was used as the cathode. A DC power supply is used to start the electrochemical reaction at a constant voltage of 6V. pH values of each compartment were measured periodically.

In both tests, the pH value of the anode compartment dropped drastically as the dominant reaction at both tests was proton generation. In contrast, the reaction at the cathode is entirely different as different cathodic buffers were used. Hydroxide generation is the dominant reaction with NaCl in the cathodic compartment. It can be validated by the increase of pH from 7.44 to 11.85 in the cathodic compartment shown in **Figure 27 (a)**. However, the pH value of the cathodic compartment with 0.1M $Cu(NO_3)_2$ solution does not change drastically, as shown in **Figure 27 (b)**.

Furthermore, there was no bubble observed at the cathode during the experiment, and a layer of copper can be seen on the stainless steel mesh cathode after the experiment. This result further validates that no hydrogen evolution reaction occurred (hydroxide generating), and copper plating was dominant at the cathode, explaining why no drastic pH change is observed. If the pH value of the bridge compartment between the two different tests is compared, it could be found that acid swing is more efficient with the use of $Cu(NO_3)_2$ solution in the cathodic compartment, as shown in **Figure 27**. This data demonstrates that using Cu(NO3)2 solution at the cathode compartment can facilitate the acid swing of the bridge compartment.

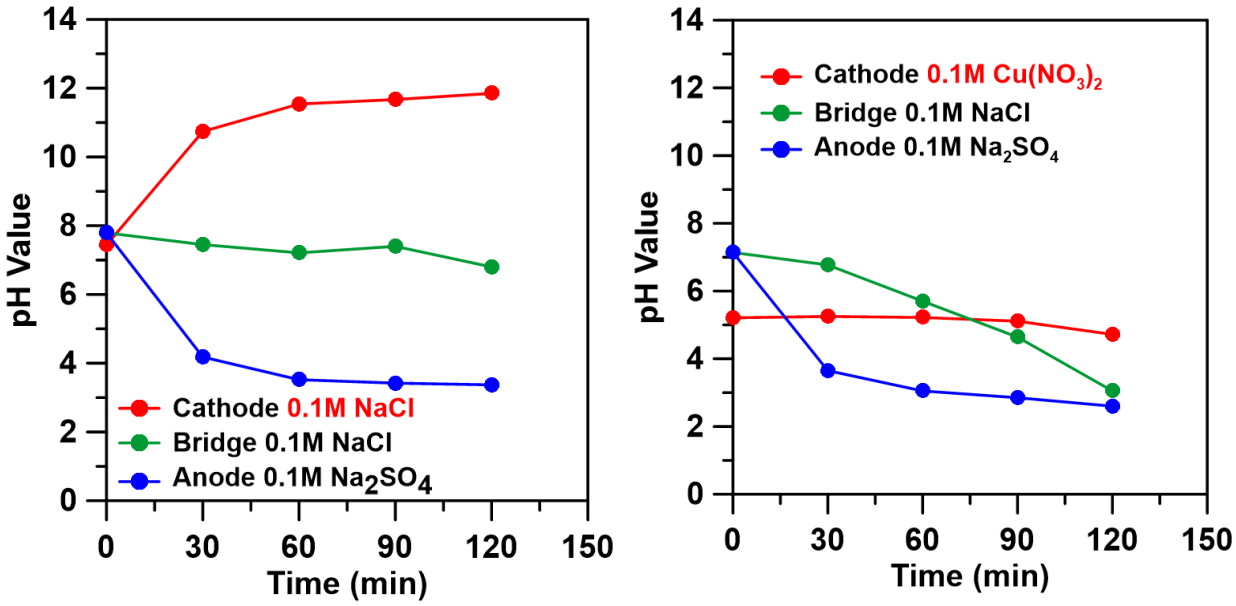


(a) (b)

**Figure 27.** Electrochemical acid swing of 0.1M NaCl solution in the bridge compartment of three-compartment cell using different cathodic buffer (a) 0.1M NaCl (b) 0.1MCu$(NO_3)_2$. The buffers placed in each compartment are shown in each figure's legend. Two cation exchange membranes were used on this cell to create three compartments. Platinum wire was used as the anode, and 316 stainless steel mesh was used. Cell potential = 6V.

After successfully demonstrating the acid swing capability of the three-compartment electrochemical cell using $Na_2SO_4$/NaCl/$Cu(NO_3)_2$ solutions in the anode/bridge/cathode compartment, the NaCl solution was replaced with a 3.6M MEA solution for further validation. Other than replacing 0.1M NaCl solution with 3.6M MEA solution, all cell configurations remained the same. The green line in **Figure 28** shows the pH change of MEA solution in the three-compartment electrochemical cell. It is shown that the pH only dropped from 12.2 to 11.86 in 5.5 hours. Even though a three-compartment cell can change the pH of NaCl solution significantly (from pH 7.14 to pH 3.5 in 2 hours), it does not decrease pH as much when the solution in the bridge compartment is substituted with 3.6M MEA. The rate and the extent of acid swing in MEA solution are both significantly lower compared to that in NaCl solution.

There are several potential explanations for this phenomenon. First, the limited pH swing in the MEA solution could result from the lack of ions in the MEA solution to maintain its electroneutrality during the acid swing process. To remain electroneutrality, the amount of cation input from the anodic compartment must be equal to the cations output to the cathode compartment. As no cations were initially present in the MEA solution, protons entering the bridge compartment cannot be balanced by other cations exiting the compartment. Therefore, the acid swing process cannot proceed without ions in the bridge solution. To test the validity of this explanation, NaCl is added to the MEA solution until a final concentration of 0.5M. Then, MEA solution with NaCl is placed in the bridge compartment of the three-compartment electrochemical cell for acid swing. The red line in **Figure *28*** shows the acid swing of MEA solution after NaCl addition. The pH can drop from 12.2 to 11.35 in 5.5 hours. This acid swing extent and rate are slightly larger than the acid swing on MEA solution without NaCl addition. However, this acid swing extent is still significantly lower than that of acid swing on NaCl solution (pH drop from 7.14 to 3.5 in 2 hours). This result indicates that electroneutrality plays a role in the acid swing of MEA solution; however, it may not be the main or the only reason that led to a stall of pH drop in MEA solution.

Another potential reason that led to the stall of pH drop in MEA solution may be the larger buffering capacity of amines than NaCl. The amine can absorb the proton transported through the cation exchange membrane and form a protonated amine. In contrast, sodium chloride cannot absorb any proton, and all protons transferred from the anodic compartment would change proton concentration ($[H^+]$) and, thus, change the pH instantly. Therefore, the difference in pH drop profile between these two solutions might not result from the different amount of proton entering the bridge compartment but from the enormous buffering capacity of the MEA solution. With the same amount of proton transferred into MEA and NaCl solution, the pH value of MEA solution

would be less sensitive to proton addition. Running the cell at a higher current for a longer time may tackle this issue. This practice could allow more protons to be generated and transferred to MEA solution, resulting in more pH change.

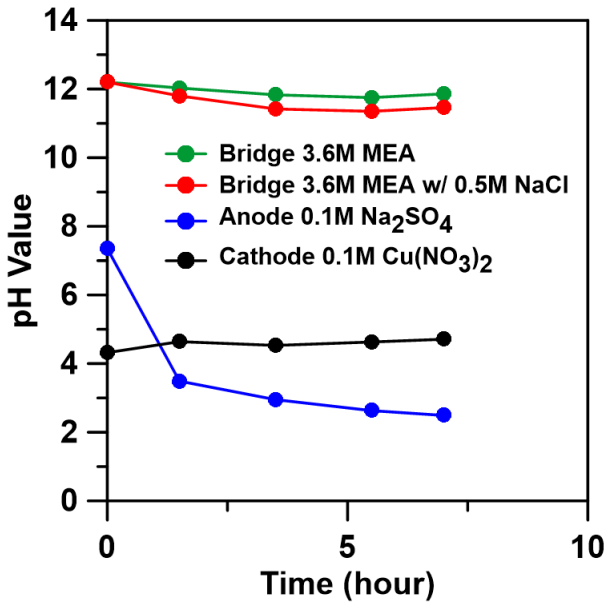


**Figure 28.** Acid swing of 3.6M MEA solution using three-compartment electrochemical cell. Two cation exchange membranes were used on this cell to create three compartments. Platinum wire was used as the anode, and 316 stainless steel mesh was used.

The other reason that leads to a stall of pH drop in MEA solution can be a result of the wrong ion exchange membrane used. In the cell design shown in **Figure 26**, two CEMs are used to create three compartments in the electrochemical cell. Proton generated from the anode can pass through CEM to enter the bridge compartment to decrease the pH of the bridge compartment. The proton inside the bridge compartment can also cross the CEM and enters the cathodic compartment. If the rate of proton transfer into and out of the bridge compartment is equal, the pH value in the bridge compartment will reach an equilibrium. Therefore, a modification is made to the electrochemical cell by replacing the CEM on the cathode side with an AEM. The schematic of this cell design is shown in **Figure 29**. The proton generated at the anode can migrate through the CME and enter the bridge compartment. However, it will be blocked by the AEM and, therefore,

would not enter the cathode compartment, securing the proton accumulation in the bridge compartment. In addition, electroneutrality can be maintained by migrating nitrate ions from the cathodic compartment. The positive charge carried by the proton can be balanced by the negative charge carried by the nitrate ion, and no NaCl needs to be added to the MEA solution. As a result, the extent of the acid swing of the bridge compartment would be dominated by the amount of nitrate ion supplied. Further experiments need to be done to validate if this new electrochemical cell design can result in a better acid swing of MEA solution.

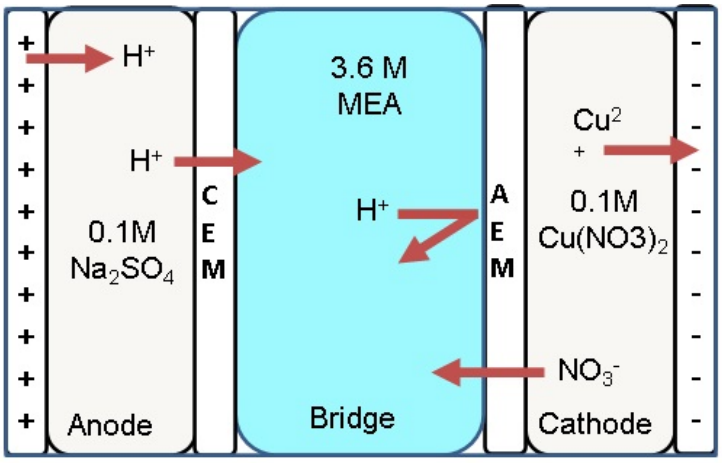


**Figure 29.** Schematic of a three-compartment electrochemical cell with a CEM and an AEM. Buffers in each compartment can be changed as required for different experiments.

To test if replacing the CEM with the AEM can result in a better acid swing result, the same solutions are used in each compartment with a different membrane usage. In this experiment, 1M of $Na_2SO_4$ and 1M of $Cu(NO_3)_2$ were used in the anodic and cathodic compartments. 3.6 M $CO_2$ loaded MEA (pH = 10) is used in bridge compartment. The $CO_2$-loaded MEA usage mimics that acid swing is performed on a $CO_2$-loaded MEA solution. The anode and cathode used were the same as in previous experiments (anode: platinum wire, cathode: 316 stainless steel mesh). The cell is operated for a longer period to ensure sufficient proton enters the bridge compartment.

This practice ensures that the proton amount entered would be significantly larger than the buffering capacity of the amine so that a larger pH change can be observed.

**Figure *30*** shows the pH swing of $CO_2$-loaded MEA solution in the three-compartment electrochemical cell. With the use of two CEMs in the electrochemical cell, the pH drops from 10 to 9.7 in the first 12 hours of cell operation (red line). No significant pH change is after 12 hours of cell operation. The pH value of the $CO_2$-loaded MEA solution is 9.67 after 24 hours of operation. This data implies that the proton concentration is in equilibrium during the 12-to-24-hour time point, and no further pH decrease is expected. When the CEM is swapped with AEM, the pH value of the $CO_2$-loaded MEA solution changes significantly. The pH value dropped from 10 to 8.34 in 24 hours and dropped to 7.59 after 44 hours (blue line). This result indicates that the three-compartment cell built with a CEM and an AEM can better facilitate the acid swing of $CO_2$-loaded MEA solution comparting to the cell built with two CEMs. When a cell built with CEM/AEM was used, bubble formation could be observed in the bridge compartment ($CO_2$-loaded MEA solution) during the acid swing. It is expected to be $CO_2$ that is released from $CO_2$-loaded MEA with the pH dropping. Another experiment using a cell with CEM/AEM configuration is performed for an even more extended time (shown in the green line in **Figure *30***). In this experiment, the cathodic compartment was replenished with fresh 1M $Cu(NO_3)_2$ at every pH measurement (t = 24 hr and t = 48 hr), and the cell was operated on for 72 hours. With the $Cu(NO_3)_2$ solution replenished periodically, it provides the cell with sufficient nitrate ions, and therefore an even larger acid swing can be achieved. As shown in **Figure *30***, pH drops from 10 to 0.5 after 72 hours of cell operation with CEM/AEM cell configuration. This extent of pH swing is sufficient for the complete $CO_2$ desorption from the MEA solution.

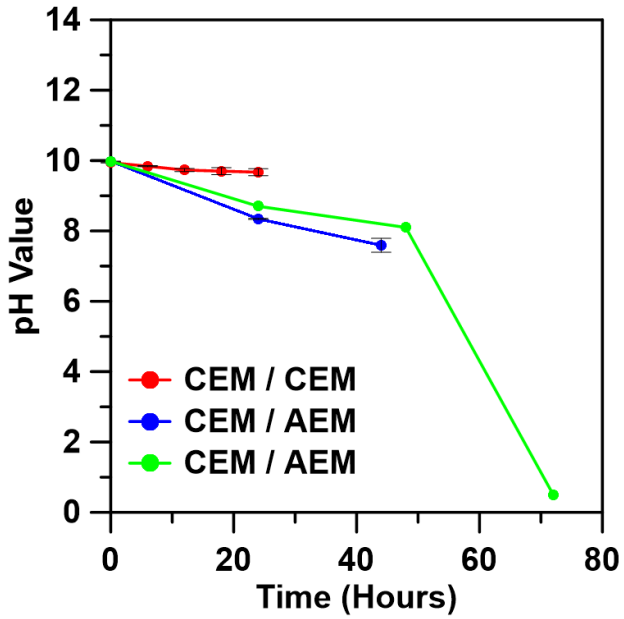


**Figure 30.** pH value of $CO_2$-loaded MEA solution (3.6M, pH=10) in bridge compartment with different membrane configurations of the three-compartment electrochemical cell. 1M $Na_2SO_4$ was used at the cathode. 1M $Cu(NO_3)_2$ solution was used at the cathode. Pt wire anode and 316 stainless steel cathode were used. Legends show the membrane used for the three-compartment electrochemical cell. Error bars indicate the standard deviation of duplicate experiments.

$CO_2$-loaded MEA solution acidified in the three-compartment electrochemical cell with CEM/AEM configuration was analyzed with IR-spectroscopy to validate the $CO_2$ desorption, protonated amine formation, and counter ion ($NO_3^-$) migration into the bridge compartment. Acidified $CO_2$-loaded MEA of pH = 8.3, 7.7, and 0.5 were collected and analyzed. In addition, fresh MEA and loaded MEA were also analyzed as standard.

**Table 8.** Peak assignment for $CO_2$-loaded MEA solution[64]

| Wavenumber ($cm^{-1}$) | Assignment |
|---|---|
| 1517 | $NH_3^+$ (protonated MEA) |
| 1486 | $COO^-$(carbamate) |
| 955 | C-$NH_2$ (MEA) |

**Figure *31*** shows the IR spectrum of these samples. **Table 8** shows the peak assignments of the IR spectrum. It is shown that the intensity of protonated MEA peak at 1517 $cm^{-1}$ increases with the decrease of the pH value of the MEA solution. This result indicates that the protonated MEA forms during the electrochemical acid swing, consistent with the reported mechanism[75]. A similar profile is also found in **Figure *17*** (b), where the MEA solution is acidified. In addition, the carbamate peak at 1486 $cm^{-1}$ decreases with a greater extent of acid swing. This result shows that $CO_2$ desorbs during the electrochemical acid swing process. Nitrate peak at 1320 $cm^{-1}$ can also validate the migration of $NO3^-$ from the cathode to the bridge compartment. With a lower pH value, a higher intensity of $NO3^-$ the peak is observed, indicating that more $NO3^-$ entered the bridge compartment to balance the proton entered from the anodic compartment.

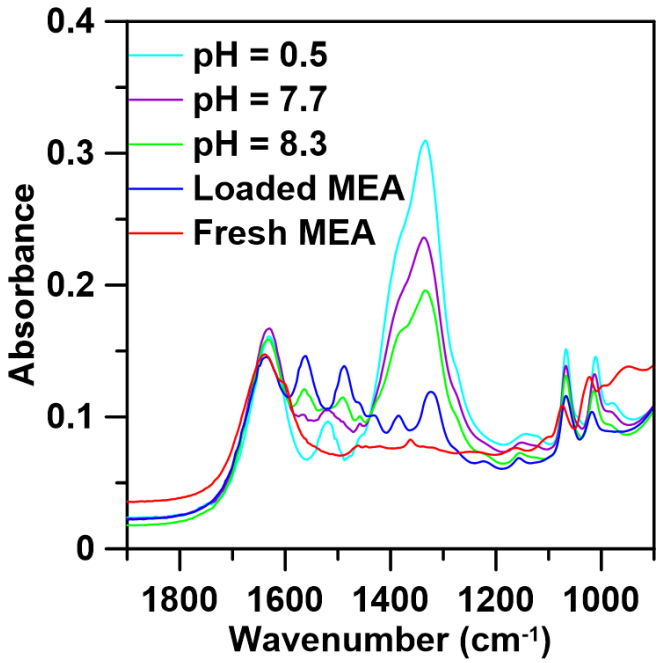


**Figure 31.** IR-spectrum of $CO_2$-loaded MEA solution acidified by three-compartment electrochemical cell with CEM/AEM configuration.

The amount of $CO_2$ desorbed during acid-swing, either by HCl addition or by electrochemical cell, is measured to validate the feasibility of $CO_2$ desorption using an electrochemical cell. 200 ml of 3.6M MEA was loaded with $CO_2$ until pH = 10. Four 50ml of aliquots were treated with different desorption methods (acid swing and subsequent temperature swing), and $CO_2$ desorption was measured during each treatment. The first 50ml aliquot of $CO_2$-loaded MEA is placed in an 80 ℃ water bath for 1 hour without any acid swing ahead. This aliquot serves as the no acid swing control for the experiment (shown in the yellow bar in **Figure *32***). Next, HCl was added to another 50 ml aliquot of $CO_2$-loaded MEA until the pH of the solution reached 7.5. The HCl-added MEA solution was placed in an 80 ℃ water bath for 1 hour. $CO_2$ desorption was measured during both processes (shown in the cyan bar in **Figure *32***). The rest two aliquots were placed in a three-compartment electrochemical cell, and the pH was decreased to 7.3 and 0.5, respectively. There were both then placed into an 80 ℃ water bath for 1 hour. $CO_2$ desorption was measured too.

**Figure *32*** shows the extent of $CO_2$ desorption of MEA using different $CO_2$ desorption methods. If the pH of the $CO_2$-loaded MEA solution is decreased to 0.5, all $CO_2$ can be desorbed during the acid swing. Subsequent temperature swings on this MEA solution cannot desorb any $CO_2$ as all $CO_2$ has been desorbed during the acid swing using a three-compartment electrochemical cell. This result indicates that complete $CO_2$ desorption can be done using an electrochemical acid swing. Also, the extent of $CO_2$ desorption is similar when pH is decreased to a similar range regardless of the method of acid swing. It is shown that 26.46% of $CO_2$ is desorbed with HCl addition to pH=7.5, and 28.91% of $CO_2$ is desorbed with an electrochemical acid swing to pH=7.3. The subsequent temperature swing at 80 ℃ further desorbs $CO_2$ to 88.62% and 98.65%, respectively. The slight difference between the $CO_2$ desorption amount resulted from the slightly

lower pH of electrochemically acidified MEA. The $CO_2$ desorption profile is similar to the trend shown in **Figure *16***.

Three-compartment electrochemical cells can be used as an acid swing method for $CO_2$-loaded MEA. It can decrease the pH of $CO_2$-loaded MEA from 10 to 0.5 with proper membrane configuration and buffer usage. The $CO_2$ desorption during the electrochemical acid swing process can be confirmed by the loss of carbamate peak in the IR spectrum of $CO_2$-loaded MEA samples. The amount of $CO_2$ desorption was also quantified, and it was found that the $CO_2$ desorption amount from electrochemical acid swing and HCl addition was similar. These data suggested that electrochemical acid swing using a three-compartment electrochemical cell can substitute HCl addition as an acid swing method for $CO_2$ desorption of $CO_2$-loaded MEA solution.

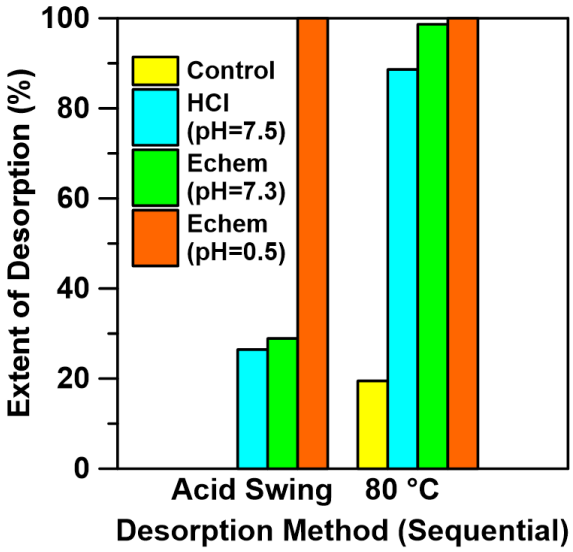


**Figure 32.** Extent $CO_2$ desorption of $CO_2$-loaded MEA solution (pH = 10) using a combination of acid swing and temperature swing. Acid swing was performed by HCl addition or three-compartment electrochemical cell to the pH value shown in the legend. Temperature swing was performed by putting MEA solution into an 80 °C water bath for 1 hour. $CO_2$ desorption amount was measured.

## 4.3 Base Swing of Acidified Amines and Four-compartment electrochemical cell

### 4.3.1 Electrochemical Base Swing

A three-compartment cell shown in **Figure *33*** is designed to attempt an electrochemical base swing. First, the base swing cell is built by reversing the electric field's polarity and changing the electrode usage. A copper plate is used as an anode, and Pt is used as a cathode. Next, the base swing is performed. The cathode would generate hydroxide, and the hydroxide would pass through AEM to enter the bridge compartment.

On the other hand, copper oxidation into copper (II) ion is the dominant anodic reaction, with copper being used as the anode. This practice prevents proton generation in the anode. However, the copper (II) ion would pass through the CEM and enter the bridge compartment as the counter ion for hydroxide generated at the cathode. Therefore, a base swing attempt is made by putting 0.1 M Cu(NO3)2 in the anode compartment and 0.1M NaOH in the cathode compartment, with the DC power supply providing 6V to the cell. The copper migration into the bridge compartment can be visualized by the color of the bridge solution. The solution turns blue, indicating the formation of the copper-MEA complex. This result is not ideal as this operation would result in copper being in contact with the MEA solution during the base swing and would result in capacity loss of MEA, as discussed in 4.2.1.

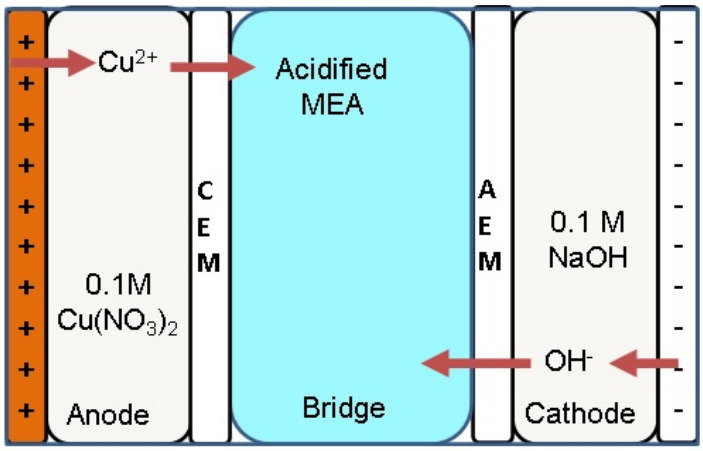


**Figure 33.** Electrochemical Base Swing Cell design. A CEM and AEM are used to separate the cell into three compartments. Copper is used as an anode, and 316 stainless steel is used as a cathode. Hydroxide generated at the cathode migrates through AEM and enters the bridge compartment for base swing. Copper is oxide at the anode and generates copper (II) ions that migrate through CEM to the bridge compartment as a counter ion.

The base swing cell is modified by replacing the CEM with an AEM to prevent copper from entering the bridge compartment. The design is shown in **Figure *34***. In this design, Pt anode replaces copper anode, and therefore the dominant reaction at anode would be oxygen evolution. Proton generated at the anode would be blocked by AEM. Hydroxide generated at the cathode can migrate through the AEM and enters the bridge compartment. The nitrate ions introduced by acid swing cell would migrate through AEM, enter the anode compartment, and balance the anion in the cathode compartment. This helps the bridge compartment to remain electrically neutral.

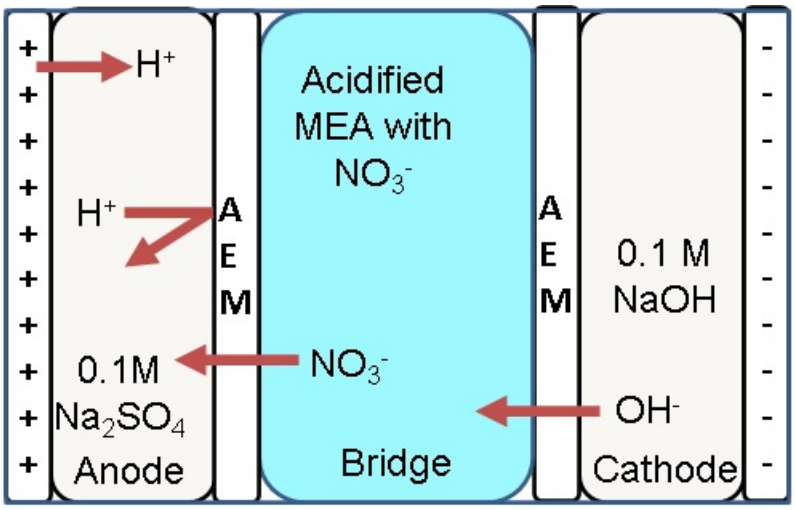


**Figure 34.** Modified three-compartment electrochemical base swing cell. The base swing cell has two AEM that separates the cell into three compartments. Pt is used as a cathode and anode.

A base swing experiment is done using the cell design shown in **Figure *34***. Platinum sheets were used as an anode and cathode. 0.1M NaOH and 0.1M $Na_2SO_4$ were placed in the cathodic and anodic compartments. An acidified MEA (by adding $HNO_3$ $CO_2$ loaded MEA solution) with pH=0.5 was placed in the bridge compartment for the base swing. The pH of acidified MEA solution is measured at 24, 48, 72, and 120 hours after the electrochemical base swing. Samples were also collected at 24- and 48-hour time points and were analyzed by IR spectrometry.

**Figure *35* (a)** shows the pH value of acidified amine under the base swing cell for 120 hours. The pH value of acidified MEA solution increases from 0.5 to 9.01 in 24 hours and further increases to 9.8 at 48- hours. However, the pH value does not further increase after 48 hours. This result indicates that the rate of hydroxide entering the bridge compartment is equal to or less than the rate of the hydroxide exiting the bridge cell, as hydroxide can pass through AEM and enters the anode compartment. This data indicates that the base swing cell can increase the pH of acidified MEA to some extent; however, a complete regeneration cannot be achieved. The IR spectrum of

acidified MEA solution during the base swing is shown in **Figure *35***. The peak intensity of protonated amine at 1517 $cm^{-1}$ decreases with the increase of pH from 0.5 to 9.8. Also, the NO3- peak at 1320 $cm^{-1}$ decreases with the pH increase. These data show that the base swing cell can successfully decrease the amount of protonated MEA while removing $NO_3^-$ at the same time. However, the nitrate is not entirely removed within the given timeframe.

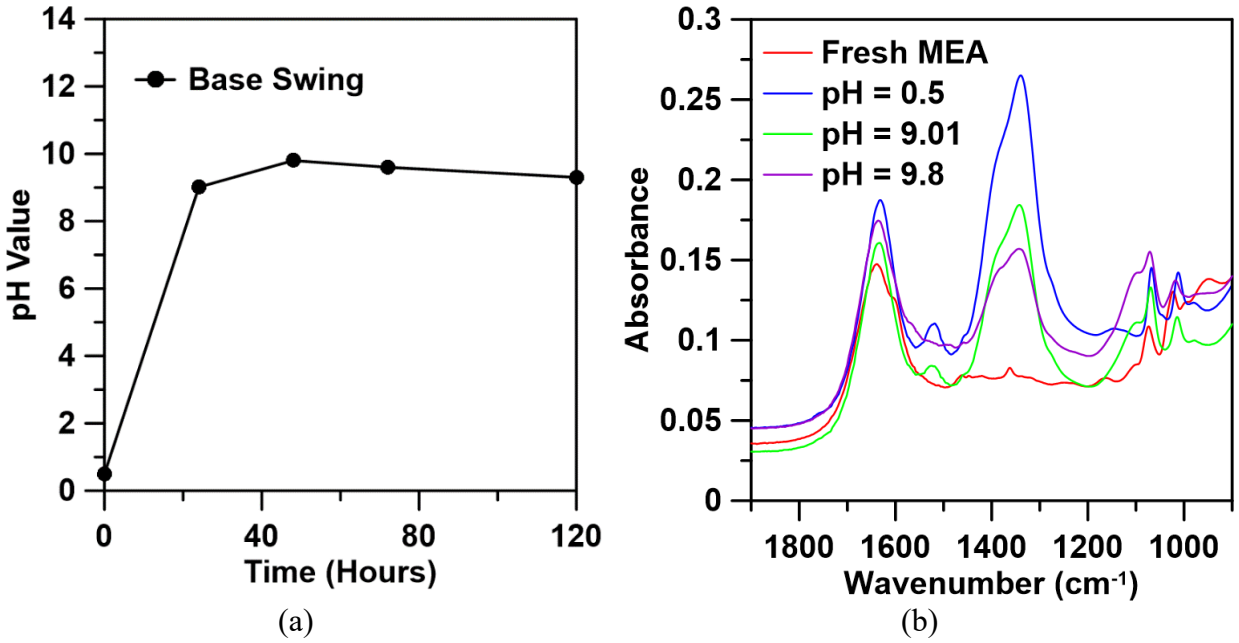


**Figure 35.** (a) pH value of acidified MEA solution under electrochemical base swing using three-compartment electrochemical base swing cell (AEM/AEM configuration). (b) IR spectrum of Acidified MEA under the electrochemical base swing.

## 4.4 Electrochemical acid-swing based amine regeneration system

### 4.4.1 Electrochemical acid swing using four-compartment acid swing cell

There are several drawbacks to the three-compartment electrochemical acid swing cell, and an improvement is needed. First, the use of copper ions in the cell must be removed. A three-compartment electrochemical cell for acid swing with copper in the cathode will result in a significant copper deposit. The copper deposit on the cathode cannot be utilized in the following

base swing process. This result implies that the acid swing process would require copper nitrate as input and have a significant amount of copper metal as output. If the copper needs to be reused, a reverse potential will be applied to oxidize copper into ions. This practice would require extra energy input, and therefore this process is not preferred. Although copper can be oxidized with the base swing process shown in **Figure *33***, it is not preferred as copper would contact MEA solution. In addition, a cheaper electrolyte other than copper nitrate would be preferred as it can reduce the cost of the overall acid swing process. Ideally, NaCl would be the best electrolyte to use, given its abundance in the ocean. Therefore, a four-compartment electrochemical cell is designed to replace the three-compartment cell for an acid swing for the reasons described.

A schematic of a four-compartment electrochemical cell is shown in **Figure *36***. CEM/AEM/CEM separates a cell into four compartments. The anode compartment is filled with 1M $H_2SO_4$ solution, generating the proton. The acid swing compartment is filled with $CO_2$-loaded MEA, which is where the acid swing is done. The salt compartment is filled with 3.6M NaCl solutions and provides counter ions to the cathode and acid swing compartments. The cathodic compartment is filled with 1M NaOH, and the cathode generates hydroxide. The CEM between the anode and acid swing compartment allows protons to migrate through, and the pH of the acid swing cell can be decreased. The hydroxide generated at the cathode would be blocked by the cation exchange membrane and stays in the cathode. NaCl in the salt compartment is essential for the extent of acid swing. Sufficient NaCl needs to be provided to achieve a greater acid swing extent.

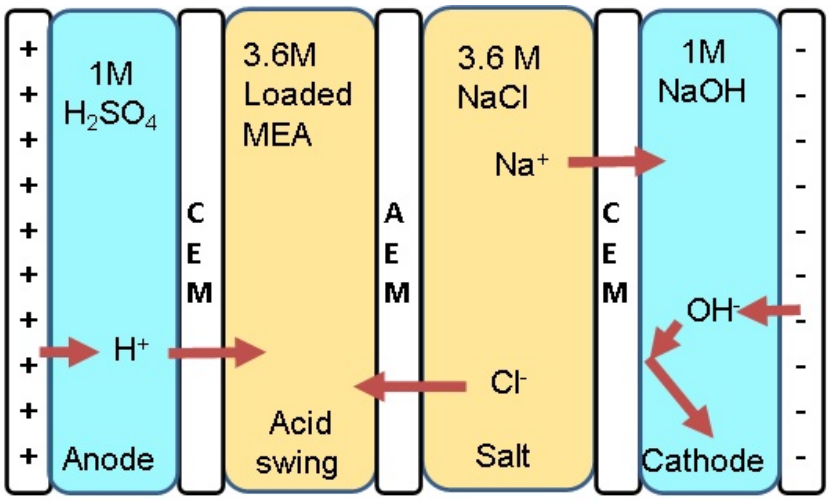


**Figure 36.** Schematics of four-compartment electrochemical acid swing cell.

The four-compartment electrochemical cell was used to validate if acid swing by electrochemical method serves as a substitute for HCl addition to facilitating CO2 desorption. 3.6M MEA solution was loaded to pH= 9 ($CO_2$ loading: ~0.5 mol$CO_2$ mol$MEA^{-1}$) and placed in the acid swing compartment of the four-compartment electrochemical cell. All other solutions used are as indicated in **Figure *36***. The acid swing of $CO_2$-loaded MEA is successful, and samples of acidified amine are collected at pH = 8, 7, 6, and 1.8. The IR spectrum of these samples is shown in **Figure *37* (a)**. It is found that the carbamate peaks decreased during the acid swing process, and the intensity of protonated amine peaks increased. This IR spectrum is the same as the $CO_2$-loaded MEA with hydrochloric acid addition, shown in **Figure *37* (b)**. This result indicates that the four-compartment electrochemical cells can successfully decrease the pH of $CO_2$-loaded MEA and fully desorb $CO_2$. Therefore, the four-compartment electrochemical acid swing cell can serve as a substitute for the acid swing using HCl or a three-compartment acid swing cell while using no copper-based solution.

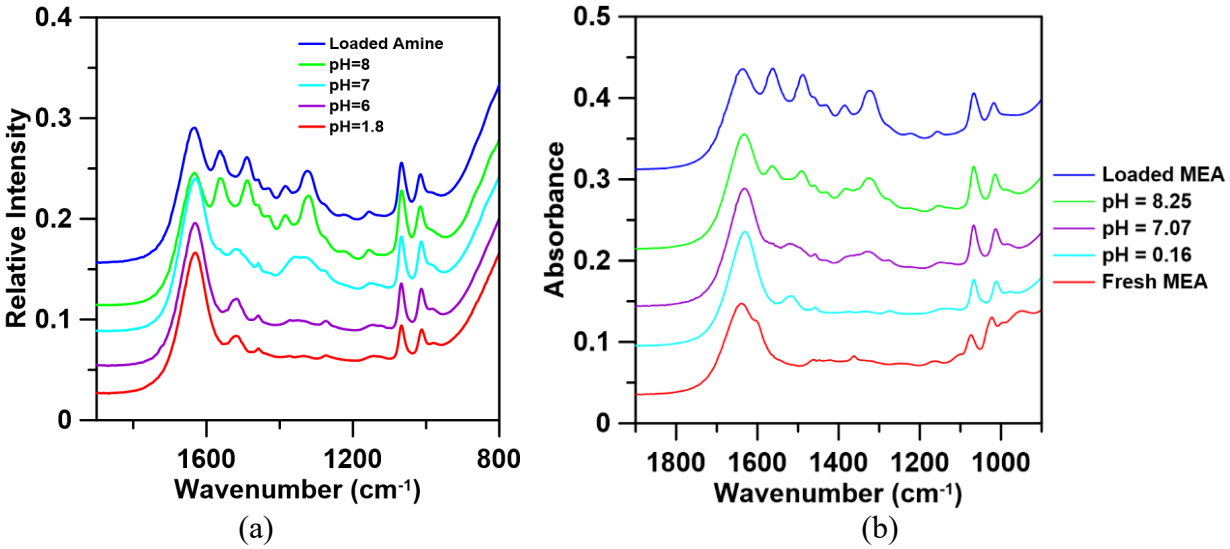


**Figure 37.** IR spectrum of $CO_2$-loaded MEA solution during an acid swing by (a) four-compartment electrochemical acid swing cell (b) HCl addition

To validate if electrochemically acidified MEA solution by the four-compartment cell can also be regenerated by a base swing, a stoichiometric amount of NaOH is added to electrochemically acidified MEA solution for MEA regeneration. After NaOH dissolves and MEA solution cools, regenerated MEA solution is placed in three neck boiling bottles for reabsorption using the method described in Chapter 2.

**Figure *38*** shows the extent of $CO_2$ reabsorption under different regenerated conditions. It is shown that the $CO_2$ reabsorption amount is 87.55 ± 4.81% of maximum capacity for MEA regenerated from electrochemically acidified MEA of pH=6. This amount is similar to the reabsorption amount of regenerated MEA acidified by the HCl addition shown in **Figure 21** (a). This result indicates that electrochemical acid swing can be a substitute acid swing method for MEA regeneration without losing the $CO_2$ absorption capacity of regenerated MEA.

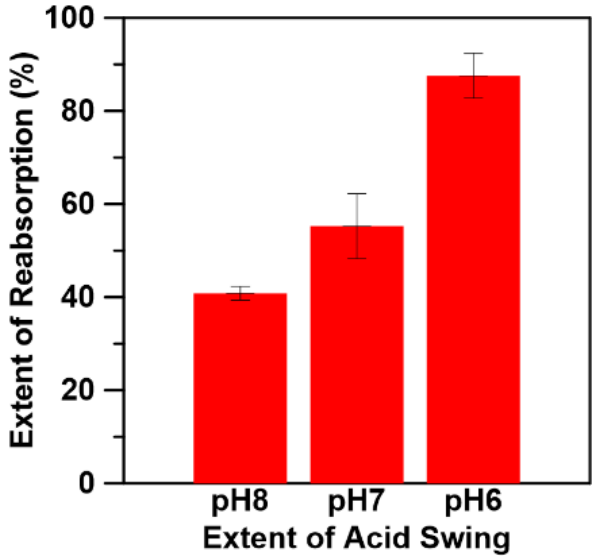


**Figure 38.** The extent of $CO_2$ reabsorption of regenerated MEA after electrochemical acid swing and NaOH base swing.

### 4.4.2 Base Swing and amine regeneration cycle via anion exchange

A base swing cell was designed based on the four-compartment electrochemical cell by reversing the electrode's polarity and swapping AEMs with CEMs. The base swing mechanism would be the opposite of that shown in **Figure *36***. In summary, hydroxide generated at the cathode would migrate through AEM and enter the base swing cell. The salt compartment would provide necessary counter ions for the base swing cell and the anode compartment. Therefore, a complete amine regeneration cycle can be done with this base swing cell. However, this amine regeneration cycle would result in NaCl accumulation in the MEA solution. Chloride enters MEA solution as a counter ion during the acid swing process, and sodium enters MEA during the base swing process. If amine absorbent is reused and no extra process is applied to remove NaCl, NaCl will accumulate a significant amount of NaCl in the MEA solution. Once the NaCl concentration exceeds its solubility, the acid-base swing cycle cannot proceed further. Therefore, a method that can remove

ions needs to be applied to the amine regeneration cycle or during acid or base swing to maintain further regeneration cycle.

Base swing of amine solution using anion exchange resin was proposed to substitute the electrochemical base swing or NaOH addition, given its ability to substitute chloride ions with hydroxide ions. Anion exchange resins are tertiary or quaternary amine functionalized styrene-divinylbenzene polymers, which can bind hydroxide and chloride ions. When the resin is charged with hydroxide ions, it can release hydroxide into a chloride-rich solution while adsorbing the chloride. This function fits our need for a method to remove ions while performing acid or base swing. IRN78-OH resin is used for the base swing of acidified MEA.

To examine if base swing NaOH addition can be replaced by anion exchange treatment, 50ml loaded MEA acidified by the electrochemical cell to various pH was prepared (pH=8, pH=7, and pH=6). Acidified MEA was mixed with IRN78-OH resin for 5 min before the resin was filtered, and the pH of MEA was tested. The pH value of MEA (acidified to pH=6) increased to pH=11.24 after mixing with 200ml of IRN78-OH (0.24 eq). To further examine if these MEA regenerated by IRN78-OH resin can reabsorb $CO_2$, MEA solutions are placed in the three-neck boiling bottle for CO2 absorption using the method described in the experiment method section.

**Figure *39*** shows the CO2 reabsorption amount of MEA regenerated by IRN78 OH. It is shown that the $CO_2$ reabsorption amount is 82.23± 1.42% of maximum capacity for regenerated MEA that is acidified to pH=6 and treated with 200ml IRN78-OH resin. This result shows that the combination of electrochemical acid swing and anion exchange base-swing can serve as a substitute method for MEA regeneration at ambient temperature without capacity loss.

IR spectrum is used to analyze the regenerated amine after different base swings. A combination of regeneration methods of HCl addition, Electrochemical acid swing, NaOH addition, and anion exchange base-swing is tested. Figure 39 (b) shows that the protonated MEA peak at 1517 cm-1 disappeared after the regeneration regardless of the acid swing and base swing method used. In addition, the appearance of the weak peak at 955 $cm^{-1}$ shows the appearance of MEA molecules. This data indicates that the MEAs are regenerated after acid and base swing. The MEA peak (955 $cm^{-1}$) intensity of amine regenerated by anion exchange resin is weaker than that of amine regenerated by NaOH addition. This data does not result from loss of MEA but the inevitable dilution of the sample during AER regeneration. The amine regenerated by AER was collected by vacuum filtration. The rinsing of DI water is required to collect all residue MEAs on the resin for CO2 quantification. GC-MS were used to quantify the amount of amine absorbent, and no significant loss of amine was found.

In summary, an electrochemical acid swing-based amine regeneration method has been developed. The electrochemical acid swing can successfully desorb $CO_2$ from MEA. Anion exchange resin can be used as a base swing method to regenerate MEA after an electrochemical acid swing. In addition, the amount of $CO_2$ that regenerated MEA can absorb is similar regardless of the method of regeneration. This result indicates that the combination of electrochemical acid swing and anion exchange base-swing can serve as a substitute method for amine regeneration.

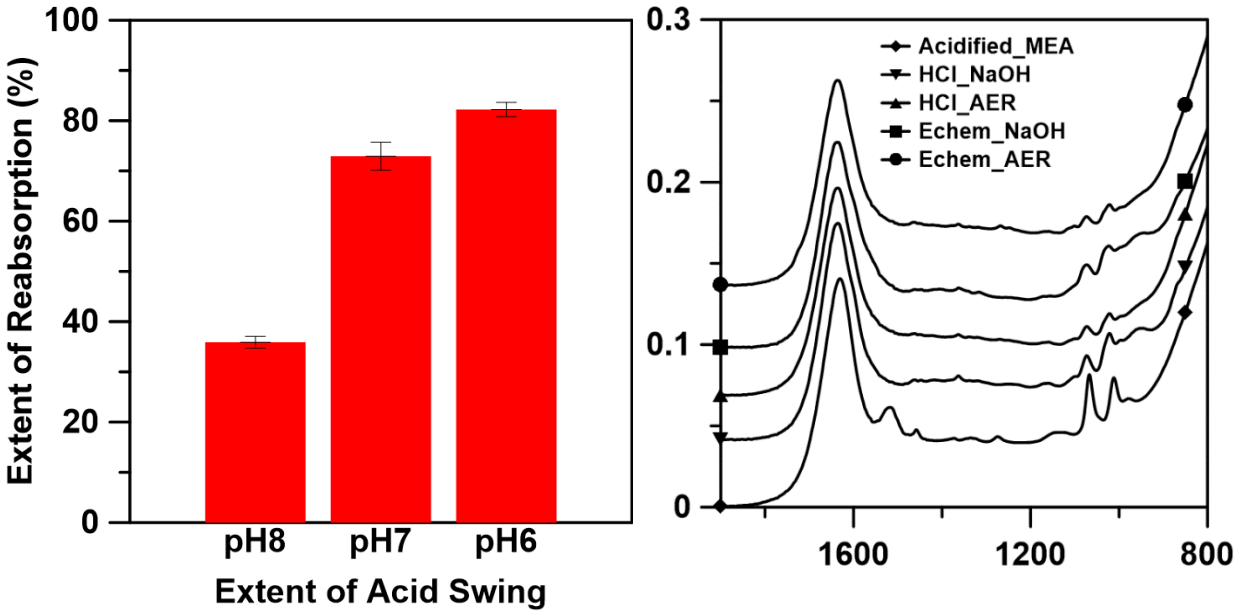


**Figure 39.** (a) The extent of $CO_2$ reabsorption of regenerated amine by electrochemical acid swing and anion exchange base swing. (b) IR spectrum of regenerated MEA by different acid swing and base swing method

# Chapter 5 Optimization Studies on Electrochemical Amine Regeneration System

Several different cell configurations and operating parameters can be studied to improve the energy efficiency of the electrochemical cell system. These parameters include but are not limited to amine absorbent usage, cell geometry selection, ion exchange membrane and resin usage, continuous process configuration, and operation parameter configurations. For example, an amine absorbent with higher maximum $CO_2$ loading and lower proton requirements for complete $CO_2$ desorption would be preferred. Amine with lower proton requirements for complete $CO_2$ desorption would result in less electrical energy required to generate proton and, therefore, less energy required to desorb $CO_2$. An amine with higher $CO_2$ loading would be preferred to increase the cyclic capacity and decrease the proton needed for $CO_2$ desorption per unit of $CO_2$. Focus on cell geometry optimization studies would decrease cell thickness and reduce cell size while maintaining $CO_2$ desorption capacities. A thinner cell would generally result in less resistance and a cell with higher efficiency. Focus on membrane studies would be mainly on increasing the ion conductivity while having selectivity and endurance of the membrane remain the same. Increasing ion conductivity would increase the reaction rate and achieve better cell efficiency. A continuous process flow configuration needs to be developed to allow a faster and more efficient operation. In addition, the operation parameter needs to be optimized. This work will be parallel with the cell geometry and continuous process configuration work. An optimized operation parameter is expected to provide better cell efficiency.

## 5.1 Energy Consumption

In the state-of-art MEA regeneration method, $CO_2$-loaded MEA solution is heated up to over 120 ℃ by a reboiler. However, even with optimal reboiler temperature, the working capacity of amine absorbent is lower than 50%. Studies show that only 0.2 mol $CO_2$ per mol MEA can be released during regeneration under reboiler temperature 120 ℃ with an initial loading of 0.5 mol $CO_2$ per mol MEA[40]. Therefore, only 40% of the maximum loading capacity is used in each absorption-regeneration cycle. Low working capacity results in a high absorbent amount needed for each absorption cycle given the same total $CO_2$ absorption amount. Also, larger units, including absorption and desorption towers, would be needed in a $CO_2$ absorption plant to increase the interaction volumes between the absorbent and $CO_2$ source. As a result, lower working capacity increases the cost of plant infrastructure and operating expenses due to the more significant absorbent amount needed.

In our electrochemical amine regeneration system, the working capacity for each absorption cycle can be increased by a greater extent of acid swing. For example, in **Figure *38***, it is shown that 80% of the maximum loading capacity is free for $CO_2$ reabsorption after electrochemical acid swing to pH=6 and then base swing with ion exchange resin. This data shows that the working capacity in each absorption cycle can reach 80% of maximum capacity by using the electrochemical regeneration method, which is at least two times higher than using the state-of-art heating regeneration method. This is to say, with an electrochemical amine regeneration system, less absorbent is needed, and therefore initial infrastructure investment and operation costs can be reduced.

To compare the energy consumption of the electrochemical and state-of-art MEA regeneration process, we estimate the energy consumption using numbers reported by previous studies and our electrochemical amine regeneration system. These energy consumption numbers are compared under operation conditions where 80% of the working capacity is achieved.

It is reported that at least 10000 kJ $kgCO_2^{-1}$ (2.52 MWh $tonCO_2^{-1}$) reboiler duty is required for $CO_2$ desorption from $CO_2$ loading of 0.5 to 0.22 $molCO_2$ $molMEA^{-1}$ [30]. If the desorption process is started with lower initial $CO_2$ loading (0.3 $molCO_2$ $molMEA^{-1}$), it will take more than 20000 kJ $kgCO_2^{-1}$ (5.04 MWh $tonCO_2^{-1}$) to desorb $CO_2$ to loading of 0.2 $molCO_2$ $molMEA^{-1}$. Another study reported that 4.6 MJ $kgCO_2^{-1}$ (1.16 MWh $tonCO_2^{-1}$) is required for $CO_2$ desorption from 0.488 to 0.347 $molCO_2$ $molMEA^{-1}$ [40]. Even though these energy consumption numbers are measured under 56%, 20%, and 28% of working capacity, they still provide useful information on energy consumption estimation. It is expected that energy requirements that allow higher working capacity would increase drastically as the $CO_2$ desorption is thermodynamically unfavored at low $CO_2$ loading. Li et al. reported that > 80% cyclic capacity would require unrealistically high energy to achieves[76]. Therefore, an energy consumption much higher than 5.04MWh $tonCO_2^{-1}$ is expected if MEA regeneration is performed under conditions with a working capacity greater than 80%.

The energy consumption of the electrochemical $CO_2$ desorption process can be estimated by the thermodynamics of the water-splitting reaction. Theoretically, the minimum energy required to dissociate a mole of water is the Gibbs Free Energy of the following equation. In contrast, the practical minimum is the enthalpy of formation to supply the absorbed heat of the entropy change.

$$H_2O \rightarrow 2e^- + 2H^+ + \frac{1}{2}O_2 \quad V = 1.229V \qquad (22)$$

$$2H_2O + 2e^- \rightarrow +2OH^- + H_2 \quad V = -0.829\,V \qquad (23)$$

However, unlike traditional electrolyzers, our four-compartment electrochemical cell undergoes a proton generation at the anode, and hydroxide is generated at the cathode, as shown in equations ( 22 ) and ( 23 ). Under pH = 0 at the anode and pH = 14 at the cathode, the minimum reaction enthalpy would be 397.49 kJ mol $H_2^{-1}$.

To compare the energy required to desorb and regenerate amines with state-of-art thermal methods, the relationship between proton generation and $CO_2$ desorption must be established. The titration previously discussed in **Figure *17*** (a) shows that ~1 mol of $H^+$ are required per mol of MEA to desorb >90% of the absorbed $CO_2$. Therefore, the $H^+$ to $CO_2$ ratio would be nearly 2 to 1 or 4 to 1, depending on whether the MEA loading was 0.5 mol$CO_2$ or 0.25 mol$CO_2$ mol$MEA^{-1}$, respectively. Assuming faradaic efficiencies of 80% at the electrodes, comparable to a state-of-the-art electrolyzer, the total electrochemical pH swing energy requirement is estimated to be 10.84 GJ $tCO_2^{-1}$ (3.01 MWh $tCO_2^{-1}$) or 21.67 GJ $tCO_2^{-1}$ (6.02 MWh $tCO_2^{-1}$), depending on the application.

However, clean hydrogen is co-produced during water electrolysis and is energy dense, with a high heating value of 285.85 kJ $mol^{-1}$. Recycling the hydrogen to power the electrochemical cell reduces the required external energy supply, effectively reducing the cell's energy demand. Assuming a modest 60% conversion efficiency of the recovered hydrogen, in line with existing fuel cell technology and projected hydrogen turbines, the total cell energy drops to 7.09 GJ $tCO_2^{-1}$ (1.97 MWh $tCO_2^{-1}$) and 14.18 GJ $tCO_2^{-1}$ (3.94 MWh $tCO_2^{-1}$), respectively.

## 5.2 Amine characterization and selection

To characterize the desorption profile and characteristics of amine solution, a variety of amines are loaded with 5% $CO_2$ until it is fully saturated. The amine tested includes monoethanolamine (MEA), diethanolamine (DEA), triethanolamine (TEA), 2-ethylaminoethanol (EMEA), 2-dimethylaminoethanol (2-DMAE), diethylenetriamine (DETA), ethylenediamine (EDA), piperazine (Pz). After full saturation, HCl was added to the $CO_2$ saturated amines until all $CO_2$ was desorbed. Finally, the amount of $CO_2$ desorbed and HCl added was recorded. The amine with higher $CO_2$ desorption and low proton requirement is preferred as it would result in lower energy consumption per unit $CO_2$ desorbed.

The amount of $CO_2$ desorption from each tested amine is shown in **Table 9**. EMEA, DETA, EDA, and Piperazine all have higher $CO_2$ desorption. Among these absorbents tested, DETA has the highest $CO_2$ desorption (1.61 mol$CO_2$ mol$DETA^{-1}$). This amount is more than three times more desorbed than the desorption amount of MEA. It is expected as DETA has three nitrogen nucleophile atoms that can absorb $CO_2$. DEA and piperazine also have two nitrogen nucleophiles, resulting in significantly more $CO_2$ absorption than MEA.

**Figure 40** visualizes the desorption performance of each absorbent by plotting the $CO_2$ desorption amount at the x-axis and proton requirement at the y-axis. The unit of the slopes would be in mol$H^+$ mol$CO_2^{-1}$. This unit is proportional to the energy consumption in the electrochemical cell required per unit of $CO_2$ desorbed. That is to say, the amine that results in a smaller slope in **Figure 40** would be preferred. Despite the higher CO2 desorption, EDA and DETA require more proton addition into the solution to achieve full $CO_2$ desorption. The proton requirement for complete $CO_2$ desorption in EDA and DETA is about 2 mol$H^+$ molAbsorbent$^{-1}$. As a result, the proton to $CO_2$ ratio would be 2.139 mol$H^+$ mol$EDA^{-1}$ and 1.235 mol$H^+$ mol$DETA^{-1}$. Piperazine

exhibits the least proton requirement for full $CO_2$ desorption. It only requires 1.02 $molH^+$ $molAbsorbent^{-1}$, which is 45.4 % less requirement than that of MEA (1.8691 $molH^+$ $molMEA^{-1}$). This result indicates that piperazine is a better absorbent for the electrochemical acid swing-based amine regeneration system.

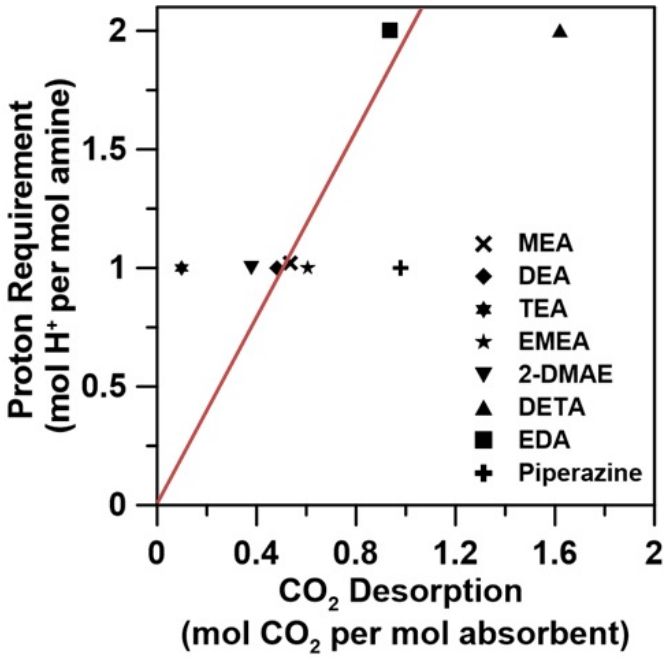


**Figure 40.** Proton requirement for complete $CO_2$ desorption with various amines. The amine was saturated with 5% $CO_2$, and an absorbent of 3.6M was used. In addition, 5M HCl was added to amine solutions until all $CO_2$ was desorbed. Finally, the amount of $CO_2$ desorption and HCl added was recorded.

**Table 9.** $CO_2$ desorption and proton requirement of amines

| Amine | Desorption Amount ($molCO_2$ $molAbsorbent^{-1}$) | Proton Requirement ($molH^+$ $molAbsorbent^{-1}$) |
|---|---|---|
| MEA | 0.535 | 1 |
| DEA | 0.483 | 1 |
| TEA | 0.098 | 1 |
| EMEA | 0.607 | 1 |
| 2-DMAE | 0.379 | 1 |
| DETA | 1.619 | 2 |
| EDA | 0.935 | 2 |
| Piperazine | 0.98 | 1 |

An interesting fact is observed on the proton requirement for DETA, Pz. It is found that the required amount of proton is less than the amount of nitrogen nucleophile for complete $CO_2$ desorption in DETA and Pz. EDTA and Pz require w $molH^+$ $molEDTA^{-1}$ and 1 $molH^+$ $molPz^{-1}$ for complete $CO_2$ desorption, while they have 3 and 2 nitrogen nucleophiles per molecule. In contrast, the proton requirement for complete $CO_2$ desorption is equivalent to nitrogen nucleophiles. EDA would require 2 $molH^+$ $molEDA^{-1}$ for complete $CO_2$ desorption. This may result from amine's structure or pKa values in protonated form.

**Figure *41*** shows the structure of Pz, DETA, and EDA. Both Pz and DETA have at least one amine connected to the other amine groups via two alkyl chains. However, EDA and other amine tested do not have a structure like this. This structural difference may have led to the difference in the amount of proton requirement for full $CO_2$ desorption; however, a future mechanistic study is required to explain this phenomenon.

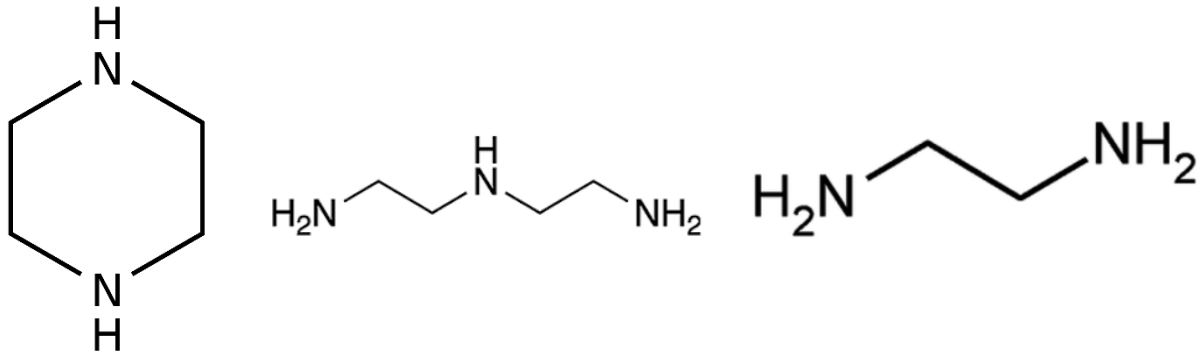


(a) (b) (c)

**Figure 41.** Structure of (a) Piperazine (b) Diethylenetriamine (c) ethylenediamine

## 5.3 Continuous electrochemical amine regeneration

The process flow diagram for the $CO_2$ absorption-desorption cycle using a four-compartment electrochemical cell and anion exchange resin is shown in **Figure *42***. First, $CO_2$ containing gas and MEA is pumped into the absorption tower. Next, $CO_2$-loaded amine is transported into the acid swing compartment of the four-compartment electrochemical cell for amine acidification and $CO_2$ desorption. Acidified amine is then pumped into an anion exchange resin-loaded column with the resin in the hydroxide form. Base swing of acidified MEA occurs in this column, and the regenerated MEA is pumped back into the absorption column for the next $CO_2$ absorption cycle. After the resin is in contact with acidified MEA, the resin will be in chloride form and need to be recharged with hydroxide form before the next base swing cycle. Therefore, at least two columns with anion exchange resin are needed. One is flushed with the acidified amine to regenerate the amine in the two anion exchange columns, and the other is flushed with hydroxide generated by the cathode. The amine regeneration process can utilize hydroxide generated at the cathode with this process. Anion exchange resin can serve as the hydroxide carrier that transfers the hydroxide from the cathode to acidified amine.

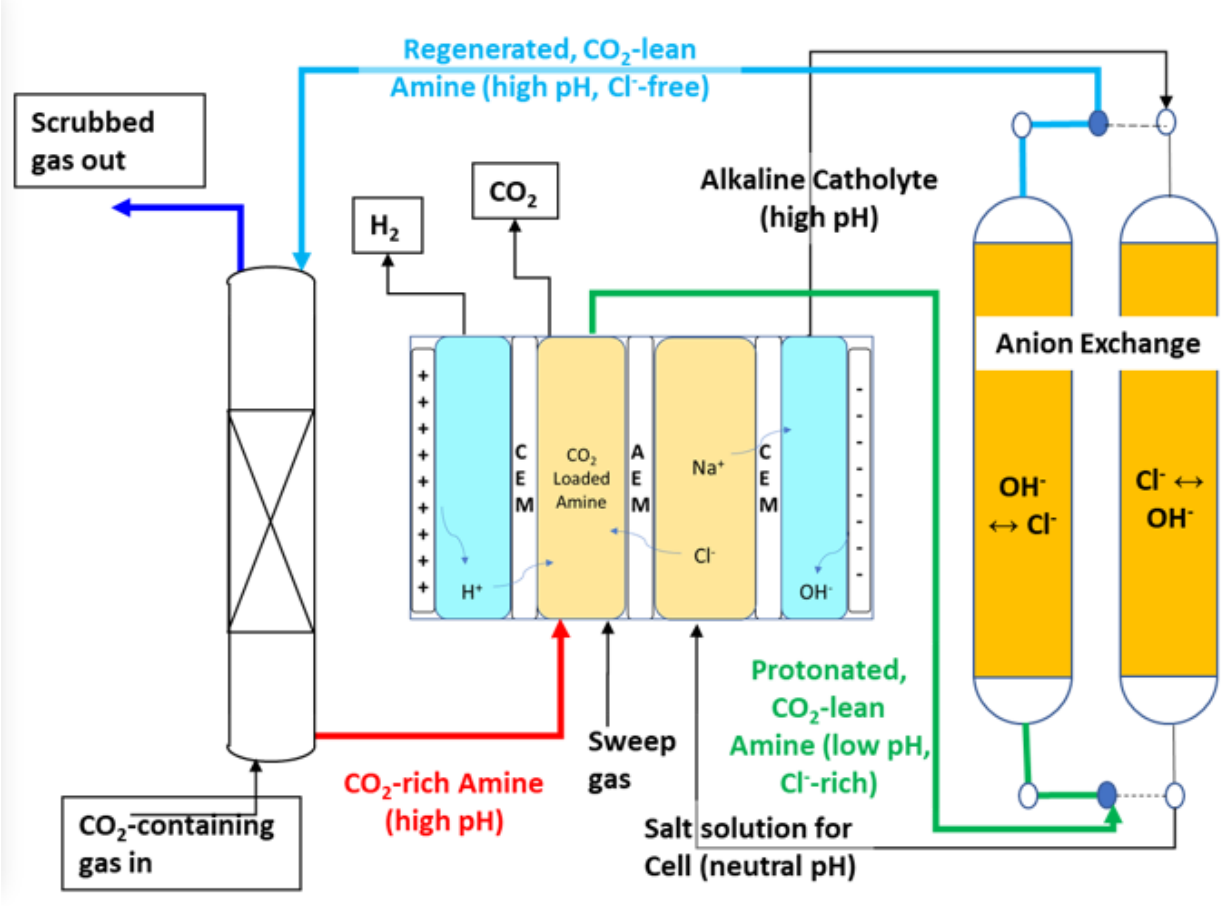


**Figure 42.** Process flow diagram of the electrochemical acid swing-based amine regeneration system

Even though this system design can allow the usage of proton and hydroxide generated from anode and cathode for acid-base swing amine regeneration, there are several disadvantages. First, the anion exchange base-swing can only be operated in a semi-batch manner. A continuous operation is not feasible due to the exchange mechanism of the ion exchange process. This is not desired as a continuous process would allow for a better operation rate and efficiency over batch or semi-batch process. Second, the main driving force of the ion exchange process is the concentration gradient of the ions. This implies that the ion exchange between hydroxide and chloride would not be in a 1-to-1 ratio. For instance, if 1 mole of chloride ions in an aqueous solution needs to be exchanged, more than 1 eq of ion in hydroxide form would be needed (1 eq,

1 equivalent, unit of exchange capacity, 1 eq = 1 mole of ion, exchange capacity). This limitation also applies to where the resin needs to be recharged with hydroxide. More than 1 mole of the hydroxide must recharge 1 eq of anion exchange resin in chloride form. This limit indicates that hydroxide generates by the cathode alone is not enough to support the regeneration cycle. Excess hydroxide would be required.

A five-compartment electrochemical cell is designed to substitute anion exchange resin as a base swing method. The schematic of the five-compartment electrochemical cell is shown in **Figure *43***. With this cell design, acid swing and base swing can be done in the same cell without using an anion exchange resin. In the 5-chamber electrochemical flow cell, $CO_2$-loaded amine is pumped into the acid swing chamber and acidified by protons generated at the anode and migrated through CEM. After the acidification of amine and desorption of $CO_2$ from the acid swing chamber, the acidified amine is pumped into the base swing chamber. Hydroxide ions generated at the cathode migrate through an AEM and enter the base swing chamber to restore alkalinity to the acidified amine for subsequent $CO_2$ absorption. The desalination chamber provides the counter ions for acid swing and base swing in the middle of the whole electrochemical cell, where regenerated amine with NaCl solution is in. As a counter ion, sodium ions migrate into the base swing chamber and chloride ions migrate into the acid swing chamber. These ions are transported by the pump and the amines and travel back to the desalination chamber to complete the counter ion cycle in the electrochemical cell. The working mechanism of the five-compartment cell is summarized in **Table 10**.

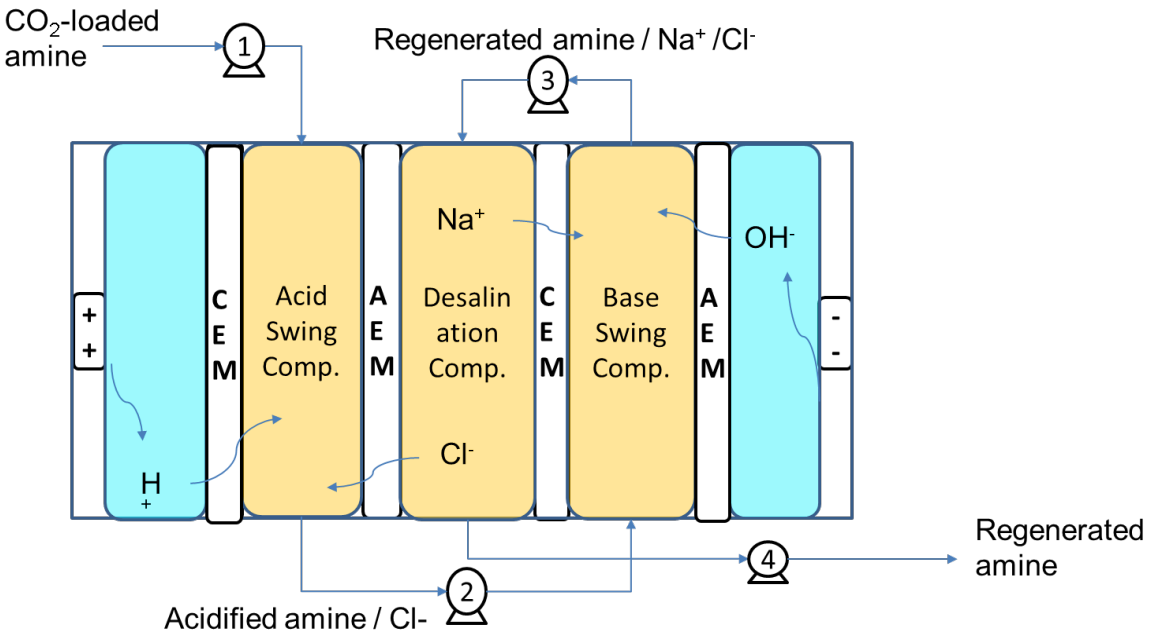


**Figure 43.** Schematic of the five-compartment electrochemical cell

**Table 10.** The working mechanism of the five-compartment electrochemical cell

| **Compartment** | **Anode** | **Acid Swing** | **Desalination** | **Base Swing** | **Cathode** |
|---|---|---|---|---|---|
| **Entering Component** | H2O | Amine-$CO_2$ | Regenerated Amine + NaCl | $AmineH^+Cl^-$ | H2O |
| **Reaction** | 2 $H_2O(l)$ → $O_2(g)$ + 4 $H^+(aq)$ + $4e^-$ | $AmineCO_2$ + HCl→ $AmineH^+Cl^-$+$CO_2$ | N/A | $AmineH^+Cl^-$ + NaOH → Amine + H2O + NaCl | 4 $H_2O(l)$ + $4e^-$ → 2 $H_2(g)$ + $4OH^-(aq)$ |
| **Ion Migration** | $H^+$ to Acid Swing | $H^+$ from Anode<br>$Cl^-$ from Desalination | Na+ to Base Swing<br>Cl- to Acid Swing | OH- from Cathode<br>Na+ from Desal | $OH^-$ to Base Swing |
| **Product** | $H_2SO_4$ | $AmineH^+Cl^-$ + $CO_2$ | Regenerated amine | Regenerated amine + NaCl | NaOH |
| **Exiting Component** | $O_2$ (vent) | $CO_2$ (vent)<br>$AmineH^+Cl^-$ (Base Swing) | Regenerated amine | Regenerated amine + NaCl | H2 (vent) |

**Table 11.** Starting solutions for continuous electrochemical amine regeneration process in the five-compartment electrochemical cell

| Compartment | Anode | Acid Swing | Desalination | Base Swing | Cathode |
|---|---|---|---|---|---|
| Main Component | 1M $H_2SO_4$ | 0.9M Piperazine | 0.9M Piperazine | 0.9M Piperazine | 1M NaOH |
| Additional Supplement | N/A | HCl addition until pH = 6 | NaCl addition to 1M | HCl & NaOH Addition (H+ : OH- : amine = 1 :1 : 1 ) | N/A |
| pH value | 0 | 6.0 | 12.0 | 12.0 | 14 |

$CO_2$ desorption and amine regeneration of the 5-compartment electrochemical cell are demonstrated by 0.9M piperazine. **Table 11** shows the solutions placed in each compartment at the start of the electrochemical cell operation. The starting solution in each compartment is intentionally determined, considering the target steady state conditions achieved during continuous operation. To regenerate piperazine continuously, 0.9M $CO_2$-loaded piperazine was pumped (by pump 1 in **Figure *43***) into the electrochemical cell at a flow rate of 0.691 ml $min^{-1}$ $A^{-1}$. This flow rate configuration would allow a 1-to-1 proton to piperazine ratio. The same flow rates were used for the rest of the pumps (pumps 2, 3, 4) to maintain a constant volume in each compartment. To keep the pH value of each compartment at its respective target value (Acid swing compartment: pH = ~6, Base Swing compartment: pH = ~12), feedback control is required. The feedback control was performed manually by measuring the pH of each cell and periodically adjusting the flow rate accordingly. The flow rate was increased if the pH of the acid swing chamber was lower than the set point and vice-versa. Samples were taken at each pH measurement and analyzed by infrared spectroscopy.

**Figure *44*** shows the pH value of each compartment during continuous operation. It is shown that the pH value of the base swing compartment fluctuates more at the early stage (0-6 hours) of the experiment. This result is believed to be inadequate feedback control. The flow rate adjustment was not frequent enough (once every 3 hours), and therefore the pH value deviated from the set point. With an improved control mechanism, the pH value of the base swing cell can achieve steady performance at its set point value (pH =12) with minimal fluctuation. This pH fluctuation can also be verified by the IR spectrum shown in **Figure *45*.**

Successful CO2 desorption, piperazine acidification, and regeneration are shown in Figures 45 **(a)** and **(b).** In **Figure *45* (b),** piperazine acidification can be verified by distinct and

characteristic peaks at 1615 $cm^{-1}$. Across all the sampled times in the acid swing chamber, the IR spectra confirm high degrees of desorption of the CO2 and no presence of $CO_2$-loaded Piperazine (characteristic peaks at 1290, 1240, and 1540 $cm^{-1}$). This data validates $CO_2$ was desorbed in an acid swing chamber during the continuous electrochemical regeneration process. Figure 45 (a) shows that protonated form of piperazine (1615 $cm^{-1}$) appears in the base swing cell at 3-hour and 7-hour-20-min time points. However, this peak disappears at 10 hours 20 min, making its spectrum identical to that of fresh Piperazine. This data validates that acidified amine can be successfully regenerated with proper pH feedback control in a continuous 5-chamber electrochemical regeneration operation. In summary, this 5-chamber electrochemical flow cell design allows us to perform electrochemical amine regeneration continuously without the need for an anion exchange resin column.

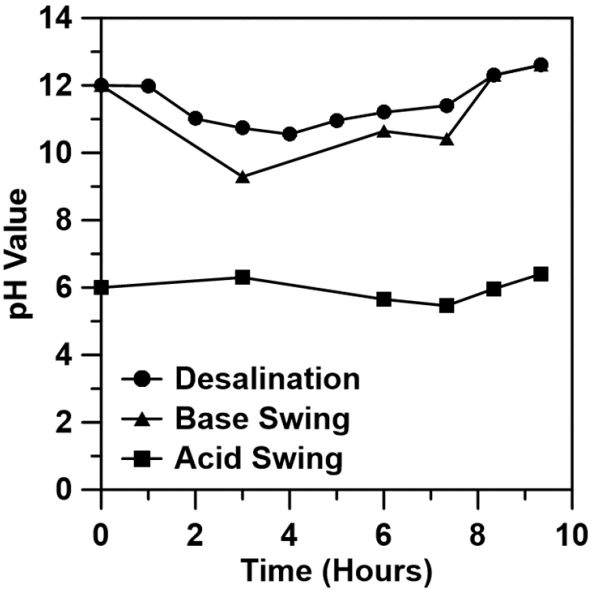


**Figure 44.** pH value of amines in five-compartment electrochemical cell during continuous electrochemical amine regeneration process

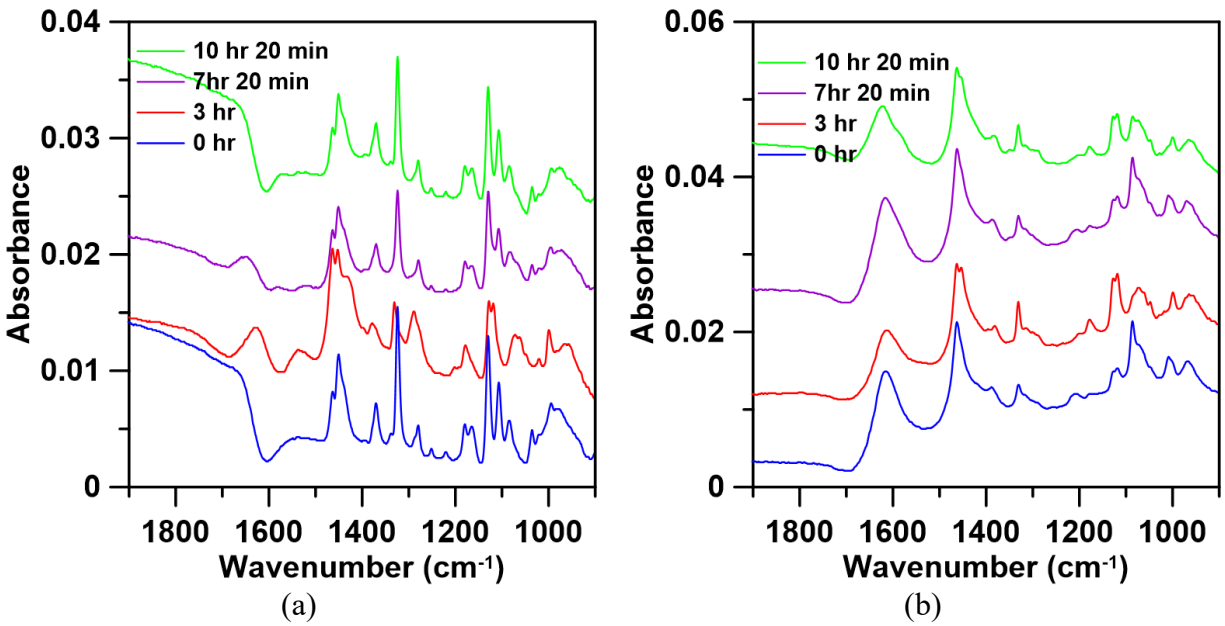


**Figure 45.** IR-spectrum of piperazine sample in **(a)** Base swing cell **(b)** Acid swing cell during continuous electrochemical amine regeneration process in the five-compartment electrochemical cell

Further cell design improvements can be implemented to reduce process complexity and enhanced energy efficiency. For example, a PVDF membrane replaces the whole desalination compartment in the five-compartment cell to reduce the number of membranes and compartments used.

**Figure 46** depicts the improved four-compartment cell design. In this design, counter ions for proton and hydroxide migrating into the acid swing and base swing compartment are not provided by the desalination compartment. Instead, the acid swing and base swing compartment provide necessary counter ions to each other to maintain their electroneutrality. The working mechanism of this cell is similar to that of the five-compartment cell and is shown in **Table 12**. This cell design can decrease the membrane amount needed and decrease the cost of the cell. In addition, cell efficiency is expected to improve with decreased electrode distance. However, the PVDF membrane is non-selective and would allow all molecules to migrate under a concentration

gradient or electric field. Further studies would need to be done to validate or optimize the operation parameter to minimize proton and hydroxide migration through the PVDF membrane.

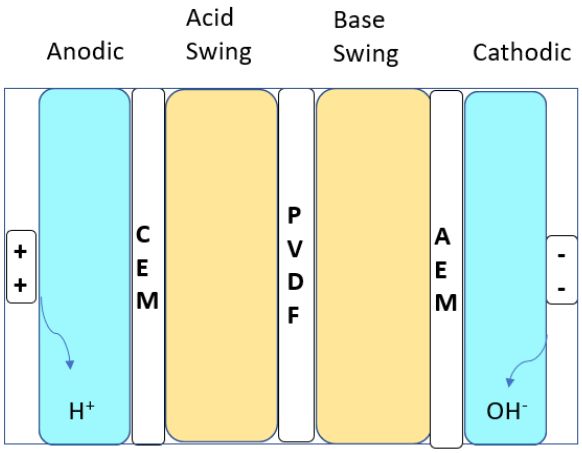


**Figure 46.** Schematic of a four-compartment electrochemical cell with the use of PVDF membrane

**Table 12.** The expected working mechanism of a four-compartment electrochemical cell with the use of PVDF membrane

| **Compartment** | **Anode** | **Acid Swing** | **Base Swing** | **Cathode** |
|---|---|---|---|---|
| **Entering Component** | H2O | NaCl + Amine-$CO_2$ | Amine$H^+Cl^-$ | H2O |
| **Reaction** | 2 $H_2O(l) \rightarrow O_2(g) + 4$ $H^+(aq) + 4e^-$ | Amine$CO_2$ + HCl→ Amine$H^+Cl^-$+$CO_2$ | Amine$H^+Cl^-$ + NaOH → Amine + H2O + NaCl | 4 $H_2O(l) + 4e^- \rightarrow 2$ $H_2(g) + 4OH^-(aq)$ |
| **Ion Migration** | $H^+$ to Acid Swing | $H^+$ from Anode<br>$Cl^-$ from Base Swing. | OH- from Cathode<br>Na+ from Acid Swing | $OH^-$ to Base Swing |
| **Product** | $H_2SO_4$ | Amine$H^+Cl^-$ + $CO_2$ | Regenerated amine + NaCl | NaOH |
| **Exiting Component** | $O_2$ (vent) | $CO_2$ (vent)<br>Amine$H^+Cl^-$ (Base Swing) | Regenerated amine + NaCl | H2 (vent) |

Besides optimizing membrane configuration in the cell, the cell stacking strategy also needs to be studied to facilitate the scale-up of the regeneration system. **Figure *47*** shows a schematic of a possible cell stacking strategy. The five-compartment-cell stack is connected in series using a bipolar membrane. A bipolar membrane can generate proton and hydroxide under reverse bias and substitute cathode and anode. Instead of duplicating the whole five-compartment cell for scale-up, connecting the cell in series can reduce the expensive Pt-coated electrodes required. The Schematic shown in **Figure *47*** is a "two" five-compartment-cell-stack connect in series. More five-five-compartment-cell-stack can be connected in series to minimize electrode number and create a more straightforward scale-up. In addition, the generation of proton and hydroxide using a bipolar membrane is less energy intensive than oxygen and hydrogen evolution reactions. This fact could decrease the energy required for the electrochemical amine regeneration system. Further studies will be required to understand the best cell stacking strategy and operation parameters.

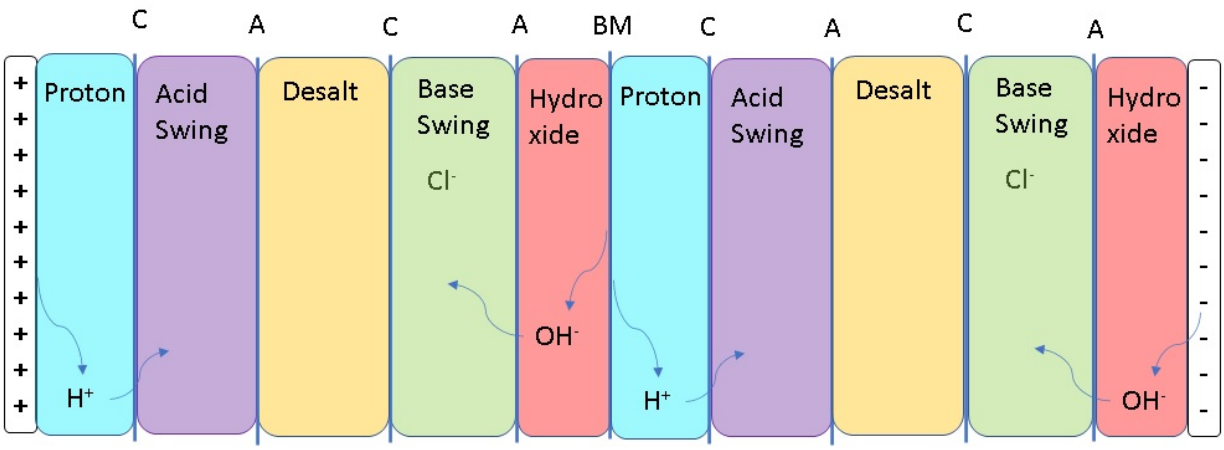


**Figure 47.** Schematics of an example of cell stacking strategy. Five-compartment-cell-stack is connected in series with the use of a bipolar membrane. C: CEM, A: AEM, BP: bipolar membrane.

# Chapter 6 Summary

This work focuses on (i) studies on acid- & base-swing based amine regeneration for $CO_2$ capture, (ii) development of electrochemical acid- & base-sing based amine regeneration system, and (iii) optimization of the configuration and operation parameters of the electrochemical amine regeneration system. It was found that absorption capacity and absorption rate remained the same after acid & base swing. In addition, hydrochloric acid addition to $CO_2$-loaded amine absorbent can desorb $CO_2$ from amine absorbent and facilitate temperature-driven $CO_2$ desorption. This result validates the feasibility of the acid & base swing amine regeneration method. Various electrochemical structures were designed to enable electrochemical acid and base swing for amine regeneration. It was found that the electrochemical acid swing can be done using a three-compartment electrochemical cell using a copper (II) ion at the cathode. However, copper usage in an electrochemical cell is not preferred, given that copper can be complex with amines. Therefore, the four-compartment electrochemical cell was developed to eliminate the use of the copper-based solution. It is shown that amine absorbent acidified by a four-compartment electrochemical cell exhibits a similar IR-spectrum with the absorbent acidified by HCl addition. This demonstrates the feasibility of acid swing using a four-compartment electrochemical cell. Base swing of acidified amine solution was done by anion exchange resin, Amberlite IRN-78 OH. It was shown that the absorption capacity of amine regenerated by HCl-NaOH and by electrochemical cell-AER are similar. IR-spectrum also validates that IRN-78 OH resin can provide hydroxide to the amine absorbent solution are regenerate protonated amine.

Optimization works were performed on amine selection, cell configuration, and operation parameters to increase energy efficiency and reduce process complexity. Piperazine has the lowest proton to $CO_2$ ratio among amine tested, indicating a minor proton requirement per unit $CO_2$

desorbed. Five-compartment cells were developed to eliminate the use of anion exchange resin as the base swing method, given its process complexity and lower hydroxide usage efficiency. It is shown that the five-compartment electrochemical cell can finish the acid- and base-swing regeneration cycle continuously without anion exchange resin usage. Several research focuses can be done to develop the electrochemical amine regeneration cell. First, mechanistic studies on proton-driven $CO_2$ desorption of amine absorbents can discover amine absorbents with fewer proton requirements per unit of $CO_2$ desorption. Studies on cell configuration can develop a more straightforward process and increase cell efficiency. The studies on cell configuration can include but are not limited to integrating bipolar membrane to the cell to connect the cell in series or integration of PVDF membrane into the to simplify the amine regeneration process and increase energy efficiency. With the potential future improvements, this electrochemical acid & base swing-based amine regeneration system can be the following generation method for $CO_2$ capture.

Appendices

**Appendix A** Python Scripts used for $CO_2$ quantification

Function definition: Import csv file recording $CO_2$ concentration $CO_2$ sensor and make it into dataframe format. Change the time format into month/day/year hh:mm:ss.sss format.

```
def CO2meter_import(start, end, filename='190521 test'):
    """
    :param path: string, The path of file to be read
    :param ptime: lambda function, convert string to timestamp format
    :param start: string, experiment start time.
    :param end: string, experiment ends time.
    :param dcount: lambda function, return day number passed from starttime
    :param scount: lambda function, return second number passed from starttime
    :param filename: string, The name of the data to be analyzed
    :return data: pandas dataframe, for future usage
    :return duration: timedelta, the duration between starttime and endtime
    :return starttime: timestamp, start time of experiment
    :return endtime: timestamp, end time of experiment
    """
    path = '/Users/byron/PycharmProjects/MEA_Absorption/Raw_data/' + filename+'.csv'
    data = pd.read_csv(path,index_col=False)

    # This line is to get rid of rows with header value created by FTIR between
    # each run
    # This problem is due to appending data to existing data
    data.pop('Unnamed: 2')
    data.pop('Unnamed: 3')
    data.columns = ['timestamp', 'CO2 (%)']
    data = data.iloc[1:]
    # Start to process time format.

    ptime = lambda x: datetime.strptime(x, '%m/%d/%y %H:%M:%S.%f')
    data['time'] = data['timestamp'].apply(ptime)

    starttime = datetime.strptime(start, '%m/%d/%Y %H:%M:%S.%f')
    endtime = datetime.strptime(end, '%m/%d/%Y %H:%M:%S.%f')
    duration = endtime-starttime
    data['timepass'] = data['time']-starttime
    dcount = lambda x: x.days
    data['day'] = data['timepass'].apply(dcount)
    scount = lambda x: x.seconds
    data['second'] = data['timepass'].apply(scount)
    # Take data only after starttime
    data = data[data['day'] == 0]
    data['min'] = round(data['second'] / 60, 5)
    data['CO2 (%)'] = pd.to_numeric(data['CO2 (%)'])
    data['CO2 (%)'] = data['CO2 (%)']/10000

    # Create another datafrome called rundata (This is data to be analyzed)
    # Then, Take the data before end time
    rundata = data[data['second'] < duration.seconds + 1]
    # Now, Rundata only consist of data in between starttime and endeimt.
```

```
    # Drop some time column that are not going to be used in the future
    rundata = rundata.drop(['time', 'timepass', 'day'], axis=1)
    #data = data.drop(['time', 'timepass', 'day'], axis=1)
    return rundata, data, duration, starttime, endtime
```

Function Defined: Calculate the saturation CO2 concentration (equCO2 in script, $X_{sat}$ in calculation work in method section)

```
def CO2equ(rundata):

    """

    :param data: pandas dataframe, include time_managed data

    :param duration: timedelta format, time duration between start and end time

    :return:

    """

    # make equilibration CO2% consistant at start and end time.

    # We try not to overestimate CO2 absorption by setting Equilibration

    # CO2 concentration to be smaller value among StartCO2% and EndCO2%

    expdata = rundata[rundata['min'] > 0]

    startCO2 = sum(expdata['CO2 (%)'].iloc[0:20]) / 20

    endCO2 = sum(expdata['CO2 (%)'].iloc[-20:]) / 20

    equCO2 = max(startCO2,endCO2)

    return expdata, startCO2, endCO2, equCO2
```

Function Defined: calculate amount of CO2 desorbed or absorbed in the following units. Gram CO2, mole CO2, molCO2 molAmine$^{-1}$, kgCO2 kgAmine$^{-1}$.

```
def result(rundata, equCO2, JN2, Soln_Molarity,

           Soln_vol, Molar_weight):

    # Unit in g, MEA amount used in this experiment

    MEA_usage = Soln_Molarity*Soln_vol/1000*Molar_weight



    # Start working on integration

    # get time difference between two data point and

    # store it in Rundata['deltat]
```

```
    rundata['deltat'] = rundata['second'] - rundata['second'].shift(1)
    # get average CO2% between two data point
    rundata['CO2% delta ave'] = (rundata['CO2 (%)'] + rundata['CO2 (%)'].shift(
        1)) / 2
    rundata['deltat'] = pd.to_numeric(rundata['deltat'])
    rundata['CO2% delta ave'] = pd.to_numeric(rundata['CO2% delta ave'])
    # Integration equation as listed
    # nCO2,out=Jn* int((X/(1-X))
    # Refer to BoxSync/Dante Lab/Data/CO2 Absorption/ Data analysis plan
    # unit in seconds
    rundata['Area'] = rundata['deltat'] * (0.01 * rundata['CO2% delta ave'] / (
                1 - 0.01 * rundata['CO2% delta ave']))
    rundata['flowout'] = rundata['Area']
    rundata['Flowin'] = rundata['deltat'] *0.01 * equCO2 /\
                        (1 - 0.01 * equCO2)
    rundata['Absorb'] = rundata['Flowin'] - rundata['flowout']
    rundata['Accu_mol'] = rundata['Absorb'].cumsum() / 60 * JN2 * 44 /\
                          MEA_usage / 44 * 61.084
    rundata['Accu_kg'] = rundata['Absorb'].cumsum() / 60 * JN2 * 44 / \
                         MEA_usage
    outIntegral = rundata['Area'].sum()
    inpIntegral = (0.01 * equCO2 / (1 - 0.01 * equCO2)) * rundata[
        'deltat'].sum()
    # Unit in mol, Total absorption amount of CO2 in this experiment
    mAbs = (inpIntegral - outIntegral) / 60 * JN2
    # Unit in gram, Total absorption CO2 in this experiment
    gAbs = mAbs * 44
```

```
    # Absorption capacity kgCO2/kgMEA

    absCap_kgCO2_per_kgMEA = gAbs / MEA_usage

    absCap_molCO2_per_molMEA = absCap_kgCO2_per_kgMEA / 44 * Molar_weight

    return absCap_kgCO2_per_kgMEA, absCap_molCO2_per_molMEA, mAbs, gAbs, rundata
```

Function defined: Create Series that reports results and running parameters of the experiment.

```
def create_series(filename, start, end, QN2, JN2, MEA_Soln_vol, mAbs, gAbs,
         absCap_kgCO2_per_kgMEA, absCap_molCO2_per_molMEA,num_of_spike):
    QN2 = round(QN2, 4)
    JN2 = round(JN2, 4)
    mAbs = round(mAbs, 4)
    gAbs = round(gAbs, 4)
    absCap_kgCO2_per_kgMEA = round(absCap_kgCO2_per_kgMEA, 4)
    absCap_molCO2_per_molMEA = round(absCap_molCO2_per_molMEA, 4)
    report = pd.Series(
        [filename, start, end, QN2, JN2, MEA_Soln_vol, mAbs, gAbs,
         absCap_kgCO2_per_kgMEA, absCap_molCO2_per_molMEA], name=num_of_spike,
        index=['Data',
               'Start Time',
               'End Time',
               'N2 Supply Flow Rate (L/min)',
               'N2 Supply Flow Rate (mol/min)',
               'MEA Amount (mL)',
               'CO2 Absorption/Desorption (mol)',
               'CO2 Absorption/Desorption (g)',
               'CO2 Absorption Capacity (kgCO2/kgMEA)',
               'CO2 Absorption Capacity (molCO2/molMEA)'])
    return report
```

Function defined: Create a dataframe that reports result and running parameters of the experiment.

```
def create_dataframe(filename, start, end, QN2, JN2, MEA_Soln_vol, mAbs, gAbs,
         absCap_kgCO2_per_kgMEA, absCap_molCO2_per_molMEA,num_of_spike):
    QN2 = round(QN2, 4)
    JN2 = round(JN2, 4)
    mAbs = round(mAbs, 4)
    gAbs = round(gAbs, 4)
    absCap_kgCO2_per_kgMEA = round(absCap_kgCO2_per_kgMEA, 4)
    absCap_molCO2_per_molMEA = round(absCap_molCO2_per_molMEA, 4)
    data = { num_of_spike: [filename, start, end, QN2, JN2, MEA_Soln_vol, mAbs, gAbs,
         absCap_kgCO2_per_kgMEA, absCap_molCO2_per_molMEA]}
    DF = pd.DataFrame(data, index=['Data',
                                   'Start Time',
                                   'End Time',
                                   'N2 Supply Flow Rate (L/min)',
                                   'N2 Supply Flow Rate (mol/min)',
                                   'MEA Amount (mL)',
                                   'CO2 Absorption/Desorption (mol)',
                                   'CO2 Absorption/Desorption (g)',
                                   'CO2 Absorption Capacity (kgCO2/kgMEA)',
                                   'CO2 Absorption Capacity (molCO2/molMEA)'])
    return DF
```

Absorption Experiment

```
#%%
from Code.Functions import *
import pandas as pd
# Input directory of Raw data
# Input directory of Each experiment trail

filename = '20220324_CO2_Desorption_2'
Addition = 'Piperazine Echem Reg Loading 0-27_I_2-45A'
start='03/24/2022 13:54:54.115'
end='03/24/2022 16:25:15.756'

N2diluenttime = 13.00#Unit=second
Soln_Molarity=0.9 #Molarity of amine absorbent (M)
Soln_vol= 100  #volume of amine absorbent solution used (mL)
Molar_weight= 86.136 # Molar weight of amine used (g/mol)

# Input experiment condition
Roomtemp = 20  # Unit=degree C
QN2 = 90/N2diluenttime*60/1000  # Unit=Liter/minute
JN2 = QN2*1/0.082/(Roomtemp+273.15)  # Unit=mol/minute
# input experiment start & end time here as a string
# Format has to be 'MM/DD/YYYY hh:mm:ss.sss'
# second to third decimal digit
# Starttime has to be at least 5 min before absorption start
# Endtime has to be at least 5 min after CO2% reach saturation
MEA_usage = Soln_Molarity*Soln_vol/1000*Molar_weight
log = lambda x: print(str(datetime.now())+x)


#%%

rundata, data, duration, starttime, endtime = CO2meter_import(start, end, filename)

expdata, startCO2, endCO2, equCO2 = CO2equ(rundata)

#%%
plot = rundata.plot(x='min', y='CO2 (%)', kind='line')
plt.legend(loc='upper right')
plt.ylabel('CO\u2082%')
plt.savefig('Figure/'+filename+'_'+Addition)

plt.show()


#%%
absCap_kgCO2_per_kgMEA, absCap_molCO2_per_molMEA, mAbs, gAbs, rundata = \
    result(rundata, equCO2, JN2, Soln_Molarity,Soln_vol, Molar_weight)

#%%
# Things to be reported
# file name
# Volumetric flowrate,
# Molar flowrate of diluent, MEA amount used, start time, end time,
# total Amount of CO2 absorbed (molar, weight)
# Absorption/desorption capacity,
```

```
report = create_series(filename, start, end, QN2, JN2, Soln_vol, mAbs, gAbs,
         absCap_kgCO2_per_kgMEA, absCap_molCO2_per_molMEA,'total')
report.to_csv('/Users/byron/PycharmProjects/MEA_Absorption/CSV_report/' +
              filename+'_'+Addition+'_Addition.csv')
Accu_data= pd.concat([rundata['min'],
                      rundata['Accu_mol'],
                      rundata['Accu_kg'],
                      rundata['CO2 (%)']],axis = 1)
Accu_data.to_csv('/Users/byron/PycharmProjects/MEA_Absorption/CSV_report/' +
              filename+'_'+Addition+'_Addition_Absorption_amount_realtime.csv')
```

Desorption Experiment

```
#%%
from Code.Functions import *
import pandas as pd
# Input directory of Raw data
# Input directory of Each experiment trail
title_of_report= 'Acid_Swing_By_HCl_Addition'
filename = '20220315_CO2_Desorption'
Addition = 'HCl_ Max CO2 loading'
start='03/15/2022 11:54:01.334'
end='03/15/2022 13:17:11.334'
N2diluenttime = 12.97 # Unit=second
Soln_Molarity=0.9 #Molarity of amine absorbent (M)
Soln_vol= 200  #volume of amine absorbent solution used (mL)
Molar_weight= 86.136 # Molar weight of amine used (g/mol)

# Input experiment condition
Roomtemp = 20  # Unit=degree C
QN2 = 90/N2diluenttime*60/1000  # Unit=Liter/minute
JN2 = QN2*1/0.082/(Roomtemp+273.15)  # Unit=mol/minute
# input experiment start & end time here as a string
# Format has to be 'MM/DD/YYYY hh:mm:ss.sss'
# second to third decimal digit
# Starttime has to be at least 10 min before absorption start
# Endtime has to be at least 10 min after CO2% reach saturation
MEA_usage = Soln_Molarity*Soln_vol/1000*Molar_weight
log = lambda x: print(str(datetime.now())+x)


#%%

rundata, data, duration, starttime, endtime = CO2meter_import(start, end, filename)

expdata, startCO2, endCO2, equCO2 = CO2equ(rundata)

#%%
plot = rundata.plot(x='min', y='CO2 (%)', kind='line')
plt.legend(loc='upper right')
plt.savefig('Figure/'+filename+'_'+Addition)
plt.show()


#%%
equCO2=0
```

```
absCap_kgCO2_per_kgMEA, absCap_molCO2_per_molMEA, mAbs, gAbs, rundata = \
       result(rundata, equCO2, JN2, MEA_Soln_vol, MEA_Soln_conc, MEA_density)
final_result = create_dataframe(filename, start, end, QN2, JN2, MEA_Soln_vol, mAbs,
                            gAbs,absCap_kgCO2_per_kgMEA,
                            absCap_molCO2_per_molMEA,'Total')
# Things to be reported
# file name
# Volumetric flowrate,
# Molar flowrate of diluent, MEA amount used, start time, end time,
# total Amount of CO2 absorbed (molar, weight)
# Absorption/desorption capacity,
report = create_series(filename, start, end, QN2, JN2, Soln_vol, mAbs, gAbs,
         absCap_kgCO2_per_kgMEA, absCap_molCO2_per_molMEA,'total')
report.to_csv('/Users/byron/PycharmProjects/MEA_Absorption/CSV_report/' +
              filename+'_'+Addition+'_Addition.csv')
Accu_data= pd.concat([rundata['min'],
                      rundata['Accu_mol'],
                      rundata['Accu_kg'],
                      rundata['CO2 (%)']],axis = 1)
Accu_data.to_csv('/Users/byron/PycharmProjects/MEA_Absorption/CSV_report/' +
              filename+'_'+Addition+'_Addition_Absorption_amount_realtime.csv')
```

**Appendix B** Supplementary Figures

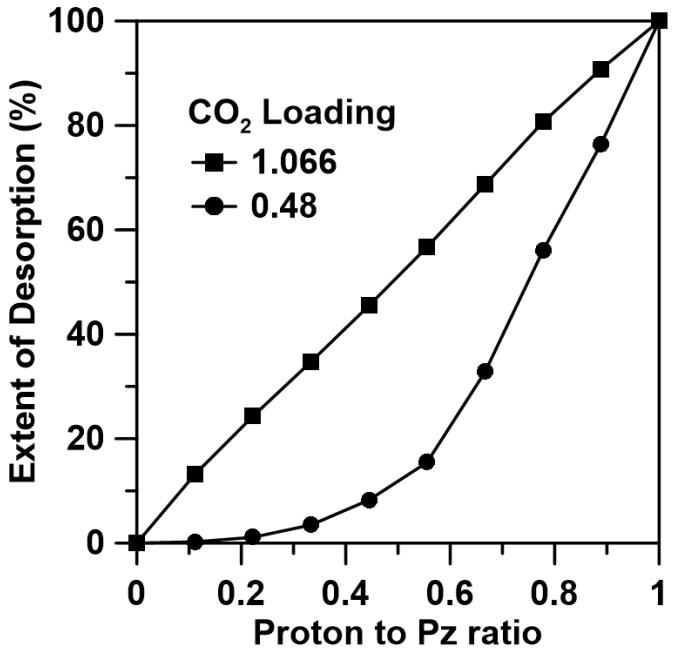


**Figure 48.** Desorption profile of Piperazine at different $CO_2$ loading ($molCO_2\ molPz^{-1}$)

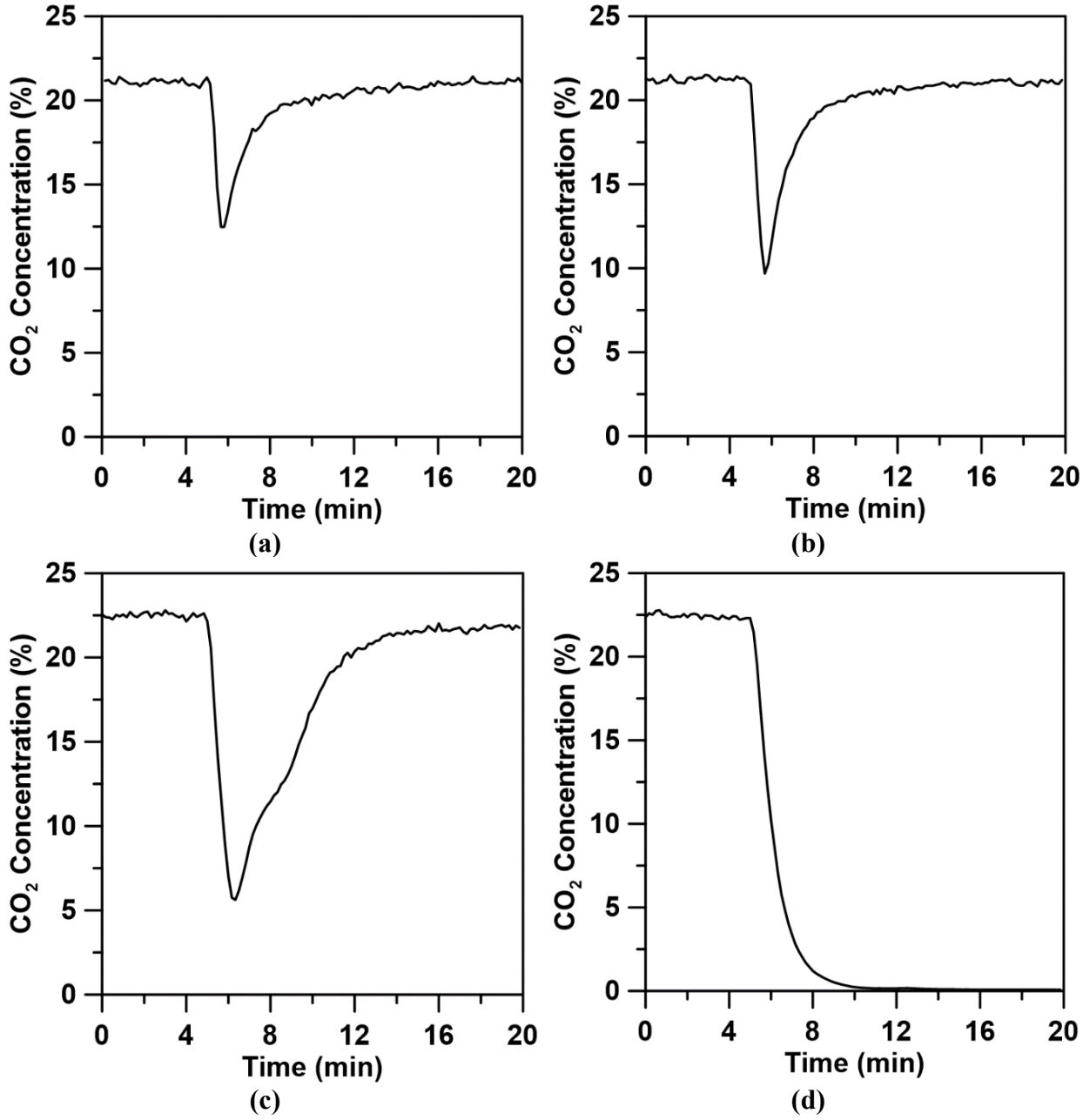


**Figure 49.** $CO_2$ breakthrough curve of NaOH solution at various pH **(a)** pH = 10 **(b)** pH = 11 **(c)** pH = 13 **(d)** pH = 14

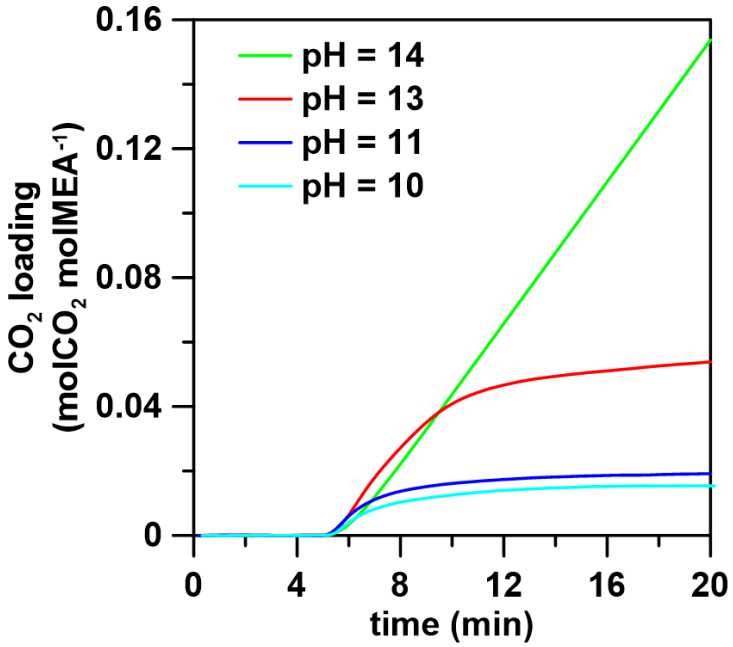


**Figure 50.** $CO_2$ loading of NaOH solution at various pH

References


1. Ian Tiseo. Annual CO2 emissions worldwide from 1940 to 2020. https://www.statista.com/statistics/276629/global-co2-emissions/#:~:text=Global carbon dioxide (CO2) emissions,to 34.81 billion metric tons. Published 2021.

2. IEA. Greenhouse Gas Emissions from Energy: Overview. 2021. https://www.iea.org/reports/greenhouse-gas-emissions-from-energy-overview.

3. Ian Tiseo. Global atmospheric concentration of carbon dioxide 1959-2021. 2022. https://www.statista.com/statistics/1091926/atmospheric-concentration-of-co2-historic/.

4. NOAA. NOAA National Centers for Environmental Information, State of the Climate: Global Climate Report for Annual 2020. https://www.ncdc.noaa.gov/sotc/global/202013. Published 2021.

5. Patel SS. A sinking feeling. *Nature*. 2006;440(7085):734-736. doi:10.1038/440734a

6. Michelle T, S. BD, L. NR, K. RD. Future warming increases probability of globally synchronized maize production shocks. *Proc Natl Acad Sci*. 2018;115(26):6644-6649. doi:10.1073/pnas.1718031115

7. International Energy Agency. Towards Susteinable Urban Energy Systems. 2016:14. doi:10.1787/energy_tech-2014-en

8. Buhre BJP, Elliott LK, Sheng CD, Gupta RP, Wall TF. Oxy-fuel combustion technology for coal-fired power generation. *Prog energy Combust Sci*. 2005;31(4):283-307.

9. Cabral RP, Mac Dowell N. A novel methodological approach for achieving £/MWh cost reduction of CO2 capture and storage (CCS) processes. *Appl Energy*. 2017;205:529-539.

doi:https://doi.org/10.1016/j.apenergy.2017.08.003

10. Aaron D, Tsouris C. Separation of CO2 from flue gas: A review. *Sep Sci Technol*. 2005;40(1-3):321-348. doi:10.1081/SS-200042244

11. Li T, Keener TC. A review: Desorption of CO2 from rich solutions in chemical absorption processes. *Int J Greenh Gas Control*. 2016;51:290-304. doi:10.1016/j.ijggc.2016.05.030

12. Vaidya PD, Kenig EY. CO2-Alkanolamine Reaction Kinetics: A Review of Recent Studies. *Chem Eng Technol*. 2007;30(11):1467-1474. doi:10.1002/ceat.200700268

13. Osman AI, Hefny M, Abdel Maksoud MIA, Elgarahy AM, Rooney DW. *Recent Advances in Carbon Capture Storage and Utilisation Technologies: A Review*. Vol 19. Springer International Publishing; 2021. doi:10.1007/s10311-020-01133-3

14. Shreyash N, Sonker M, Bajpai S, et al. The review of carbon capture-storage technologies and developing fuel cells for enhancing utilization. *Energies*. 2021;14(16). doi:10.3390/en14164978

15. MacDowell N, Florin N, Buchard A, et al. An overview of CO 2 capture technologies. *Energy Environ Sci*. 2010;3(11):1645-1669.

16. Jansen D, Gazzani M, Manzolini G, Dijk E Van, Carbo M. Pre-combustion CO2 capture. *Int J Greenh Gas Control*. 2015;40:167-187. doi:10.1016/j.ijggc.2015.05.028

17. Alves HJ, Bley Junior C, Niklevicz RR, Frigo EP, Frigo MS, Coimbra-Araújo CH. Overview of hydrogen production technologies from biogas and the applications in fuel cells. *Int J Hydrogen Energy*. 2013;38(13):5215-5225. doi:10.1016/j.ijhydene.2013.02.057

18. Gazzani M, Macchi E, Manzolini G. CO2 capture in natural gas combined cycle with SEWGS. Part A: Thermodynamic performances. *Int J Greenh Gas Control*. 2013;12:493-501. doi:10.1016/j.ijggc.2012.06.010

19. Manzolini G, Macchi E, Gazzani M. CO2 capture in natural gas combined cycle with SEWGS. Part B: Economic assessment. *Int J Greenh Gas Control*. 2013;12:502-509. doi:10.1016/j.ijggc.2012.06.021

20. Leung DYC, Caramanna G, Maroto-Valer MM. An overview of current status of carbon dioxide capture and storage technologies. *Renew Sustain Energy Rev*. 2014;39:426-443. doi:10.1016/j.rser.2014.07.093

21. Kheirinik M, Ahmed S, Rahmanian N. Comparative techno-economic analysis of carbon capture processes: Pre-combustion, post-combustion, and oxy-fuel combustion operations. *Sustain*. 2021;13(24). doi:10.3390/su132413567

22. Koohestanian E, Shahraki F. Review on principles, recent progress, and future challenges for oxy-fuel combustion CO2capture using compression and purification unit. *J Environ Chem Eng*. 2021;9(4):105777. doi:10.1016/j.jece.2021.105777

23. Wall T, Liu Y, Spero C, et al. An overview on oxyfuel coal combustion-State of the art research and technology development. *Chem Eng Res Des*. 2009;87(8):1003-1016. doi:10.1016/j.cherd.2009.02.005

24. Danckwerts P V. The reaction of CO2 with ethanolamines. *Chem Eng Sci*. 1979;34(4):443-446. doi:10.1016/0009-2509(79)85087-3

25. Blauwhoff PMM, Versteeg GF, Van Swaaij WPM. A study on the reaction between CO2

and alkanolamines in aqueous solutions. *Chem Eng Sci*. 1983;38(9):1411-1429. doi:10.1016/0009-2509(83)80077-3

26. Lv B, Guo B, Zhou Z, Jing G. Mechanisms of CO 2 Capture into Monoethanolamine Solution with Di ff erent CO 2 Loading during the Absorption / Desorption Processes. 2015. doi:10.1021/acs.est.5b02356

27. Boettinger W, Maiwald M, Hasse H. Online NMR spectroscopic study of species distribution in MEA-H2O-CO2 and DEA-H2O-CO2. *Fluid Phase Equilib*. 2008;263(2):131-143. doi:10.1016/j.fluid.2007.09.017

28. Lin YJ, Madan T, Rochelle GT. Regeneration with rich bypass of aqueous piperazine and monoethanolamine for CO2 capture. *Ind Eng Chem Res*. 2014;53(10):4067-4074. doi:10.1021/ie403750s

29. Nakagaki T, Yamabe R, Furukawa Y, Sato H, Yamanaka Y. Experimental Evaluation of Temperature and Concentration Effects on Heat of Dissociation of CO2-loaded MEA Solution in Strippers. *Energy Procedia*. 2017;114(November 2016):1910-1918. doi:10.1016/j.egypro.2017.03.1322

30. Sakwattanapong R, Aroonwilas A, Veawab A. Behavior of reboiler heat duty for CO2 capture plants using regenerable single and blended alkanolamines. *Ind Eng Chem Res*. 2005;44(12):4465-4473. doi:10.1021/ie050063w

31. Chowdhury FA, Yamada H, Higashii T, Goto K, Onoda M. CO2 capture by tertiary amine absorbents: A performance comparison study. *Ind Eng Chem Res*. 2013;52(24):8323-8331. doi:10.1021/ie400825u

32. Sartorl G, Savage DW. Sterically Hindered Amines for CO2 Removal from Gases. *Ind Eng Chem Fundam*. 1983;22(2):239-249. doi:10.1021/i100010a016

33. Kim YE, Lim JA, Jeong SK, Yoon Y Il, Bae ST, Nam SC. Comparison of Carbon Dioxide Absorption in Aqueous MEA , DEA , TEA , and AMP Solutions. 2013;34(3):783-787.

34. Huertas JI, Gomez MD, Giraldo N, Garzón J. CO 2 Absorbing Capacity of MEA. 2015;2015(2).

35. Aronu UE, Ghondal S, Hessen ET, Haug-warberg T, Hoff KA, Svendsen HF. Equilibrium in the H2O-MEA-CO2 system: new data and modeling. *1st Post Combust Capture Conf Equilib*. 2010:30-32. https://www.ieaghg.org/docs/General_Docs/PCCC1/Abstracts_Final/pccc1Abstract00040.pdf.

36. Dugas RE, Rochelle GT. CO2 absorption rate into concentrated aqueous monoethanolamine and piperazine. *J Chem Eng Data*. 2011;56(5):2187-2195. doi:10.1021/je101234t

37. Choi BK, Kim SM, Lee JS, et al. Effect of Blending Ratio and Temperature on CO2Solubility in Blended Aqueous Solution of Monoethanolamine and 2-Amino-2-methyl-propanol: Experimental and Modeling Study Using the Electrolyte Nonrandom Two-Liquid Model. *ACS Omega*. 2020;5(44):28738-28748. doi:10.1021/acsomega.0c04046

38. Maneeintr K, Photien K, Charinpanitkul T. Mixture of MEA/2-MAE for effective CO2 capture from flue gas stream. *Chem Eng Trans*. 2018;63:229-234. doi:10.3303/CET1863039

39. Pei Z, Yao SHI. Regeneration of amino for carbon dioxide absorption. 2008;20:39-44.

40. Li K, Cousins A, Yu H, et al. Systematic study of aqueous monoethanolamine-based CO2 capture process: Model development and process improvement. *Energy Sci Eng*. 2016;4(1):23-39. doi:10.1002/ese3.101

41. Salem RR. Theory of the electrolysis of water. *Prot Met*. 2008;44(2):120-125. doi:10.1007/s11124-008-2002-x

42. López-Fernández E, Sacedón CG, Gil-Rostra J, Yubero F, González-Elipe AR, de Lucas-Consuegra A. Recent advances in alkaline exchange membrane water electrolysis and electrode manufacturing. *Molecules*. 2021;26(21):1-24. doi:10.3390/molecules26216326

43. Shiva Kumar S, Himabindu V. Hydrogen production by PEM water electrolysis – A review. *Mater Sci Energy Technol*. 2019;2(3):442-454. doi:10.1016/j.mset.2019.03.002

44. Grigoriev SA, Millet P, Fateev VN. Evaluation of carbon-supported Pt and Pd nanoparticles for the hydrogen evolution reaction in PEM water electrolysers. *J Power Sources*. 2008;177(2):281-285. doi:10.1016/j.jpowsour.2007.11.072

45. Nikolaidis P, Poullikkas A. A comparative overview of hydrogen production processes. *Renew Sustain Energy Rev*. 2017;67:597-611. doi:10.1016/j.rser.2016.09.044

46. Grigoriev SA, Porembsky VI, Fateev VN. Pure hydrogen production by PEM electrolysis for hydrogen energy. *Int J Hydrogen Energy*. 2006;31(2):171-175. doi:10.1016/j.ijhydene.2005.04.038

47. Millet P, Ngameni R, Grigoriev SA, et al. PEM water electrolyzers: From electrocatalysis to stack development. *Int J Hydrogen Energy*. 2010;35(10):5043-5052.

doi:10.1016/j.ijhydene.2009.09.015

48. Cheng J, Zhang H, Chen G, Zhang Y. Study of IrxRu1-xO2 oxides as anodic electrocatalysts for solid polymer electrolyte water electrolysis. *Electrochim Acta*. 2009;54(26):6250-6256. doi:10.1016/j.electacta.2009.05.090

49. Esposito E, Minotti A, Fontananova E, Longo M, Jansen JC, Figoli A. Green H2 Production by Water Electrolysis Using Cation Exchange Membrane: Insights on Activation and Ohmic Polarization Phenomena. *Membranes (Basel)*. 2022;12(1). doi:10.3390/membranes12010015

50. Hinnemann B, Moses PG, Bonde J, et al. Biomimetic hydrogen evolution: MoS2 nanoparticles as catalyst for hydrogen evolution. *J Am Chem Soc*. 2005;127(15):5308-5309. doi:10.1021/ja0504690

51. Gouda MH, Elnouby M, Aziz AN, Youssef ME, Santos DMF, Elessawy NA. Green and Low-Cost Membrane Electrode Assembly for Proton Exchange Membrane Fuel Cells: Effect of Double-Layer Electrodes and Gas Diffusion Layer. *Front Mater*. 2020;6(January):1-9. doi:10.3389/fmats.2019.00337

52. Bernt M, Hartig-Weiß A, Tovini MF, et al. Current Challenges in Catalyst Development for PEM Water Electrolyzers. *Chemie-Ingenieur-Technik*. 2020;92(1-2):31-39. doi:10.1002/cite.201900101

53. Hegge F, Lombeck F, Cruz Ortiz E, et al. Efficient and Stable Low Iridium Loaded Anodes for PEM Water Electrolysis Made Possible by Nanofiber Interlayers. *ACS Appl Energy Mater*. 2020;3(9):8276-8284. doi:10.1021/acsaem.0c00735

54. Pärnamäe R, Mareev S, Nikonenko V, et al. Bipolar membranes: A review on principles, latest developments, and applications. *J Memb Sci*. 2021;617. doi:10.1016/j.memsci.2020.118538

55. Zeigerson E. Division oj Chemistry , Negev Institute oj Arid Zone. 1971;9:483-497.

56. Kunst B, Lovrecek B. Electrochemical Properties of the Ion-Exchange Membranes Junction. II.*. 1962;34:219-229.

57. Onsager L. Deviations from Ohm ' s Law in Weak. *J Chem Phys*. 1934;2(May 1934):599-615.

58. Alcaraz A, Ramírez P, Mafé S, Holdik H. A simple model for ac impedance spectra in bipolar membranes. *J Phys Chem*. 1996;100(38):15555-15561. doi:10.1021/jp961187c

59. Simons R. Strong electric field effects on proton transfer between membrane-bound amines and water [4]. *Nature*. 1979;280(5725):824-826. doi:10.1038/280824a0

60. Strathmann H, Krol JJ, Rapp HJ, Eigenberger G. Limiting current density and water dissociation in bipolar membranes. *J Memb Sci*. 1997;125(1):123-142. doi:10.1016/S0376-7388(96)00185-8

61. Feng B, Du M, Dennis TJ, Anthony K, Perumal MJ. Reduction of energy requirement of CO2 desorption by adding acid into CO2-loaded solvent. *Energy and Fuels*. 2010;24(1):213-219. doi:10.1021/ef900564x

62. Du M, Feng B, An H, Liu W, Zhang L. Effect of addition of weak acids on CO2 desorption from rich amine solvents. *Korean J Chem Eng*. 2012;29(3):362-368. doi:10.1007/s11814-011-0184-4

63. Du M. Effect of pH on desorption of CO2 from alkanolamine - Rich solvents. *AIP Conf Proc*. 2017;1864(August 2017). doi:10.1063/1.4992908

64. Sun C, Dutta PK. Infrared Spectroscopic Study of Reaction of Carbon Dioxide with Aqueous Monoethanolamine Solutions. *Ind Eng Chem Res*. 2016;55(22):6276-6283. doi:10.1021/acs.iecr.6b00017

65. Jackson WA, Lacourse WR, Dobberpuhl D, Johnson DC. The voltammetric response of ethanolamine at gold electrodes in alkaline media. *Electroanalysis*. 1991;3(7):607-616. doi:10.1002/elan.1140030704

66. Betowska-Brzezinska M, Łuczak T, Holze R. Electrocatalytic oxidation of mono- and polyhydric alcohols on gold and platinum. *J Appl Electrochem*. 1997;27(9):999-1011. doi:10.1023/a:1018422206817

67. Cheng C hung, Li K, Yu H, Jiang K, Chen J, Feron P. Amine-based post-combustion CO2 capture mediated by metal ions: Advancement of CO2 desorption using copper ions. *Appl Energy*. 2018;211(November 2017):1030-1038. doi:10.1016/j.apenergy.2017.11.105

68. Zelewsky A von. *Stereochemistry of Coordination Compounds*.; 1996.

69. Lin JM, Shan X, Hanaoka S, Yamada M. Luminol chemiluminescence in unbuffered solutions with a Cobalt(II) - Ethanolamine complex immobilized on resin as catalyst and its application to analysis. *Anal Chem*. 2001;73(21):5043-5051. doi:10.1021/ac010573+

70. Masoud MS. Coordination compounds of ethanolamines with nickel(II) salts. *J Inorg Nucl Chem*. 1977;39(3):413-415. doi:10.1016/0022-1902(77)80052-3

71. Vaseem M, Lee SK, Kim JG, Hahn YB. Silver-ethanolamine-formate complex based

transparent and stable ink: Electrical assessment with microwave plasma vs thermal sintering. *Chem Eng J*. 2016;306:796-805. doi:10.1016/j.cej.2016.08.003

72. Karadag A, Yilmaz VT, Thoene C. Di- and triethanolamine complexes of Co(II), Ni(II), Cu(II) and Zn(II) with thiocyanate: Synthesis, spectral and thermal studies. Crystal structure of dimeric Cu(II) complex with deprotonated diethanolamine, [Cu2(μ-dea)2(NCS)2]. *Polyhedron*. 2001;20(7-8):635-641. doi:10.1016/S0277-5387(01)00720-3

73. Pait M, Kundu B, Kundu SC, Ray D. Copper(II) complexes of piperazine based ligand: Synthesis, crystal structure, protein binding and evaluation of anti-cancerous therapeutic potential. *Inorganica Chim Acta*. 2014;418:30-41. doi:10.1016/j.ica.2014.04.019

74. Inada Y, Ozutsumi K, Funahashi S, Soyama S, Kawashima T, Tanaka M. Structure of Copper(II) Ethylenediamine Complexes in Aqueous and Neat Ethylenediamine Solutions and Solvent-Exchange Kinetics of the Copper(II) Ion in Ethylenediamine As Studied by EXAFS and NMR Methods. *Inorg Chem*. 1993;32(14):3010-3014. doi:10.1021/ic00066a009

75. Lv B, Guo B, Zhou Z, Jing G. Mechanisms of CO2 Capture into Monoethanolamine Solution with Different CO2 Loading during the Absorption/Desorption Processes. *Environ Sci Technol*. 2015;49(17):10728-10735. doi:10.1021/acs.est.5b02356

76. Li S, Li H, Yu Y, Chen J. Aqueous Solvents of N - ( 2-Hydroxyethyl ) Piperazine and. 2021.